A NOVEL QUANTITATIVE ANGIOGRAPHY TECHNIQUE FOR GUIDING IMAGE-GUIDED VASCULAR INTERVENTIONS

By:

Sarvesh Periyasamy

A dissertation submitted in partial fulfillment of the requirements for the degree of

Doctor of Philosophy

(Biomedical Engineering)

At the

UNIVERSITY OF WISCONSIN - MADISON

2022

Date of final oral examination: May 31st, 2022

The dissertation is approved by the following members of the Final Oral Committee:

Dr. Paul F. Laeseke, MD, PhD, Assistant Professor, Radiology, Biomedical Engineering
Dr. Chris L. Brace, PhD, Associate Professor, Radiology, Biomedical Engineering
Dr. Michael A. Speidel, PhD, Associate Professor, Medical Physics, Medicine
Dr. Melissa C. Skala, PhD, Professor, Biomedical Engineering
Dr. John-Paul J. Yu MD, PhD, Assistant Professor, Radiology, Psychiatry, Biomedical Engineering

Acknowledgements

Writing this thesis has been a great reflection on my scientific experience over the last four years, but it has also been a wonderful reflection on all the incredible people that have helped make my graduate school experience one of the most memorable and joyful periods in my life. So, to the following people, I would like to say *thank you*:

To my thesis advisor, Paul, who I could not be more thankful to have worked with over the last several years. Four years ago I had no idea what I wanted to do, both in medicine and science. I would consider our first meeting a true bit of serendipity as it completely changed my physician-scientist journey for the better. I have learned more than I could possibly described about being a good clinician, scientist, and mentor from you. Very few times do you get to truly follow in the footsteps of your role model, and for that I am truly grateful.

To the rest of my thesis committee, Chris, Mike, Melissa, and JP, all of whom have been the most open and encouraging mentors throughout my academic career. I have been fortunate enough that I have gotten to work or collaborate with all of you in some capacity, in addition to the guidance you have provided me through my doctorate.

To the University of Wisconsin MSTP leadership, who gave me the opportunity of a lifetime. I still vividly remember meeting Anna, Mark, and Scott on my interview weekend and thinking how lucky I would be to be invited into this amazing program. Perhaps the biggest thank you of all to Chelsea and Nichole, who have undoubtedly been two of the most important people in getting me through this journey. Even in the busiest, toughest days, chatting with you two in your office was always a welcome break.

To the Image-Guided Interventions Lab, one of the most collaborative and helpful groups I have ever worked with. In particular Martin, Carson, Joe, and Erick, whose foundational work was critical to everything in this thesis. I attribute a lot my of day-to-day growth as a scientist to your partnerships.

To the Cardiovascular Research Core (Hacker Lab), Tim, Allie, Jamie, and especially EJ and Sarah. I am entirely certain that nothing in this dissertation would have been possible without your tireless help. I would venture to say I spent more time with you (hundreds, if not thousands of hours?) than anyone else in my life over the last four years. And I could not think of a better group of friends to have spent it with.

To all my mentors and collaborators in the Department of Radiology: Dr. Scott Reeder, Dr. Ali Pirasteh, Dr. Tim Ziemlewicz, Dr. Fred Lee, Dr. Mark Kleedehn, Dr. Orhan Ozkan, Jim White, Sebastian Schaefer, James Scheuermann, among many others. I

am always grateful to have worked in a department where I have so many people to turn to for wisdom.

To my MSTP cohort (*The Lifeblood*) who have been one of the few constants in my life for the better part of seven years. I could not have asked for a better group to undertake this eight year journey with.

To my friends, Kate, Alli, & Lola, who made my four years of graduate school some of the most memorable and fun of my life. During a pandemic where I was feeling especially isolated, you were the most loving, supportive, and caring friends. A lot of my favorite memories related to this time in my life are with you guys and I will forever cherish that.

Most importantly, to Mom, Dad, Vish, and Abu. Your support throughout my entire life has made this possible. You were always there for me when I needed it the most, offering encouragement, guidance, and love. I consider this your achievement just as much as it is mine.

Table of Contents

Abstract

A Novel Quantitative Angiography Technique for Guiding Image-Guided Vascular Interventions

Sarvesh Periyasamy

Under the supervision of Dr. Paul F. Laeseke, MD, PhD, Assistant Professor of Radiology & Biomedical Engineering at the University of Wisconsin - Madison

Image-guided vascular interventions are a common method of treating a number of oncologic and non-oncologic diseases. Such procedures are guided by x-ray based contrast-enhanced imaging of blood vessels (angiography). These procedures, including angioplasty, stent placement, and embolization are largely qualitative, relying on subjective, visual assessment of digital subtraction angiography (DSA) images to diagnose pathology, determine procedural endpoints, and evaluate treatment efficacy. Angiographic assessment using DSA depends on factors such as observer experience and perceptual bias, both of which have been previously shown to be a significant source of interpretive error in radiology. This leads to a high degree of interobserver variability and decrease in reproducibility. An objective, quantitative angiographic technique for determining procedural endpoints would help standardize vascular interventions, and

ultimately build the quantitative link between endpoints and patient outcomes needed to improve procedure safety and efficacy.

We have developed two quantitative angiography techniques which can be used to determine objective treatment endpoints during arterial and venous vascular interventions: quantitative digital subtraction angiography (qDSA) and quantitative digital subtraction venography (qDSV). In this dissertation, the feasibility of using qDSA and qDSV is investigated. qDSA was validated in phantom and in vivo models as an accurate technique for performing intra-procedural blood velocity quantitation. In the oncologic application of liver embolizations, qDSA was able to quantitatively discriminate treatment endpoints, characterize intra-procedural blood velocity changes better than a commercially available technique, and correlated with histopathologic and functional imaging measures of tissue perfusion. In developing advanced techniques, evaluations of super-selective qDSA, volumetric qDSA, and motion-compensation for 3D-DSAs demonstrated strong feasibility for integration into angiographic procedure workflow. In the non-oncologic application of splenic embolization, qDSA was able to characterize intra-procedural blood velocity changes, discriminate blood velocity changes due to different size particles, and correlated with multi-modal imaging measures of reduced portal venous blood flow. In the application of venous intervention, qDSV was

accurate across a range of time-modulated injection protocols and methods, accurate in in vivo models, and was able to characterize intra-procedural blood velocity changes in an in vivo model of iliac vein stenosis.

This complete body of work successfully demonstrates the strong potential of these quantitative angiography techniques for improving patient outcomes related to image-guided vascular interventions.

Chapter 1: Introduction

Portions of this chapter were co-authored and published in a peer-reviewed journal:

Hoffman C, **Periyasamy S**, Longhurst C, Medero R, Roldan-Alzate A, Speidel MA, Laeseke PF. A technique for intra-procedural blood velocity quantitation using time-resolved 2D digital subtraction angiography. CVIR Endovasc. 2021 Jan 7;4(1):11. doi: 10.1186/s42155-020-00199-y. PMID: 33411087; PMCID: PMC7790988.

1.1 Image-Guided Vascular Interventions

Interventional radiology is a medical specialty which uses image-guidance to perform minimally-invasive procedures to treat patients. Interventional radiologists treat up to 10% of all inpatients in the United States, many of whom undergo image-guided vascular interventions (1,2). These are procedures in which the physician navigates and treats different organs and regions throughout the body using blood vessels (e.g. arteries, veins). The aim of many of these vascular interventions is to alter blood flow. In procedures such as transarterial embolization, the aim is to reduce arterial blood flow through occlusion of the vessel using different types of particles (Figure 1). This can be used to starve a tumor of its blood supply (and subsequently, oxygen and nutrients) or it can be used to control bleeding from an injured vessel. In other procedures, such as angioplasty (ballooning) or stenting, the aim is to restore blood flow by increasing patency in a stenotic (narrowed) vessel. These procedures are performed by accessing the vascular system (e.g. the femoral artery) through a small incision and needle, and guiding wires and catheters to the target location in order to deliver the therapy.

Vascular interventions are typically guided by real-time x-ray imaging (fluoroscopy) using a C-arm x-ray system. Angiography, the visualization of blood vessels

and blood flow, is achieved through injection of iodinated contrast. Currently, vascular interventions largely rely on qualitative assessments of angiographic images acquired during the procedure to diagnose pathology, determine procedural endpoints, and evaluate treatment efficacy. In embolizations for example, these assessments include the appearance of sluggish contrast flow in the artery or decreased contrast-enhancement of the tumor. In angioplasties, these assessments include the appearance of increased contrast flow past the area of stenosis and increased contrast-enhancement of the downstream organ. These assessments are subjective and can depend on factors such as observer experience and perceptual bias; both of these factors have been previously shown to be a significant source of interpretive error in radiology (3). This leads to a high degree of interobserver variability and a decrease in reproducibility, ultimately affecting procedural outcomes (4-6). For example, in peripheral arterial balloon angioplasty, there is up to a 52% reduction in success rate based solely on how success is defined (7). In hepatic transarterial embolization, an optimal treatment endpoint improves clinical outcomes, including a 9-moth survival benefit, but the correlation between subjective angiographic endpoints and MR-based tumoral perfusion is poor (8-10). An objective, quantitative angiographic technique for determining procedural endpoints would help standardize vascular interventions, and ultimately build the quantitative link between endpoints and patient outcomes needed to improve procedure safety and efficacy.

1.1.1 Figures

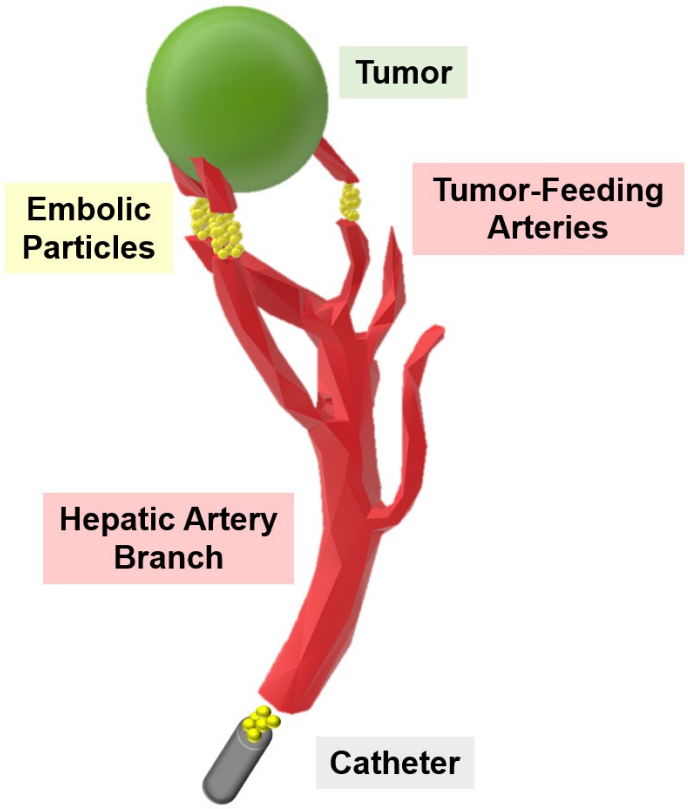

Figure 1: Illustration of how embolization reduces tumor perfusion

In transarterial embolization of a tumor, a catheter is advanced into a target artery (e.g. hepatic artery branch). Embolic agents (microspheres, liquid embolics, gelatin sponges, etc.) are injected into the tumor-feeding arteries and occlude blood flow to reduce perfusion, effectively starving the tumor of oxygen and nutrients. This can be combined with chemotherapeutics or radionuclides for combined therapeutic effects.

1.2 Digital Subtraction Angiography (DSA)

Digital subtraction angiography (DSA) is an x-ray based vascular imaging technique first developed at the University of Wisconsin – Madison in the 1970's by Dr. Charles Mistretta and Dr. Andrew Crummy (11-19). This technique has revolutionized many fields of medicine including interventional neurology, interventional cardiology, and interventional radiology. It plays a critical role in abdominal and peripheral vascular procedures such as angioplasty, stent placement, and transarterial embolization as it is used universally for vascular image-guidance.

The technique helps improve visibility of vascular structures by *subtracting* away background soft tissue and bony anatomy from the final images (Figure 1). In a typical DSA acquisition, iodinated contrast medium is injected into an artery in the fluoroscopic field of view. Frames in the image sequence are digitally subtracted from the first frames, which do not contain contrast. The first frame is traditionally called *the mask*. Subsequent frames containing contrast will be referred to as *the fill* in this work. A logarithmic subtraction is performed in order to account for the exponential attenuation of x-rays in the presence of the additional contrast. This subtraction is described in the following equations where I_{mask} is the intensity of the mask image, I_0 is the intensity of the incident

x-ray, μ_b is the linear attenuation coefficient of the background, x_b is the thickness of the background, I_{fill} is the intensity of the fill image, μ_c is the linear attenuation coefficient of the contrast agent, and x_c is the thickness of the region of contrast. This subtraction may be reversed (fill-mask), which will result in a similar image with inverse polarity.

$$I_{mask} = I_0\, e^{-\mu_b x_b} \qquad I_{fill} = I_{mask}\, e^{-\mu_c x_c}$$

$$DSA = \ln I_{mask} - \ln I_{fill}$$

$$DSA = \mu_c x_c$$

This subtraction, assuming a monoenergetic x-ray beam, no x-ray scatter, and no motion of the structures within the image, results in an image with minimal background signal and image attenuation largely concentrated in the regions where the contrast has been injected into the blood vessels.

Given that DSA is the gold-standard for guiding and assessing angiographic procedures, a robust quantitative technique utilizing DSA would be minimally intrusive to the procedural workflow and provide a quantitative complement to current assessment methods. This would result in a paradigm shift in clinical practice from the use of subjective criteria towards quantitative, tailored, and established therapeutic endpoints (Figure 2). Standardized endpoints are also a first and requisite step toward automated, closed-loop angiographic procedures to further reduce operator dependence.

1.2.1 Figures

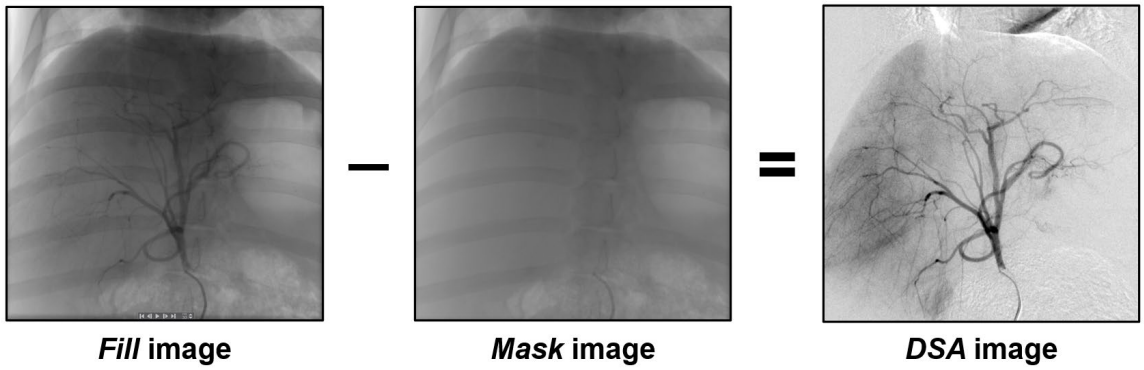

Figure 1: Example of digital subtraction angiography image processing

An example of how a digital subtraction angiography (DSA) image is generated. Contrast is injected into the common hepatic artery (left) and fills the hepatic vasculature. A frame prior to contrast injection (middle) includes all the background anatomy including the soft tissue of the liver, stomach, bowel, ribs and other bone. When the two images are subtracted, the resulting DSA image has high contrast visualization of the vasculature with minimal attenuating signal from the background anatomy. There is some subtraction artifact at the top of the image from cardiac motion and some artifact near the bottom of the image from movement of bowel gas. Additionally, there is contrast-enhancement of the right hemi-liver indicating tissue perfusion.

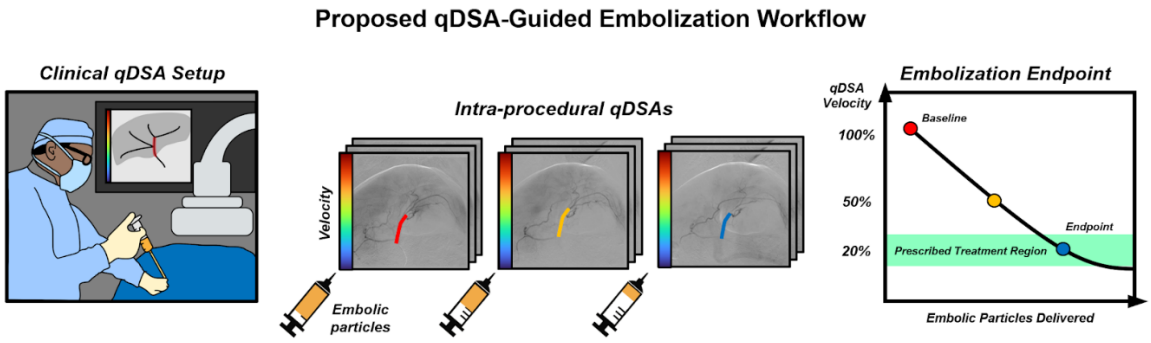

Figure 2: Proposed quantitative angiography-guided procedural workflow

A proposed-quantitative angiography guided workflow, using DSA, for performing embolization procedures. The interventionalist acquires quantitative angiographic images throughout the procedure with real-time access to blood flow data. They are able to use this information to select the optimal treatment endpoint, mitigating concern for under- or over-treatment.

1.3 Quantitative Digital Subtraction Angiography (qDSA)

1.3.1 qDSA Validation Study

Purpose

In response to the need for a method for determining objective intra-procedural treatment endpoints, we proposed a quantitative digital subtraction angiography (qDSA) technique which uses the naturally occurring, under-exploited inherent cardiac pulsatility of arterial flow in addition to spatial information within an artery to compute blood velocity. After initial development of the technique, we conducted a study to validate qDSA (20). The objective of the study was to assess the accuracy and precision of a time-resolved quantitative 2D DSA (qDSA) technique and to determine its feasibility for in vivo measurement of blood velocity.

Materials and Methods

A quantitative DSA technique was developed to calculate intra-procedural blood velocity.

The proposed technique uses the inherent cardiac pulsatility of arterial flow in addition to spatial information within an artery to compute blood velocity. Pulsatility of

arterial blood flow during a contrast injection results in an time-oscillating contrast signal in the time-attenuation curve (TAC) of a given pixel in the DSA image sequence. This oscillation of signal represents a trackable marker of blood flow. Given two pixels along a vessel separated by distance ***d***, the TACs from the two pixels will have similar time-oscillating signals, offset by some temporal shift ***t***. This temporal shift corresponds to the time a contrast bolus travels through a vessel. A shifted-least squares approach is employed to calculate the temporal shift. Distances and temporal shifts can be computed for pairs of points along the vessel centerline to improve statistical power and results in a spatially averaged blood velocity ***v***.

$$v = \frac{d}{t}$$

In vitro validation was performed by comparing velocities from the qDSA method and an ultrasonic flow probe in a bifurcation phantom. Parameters of interest included baseline flow rate, contrast injection rate, projection angle, and magnification. In vivo qDSA analysis was completed in five different branches of the abdominal aorta in two 50 kg swine and compared to 4D Flow MRI. Linear regression, Bland-Altman, Pearson's correlation coefficient and chi squared tests were used to assess the accuracy and precision of the technique.

Results

In vitro validation showed strong correlation between qDSA and flow probe velocities over a range of contrast injection and baseline flow rates (slope = 1.012, 95% CI [0.989,1.035], Pearson's r = 0.996, $p < .0001$) (Figure 1). The application of projection angle and magnification corrections decreased variance to less than 5% the average baseline velocity ($p = 0.999$ and $p = 0.956$, respectively). In vivo validation showed strong correlation with a small bias between qDSA and 4D Flow MRI velocities for all five abdominopelvic arterial vessels of interest (slope = 1.01, Pearson's r = 0.880, $p = <.01$, Bias = 0.117 cm/s) (Figures 2).

Conclusions

The proposed method allows for accurate and precise calculation of blood velocities, in near real-time, from time resolved 2D DSAs.

1.3.2 Figures

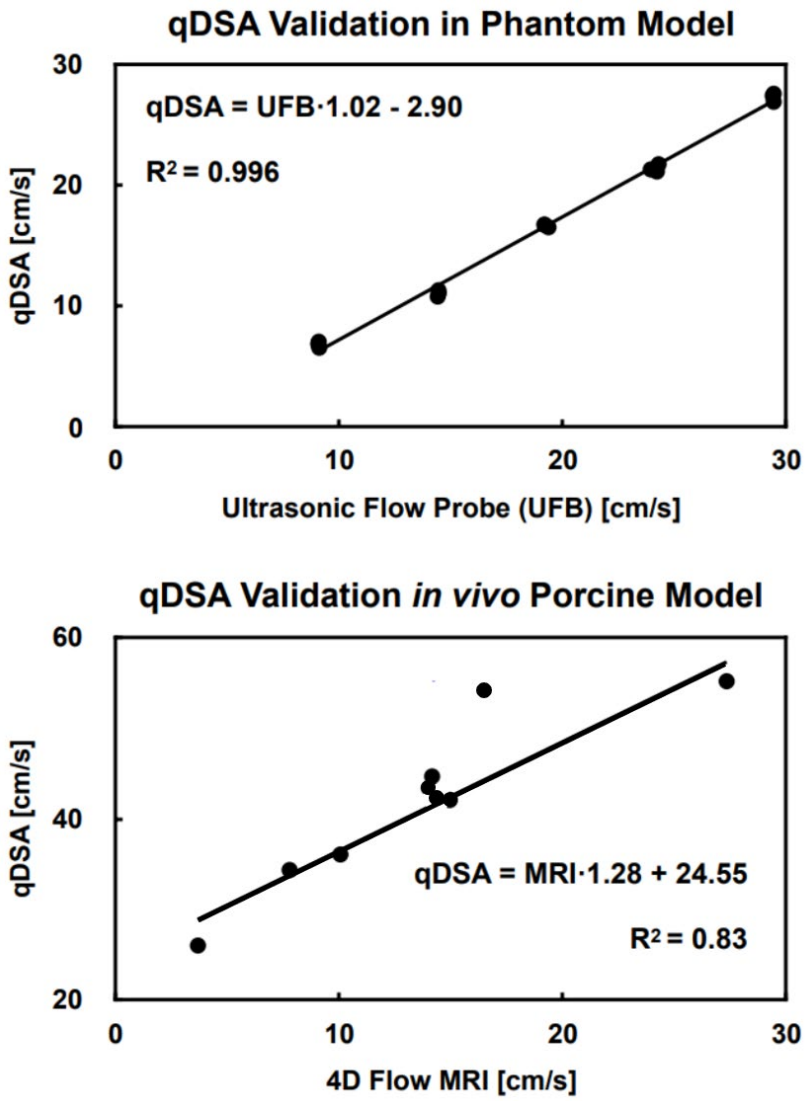

Figure 1: Phantom and in vivo validation of qDSA

The velocity calculations using qDSA are consistent and accurate across different flow rates in a phantom model (top). The velocity calculations using qDSA are strongly correlated with velocities measured using 4D Flow MR in an in vivo model (bottom).

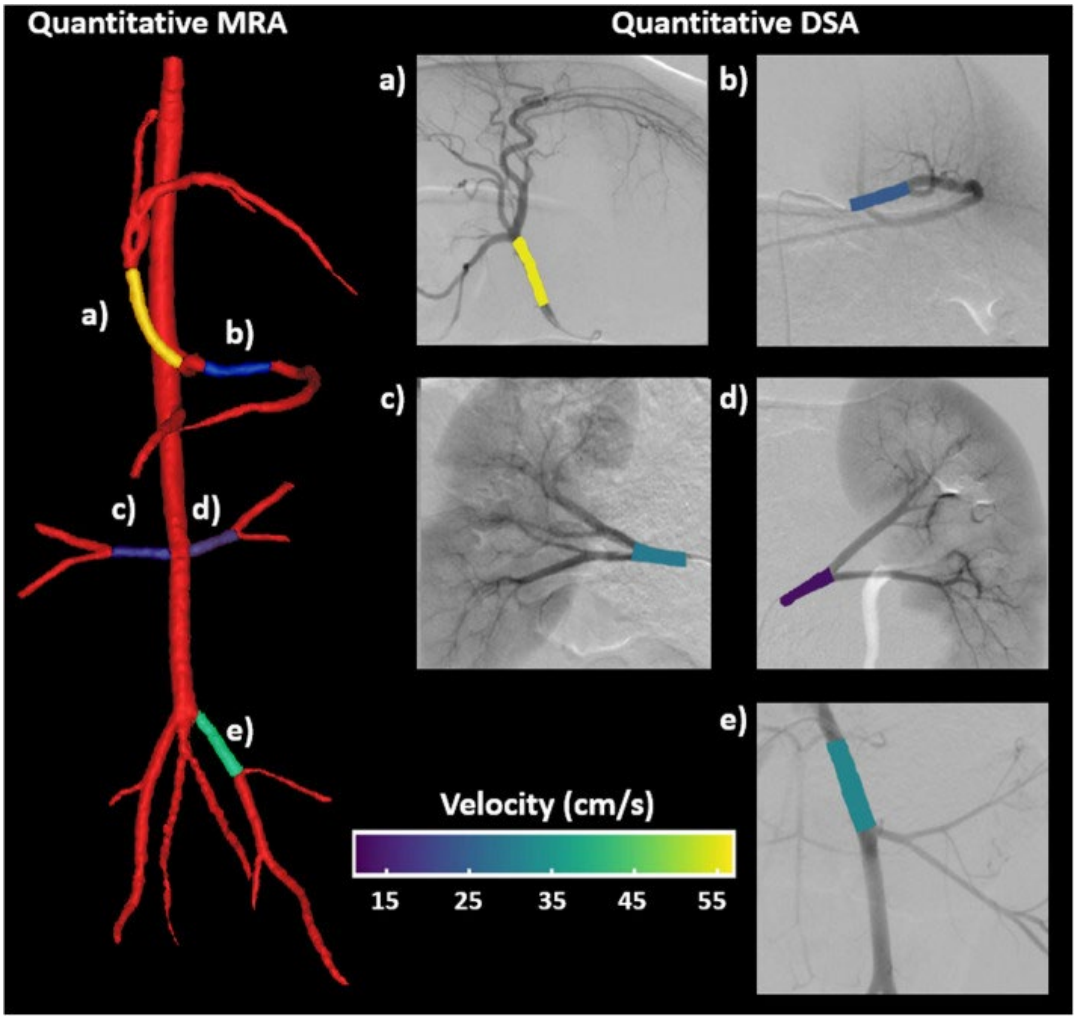

Figure 2: In vivo correlation of qDSA and 4D Flow MRI

Quantitative angiographic images for both the 4D Flow MRI and qDSA methods from Swine 1. The magnetic resonance angiogram (MRA) 3D reconstruction was manually segmented and average velocities were calculated for the associated DSA vessels. The distribution of velocities was similar between both imaging modalities. (Adapted from Hoffman, CVIR Endovasc, 2021)

1.4 Prelude

The following dissertation provides an in-depth exploration of quantitative digital subtraction angiography and venography (qDSA and qDSV) and their potential applications. **Chapter 2** investigates the use of qDSA for oncologic applications, specifically, embolization of liver tumors. **Chapter 3** investigates advanced qDSA techniques which would increase the robustness and translatability of the method, particularly in the liver. **Chapter 4** investigates the use of qDSA for non-oncologic applications, specifically, embolization of the spleen. **Chapter 5** investigates qDSV, a sister-technique which employs temporally-modulated injections for use in venous interventions. **Chapter 6** discusses ongoing investigation and future avenues of research for qDSA and qDSV.

1.5 References

1. Shah, S. S.; Tennakoon, L.; O'Beirne, E.; Staudenmayer, K. L.; Kothary, N. The Economic Footprint of Interventional Radiology in the United States: Implications for Systems Development. J Am Coll Radiol 2021, 18 (1), 53–59. https://doi.org/10.1016/j.jacr.2020.07.038.

2. Balthazar, P.; Hawkins, C. M.; Vijayasarathi, A.; Loehfelm, T. W.; Duszak, R. Current Clinical Practice Patterns of Self-Identified Interventional Radiologists. Ajr Am J Roentgenol 2018, 210 (3), 663–668. https://doi.org/10.2214/ajr.17.18592.

3. Lee, C. S.; Nagy, P. G.; Weaver, S. J.; Newman-Toker, D. E. Cognitive and System Factors Contributing to Diagnostic Errors in Radiology. Am J Roentgenol 2013, 201 (3), 611–617. https://doi.org/10.2214/ajr.12.10375.

4. Koelemay, M. J. W.; Legemate, D. A.; Reekers, J. A.; Koedam, N. A.; Balm, R.; Jacobs, M. J. H. M. Interobserver Variation in Interpretation of Arteriography and Management of Severe Lower Leg Arterial Disease. Eur J Vasc Endovasc 2001, 21 (5), 417–422. https://doi.org/10.1053/ejvs.2001.1328.

5. Paul, J. F.; Cherrak, I.; Jaulent, M. C.; Chatellier, G.; Plouin, P. F.; Degoulet, P.; Gaux, J. C. Interobserver Variability in the Interpretation of Renal Digital Subtraction Angiography. Am J Roentgenol 1999, 173 (5), 1285–1288. https://doi.org/10.2214/ajr.173.5.10541106.

6. Vries, A. R. de; Engels, P. H.; Overtoom, T. T.; Saltzherr, T. P.; Geyskes, B. G. Interobserver Variability in Assessing Renal Artery Stenosis by Digital Subtraction Angiography. Diagn Imag Clin Med 1984, 53 (6), 277–281.

7. Gardiner, G. A.; Sullivan, K. L.; Halpern, E. J.; Parker, L.; Beck, M.; Bonn, J.; Levin, D. C. Angiographic Assessment of Initial Balloon Angioplasty Results. J Vasc Interv Radiol 2004, 15 (10), 1081–1087. https://doi.org/10.1097/01.rvi.0000137398.73970.d5.

8. Jin, B.; Wang, D.; Lewandowski, R. J.; Riaz, A.; Ryu, R. K.; Sato, K. T.; Larson, A. C.; Salem, R.; Omary, R. A. Chemoembolization Endpoints: Effect on Survival among Patients with Hepatocellular Carcinoma. AJR. American journal of roentgenology 2011, 196 (4), 919–928. https://doi.org/10.2214/ajr.10.4770.

9. Lewandowski, R. J.; Wang, D.; Gehl, J.; Atassi, B.; Ryu, R. K.; Sato, K.; Nemcek, A. A.; Miller, F. H.; Mulcahy, M. F.; Kulik, L.; Larson, A. C.; Salem, R.; Omary, R. A. A Comparison of Chemoembolization Endpoints Using Angiographic versus Transcatheter Intraarterial Perfusion/MR Imaging Monitoring. Journal of vascular and interventional radiology : JVIR 2007, 18 (10), 1249–1257. https://doi.org/10.1016/j.jvir.2007.06.028

10. Jin, B.; Wang, D.; Lewandowski, R. J.; Ryu, R. K.; Sato, K. T.; Larson, A. C.; Salem, R.; Omary, R. A. Quantitative 4D Transcatheter Intraarterial Perfusion MRI for Standardizing Angiographic Chemoembolization Endpoints. AJR. American journal of roentgenology 2011, 197 (5), 1237–1243. https://doi.org/10.2214/ajr.10.5821.

11. Crummy, A. B., Mistretta, C. A., Cline, R., Terry, W., Ort, M. G., Kelcz, F., & Cameron, J. R. (1974). An inexpensive storage system for selective catheterization procedures. Radiology, 110(2), 369-372.

12. R. A. Kruger, C. A. Mistretta, J. Lancaster, T. L. Houk, M. Goodsitt, C. G. Shaw, S. J. Riederer, J. Hicks, J. Sackett, A. B. Crummy, and D. Fleming, 1978, "A Digital Video Image Processor for Real-Time X-Ray Subtraction Imaging," Optical Engineering, 17(6), pp. 652–657.

13. Mistretta, C. A., 1980, "Real-Time Digital X-Ray Subtraction Imaging," p. 22.

14. Strother, C. M., Sackett, J. F., Crummy, A. B., Lilleas, F. G., Zwiebel, W. J., Turnipseed, W. D., Javid, M., Mistretta, C. A., Kruger, R. A., Ergun, D. L., and Shaw, C. G., 1980, "Clinical Applications of Computerized Fluoroscopy: The Extracranial Carotid Arteries.," Radiology, 136(3), pp. 781–783.

15. Kruger, R. A., Mistretta, C. A., and Riederer, S. J., 1981, "Physical and Technical Considerations of Computerized Fluoroscopy Difference Imaging," IEEE Transactions on Nuclear Science, 28(1), pp. 205–212.

16. Crummy, A. B., Stieghorst, M. F., Turski, P. A., Strother, C. M., Lieberman, R. P., Sackett, J. F., Turnipseed, W. D., Detmer, D. E., and Mistretta, C. A., 1982, "Digital Subtraction Angiography: Current Status and Use of Intra-Arterial Injection.," Radiology, 145(2), pp. 303–307.

17. Crummy, A. B., Strother, C. M., and Mistretta, C. A., 2018, "The History of Digital Subtraction Angiography," Journal of Vascular and Interventional Radiology, 29(8), pp. 1138–1141.

18. Mistretta, C. A., Crummy, A. B., and Strother, C. M., 1981, "Digital Angiography: A Perspective.," Radiology, 139(2), pp. 273–276. 173

19. Crummy, A., Strother, C., Sackett, J., Ergun, D., Shaw, C., Kruger, R., Mistretta, C., Turnipseed, W., Lieberman, R., Myerowitz, P., and Ruzicka, F., 1980, "Computerized Fluoroscopy: Digital Subtraction for Intravenous Angiocardiography and Arteriography," American Journal of Roentgenology, 135(6), pp. 1131–1140.

20. Hoffman, C.; Periyasamy, S.; Longhurst, C.; Medero, R.; Roldan-Alzate, A.; Speidel, M. A.; Laeseke, P. F. A Technique for Intra-Procedural Blood Velocity Quantitation Using Time-Resolved 2D Digital Subtraction Angiography. Cvir Endovascular 2021, 4 (1), 11. https://doi.org/10.1186/s42155-020-00199-y.

Chapter 2: Quantitative Digital Subtraction Angiography (qDSA): Oncologic Application

Portions of this chapter were published in a peer-reviewed journal:

Periyasamy S, Hoffman CA, Longhurst C, Schefelker GC, Ozkan OS, Speidel MA, Laeseke PF. A Quantitative Digital Subtraction Angiography Technique for Characterizing Reduction in Hepatic Arterial Blood Flow During Transarterial Embolization. Cardiovasc Intervent Radiol. 2021 Feb;44(2):310-317. doi: 10.1007/s00270-020-02640-0. Epub 2020 Oct 6. PMID: 33025244; PMCID: PMC7855448.

and presented at the following scientific meetings:

Periyasamy S, Hoffman CA, Laeseke PF. Quantitative Angiography: A New Frontier in Hepatic Interventions. AAPM NCC Annual Meeting 2019. La Crosse, WI. April 2019. Oral

Hoffman CA, **Periyasamy S**, Wu Y, Speidel M, Laeseke PF. Quantitative 2D DSAQ: a novel method for determining treatment endpoints during transarterial embolization. RSNA 2019. Chicago, IL. November 2019. Oral

Periyasamy S, Hoffman CA, Schefelker G, Speidel M, Laeseke PF. A Quantitative 2D-Digital Subtraction Angiography Method for Characterizing Changes in Hepatic Perfusion During Transarterial Embolization. SIO 2020. New Orleans, LA. January 2020. Poster

Periyasamy S, Hoffman CA, Schefelker G, Speidel M, Laeseke PF. A Quantitative 2D-Digital Subtraction Angiography Method for Characterizing Changes in Hepatic Perfusion During Transarterial Embolization. GEST 2020. New York, NY. May 2020. Oral

Periyasamy S, Hoffman CA, Longhurst C, Schefelker G, Ozkan O, Speidel M, Laeseke PF. A comparison of velocity and color-coded DSA techniques for intra-procedural characterization of blood flow reduction during transarterial embolization of the liver. CIRSE 2020. Virtual. September 2020. Oral

Hoffman CA, **Periyasamy S**, Longhurst C, Speidel M, Laeseke PF. Intra-Procedural Blood Velocity Quantitation Using Time-Resolved 2D Digital Subtraction Angiography. GEST 2020. New York, NY. May 2020. Oral

Periyasamy S, Pirasteh A, Whitehead J, Hoffman CA, Speidel M, Laeseke PF. Characterization of Functional Hypoxia Changes Using [18F] FMISO PET/MR Following Quantitative DSA-Guided Transarterial Embolization of the Liver. SIO 2022. San Francisco, CA. March 2022.

2.1 Introduction

Following successful development and validation of quantitative digital subtraction angiography (qDSA) for intra-procedural blood velocity quantitation, we sought to determine how qDSA could be used for application in vascular intervention of cancer, in particular, liver embolizations. This chapter explores the feasibility of performing intra-procedural hepatic qDSA, how it compares to currently available techniques, and how it correlates with tissue-level changes.

2.2 Motivation

Primary liver cancer, or hepatocellular carcinoma (HCC), is the sixth most common malignancy worldwide and the fourth leading cause of cancer death, with over 841,000 new cases and 781,000 deaths annually (1,2). The incidence of HCC in developed countries, including the US, has risen dramatically in the last two decades due to the increased prevalence of hepatitis B and C, alcoholic liver disease, and non-alcoholic fatty liver disease. Many of these conditions lead to chronic liver disease and the development of cirrhosis, a known nidus for HCC pathogenesis. In addition to primary tumors, the liver is also a common site of metastatic disease for a number of other primary cancers. Surgical resection is considered the gold-standard for patients with early stage HCC or limited metastatic disease; liver transplantation represents another curative option as it cures the tumor and can treat any underlying cirrhosis (3). Unfortunately, as few as 30% of patients are considered operable because of tumor size, number, and medical co-morbidities (4). In the US, as few as 5% are suitable candidates due to concomitant cirrhosis (5). For patients who have unresectable intermediate stage disease (Stage B, Barcelona Clinic Liver Cancer Staging), intra-arterial therapies, such as transarterial chemoembolization (TACE), are the mainstay of treatment (6). TACE involves the

targeted delivery of embolic material to arteries feeding a tumor using drug-eluting beads or a chemotherapeutic-embolic particle emulsion. The embolization induces tumor necrosis by interrupting the tumor's blood supply whilst simultaneously increasing the dwell time and cytotoxicity of the chemotherapeutic agents. TACE can significantly prolong survival in HCC patients, with a 2-year survival rate of 63% compared to 27% in patients under conservative treatment (7,8). Additionally, TACE can serve as a bridge to transplantation by delaying disease progression to a degree that patients will maintain or satisfy Milan criteria, the inclusion criteria by which most transplant centers select liver transplant candidates (9-11).

Outcomes after TACE are influenced by variations in how the procedure is performed, including embolic agents and drugs delivered, drug dose, and lipiodol use. Regardless of how it is performed, the efficacy of all TACE procedures depends on achieving the appropriate degree of blood flow stasis in the target vasculature (12). If too little stasis is achieved, there will be insufficient tumor necrosis. If complete stasis is achieved (overembolization), non-target parenchyma will suffer and the procedure can increase liver toxicity, accelerate liver failure, and lead to increased mortality (13). Complete stasis can also upregulate angiogenic factors within the tumor and lead to increased tumor growth (14-17). Sub-stasis, the optimal endpoint, facilitates tumor

necrosis with minimal injury to surrounding liver, but currently cannot be determined via objective reproducible means.

Currently, TACE procedures are guided by digital subtraction angiography (DSA), an imaging technique that uses contrast injection and image subtraction to highlight vasculature whilst minimizing distracting anatomical background (18,19). During the course of a procedure, an interventional radiologist will continue injecting embolic particles into the tumor-feeding arteries until it appears on DSA that the artery is sufficiently blocked (e.g. the appearance of sluggish antegrade flow contrast flow within the vessel) and the blush (tumor parenchymal contrast enhancement from perfusion) in the region of the tumor is eliminated. The difference between sub-stasis and complete stasis requires visual determination of minimal vs no antegrade flow and parenchymal enhancement respectively. This visual assessment, an angiographic endpoint, is entirely subjective and is dependent on factors like operator experience, perception, and bias. Perceptual variation has been shown to be an important source of interpretive error in radiology (20). As such, subjective angiographic endpoints have been shown to have minimal correlation with actual tumor perfusion, which can lead to a wide variation in procedural outcomes (21). There is no objective and standardized intra-procedural method for determining the optimal embolization endpoint.

Attempts have been made to develop an objective embolization endpoint. One, quantitative 4D transcatheter intra-arterial perfusion MRI, showed promise as an intra-procedural metric (22-24); this technique, however, lacks feasibility as it requires a complex hybrid angiography/MR suite only available at select institutions, and also requires significant time and cost. There are also investigations into using pre- and post-procedure perfusion imaging in order to quantitatively assess the effectiveness of an embolization, but these techniques only provide peri-procedural assessment and do not allow for intra-procedural guidance (25-27). Recently, color-coded DSA (ccDSA) analysis has demonstrated validity as a tool for quantifying embolization endpoints (28). The technique, however, is susceptible to variability from factors such as vessel size, vessel/tissue overlap, turbulent flow, contrast injection rate, catheter position, and motion artifact (29-31).

We propose a quantitative angiography method (qDSA) that extracts blood flow information from time-resolved 2D DSA and correlates with tissue perfusion. Our method uses the inherent cardiac pulsatility in arteries to measure the distance travelled and transit time of transient contrast boluses developed during contrast injection. Using this time and distance information, the blood flow velocity (BFV) of blood in a segment can be calculated. This velocity information can be combined with cross-sectional data

from three-dimensional scans (e.g. cone-beam CT, 3D-DSA) to calculate blood flow. While blood flow is the factor of primary interest, we will predominantly evaluate velocity given that the cross-sectional area of the target arteries does not significantly change during an embolization. During the course of an embolization procedure, DSA acquisitions can be serially acquired and the real-time changes in blood flow of an embolized vessel can be measured using qDSA. Ultimately, an optimal sub-stasis endpoint can be identified which corresponds with a particular reduction in blood flow calculated using the qDSA method. The endpoint would be reproducible across operator, equipment, and institution. This method would be minimally intrusive to the current embolization workflow, as the interventional radiologist is already acquiring DSAs during the procedure and it would only require modification to the acquisition parameters. This method also minimizes risk to the patient, as there is no introduction of new devices and no dramatic changes to the procedure. We believe our qDSA method will improve the efficacy of TACE by allowing for the achievement of standardized, reproducible, and objective sub-stasis endpoints. It will also improve the safety of TACE by helping radiologists avoid complete-stasis endpoints that can otherwise increase liver toxicity and mortality.

We hypothesize that (1) qDSA is able to characterize real-time changes in blood flow during embolization and discriminate angiographic embolization endpoints, (II) qDSA is as effective or superior to a commercially available quantitative technique for characterizing blood flow changes during embolization, and (III) the changes in blood flow characterized by qDSA correlate with tissue-level perfusion changes. The objective of this study was to demonstrate the feasibility of using qDSA to characterize intra-procedural changes in hepatic arterial blood flow in response to transarterial embolization (TAE) in an in vivo porcine model.

2.3 Characterizing Reductions in Hepatic Arterial Blood Flow During Transarterial Embolization Using qDSA

2.3.1 Materials and Methods

All procedures were approved by the institutional research animal care and use committee and were compliant with regulatory guidelines. Transarterial embolization was performed in the livers of eight swine (mean weight, 49.4 ± 2.0 kg). Subjects were sedated with an intramuscular administration of 7 mg/kg of tiletamine hydrochloride-zolazepam hydrochloride (Xyla-Ject; Phoenix Pharmaceutical, St. Joseph, Missouri), endotracheally intubated, and then underwent anesthesia induction and maintenance with 2% inhaled isoflurane (Halocarbon Laboratories, River Edge, New Jersey).

Transarterial Embolization

All procedures were performed in an angiography suite (Artis zee; Siemens Healthineers, Forcheim, Germany). Femoral arterial access was obtained and the common hepatic artery selected with a 5 Fr angled glide catheter. A 3D-DSA was acquired to delineate hepatic arterial anatomy and determine an optimal projection angle. Prior to embolization, a 30 frames per second (fps) 2D-DSA of the common hepatic artery was acquired using an injection of iohexol 300 mg/mL (Omnipaque 300; GE

Healthcare, Waukesha, Wisconsin) (see Table 1 for imaging parameters). All DSA images were acquired with breath holds.

In each animal, up to two (of four) hepatic lobes were selected for embolization (see Table 1 for embolization and DSA acquisition parameters). Bland embolizations (n=10) were performed given that the primary objective of the study was to characterize reductions in blood flow velocity. A 0.014" guidewire was used to select a second-order hepatic artery branch supplying the target lobe, after which a 2.8 Fr microcatheter was advanced into the vessel. Once the microcatheter was correctly positioned, an embolization was performed using 100-300 um microspheres (Embosphere Microsphere; Merit Medical Systems, South Jordan, Utah) diluted in 10 mL of ioxhexol 300 mg/mL. Embolizations were performed to partial- or sub-stasis based on a version of the SACE scale modified for normal liver tissue (Table 2) [7]. In a subset of embolizations (n=7), additional intraprocedural DSA images were acquired after delivery of embolic particle aliquots (0.5-3 mL) in order to generate BFV reduction-embolization curves to better characterize changes in velocity throughout a liver embolization. After each aliquot, the microcatheter was withdrawn, a 2D-DSA (with same imaging parameters as the baseline) was acquired via the stationary base catheter positioned in the common hepatic artery, the target vessel was reselected with the microcatheter and the embolization resumed. In

these embolizations, there was a minimum of two minutes between microcatheter withdrawal and subsequent imaging in order to minimize any effects of transient arterial spasm.

qDSA Method

The qDSA method uses inherent oscillations in the image contrast caused by arterial flow pulsatility as a trackable marker of BFV in the artery. The oscillatory image signal is measured in the time-attenuation curves (TAC) of pixels along the centerline of a vessel. When two TACs from two pixels along the centerline of the vessel (separated by a distance) are superimposed, the temporal shift between the two functions represents the time of contrast transit along the vessel. An in vivo example of the TAC shift in a porcine model is illustrated in Figure 1. Distances and temporal shifts (using a shifted-least squares approach (32)) can be found for all pairs of points along the centerline of a vessel in order to calculate a spatially-averaged BFV in the vessel of interest. An algorithm employing the qDSA method was implemented in MATLAB (MATLAB R2018b version 9.5, MathWorks, Natick, Massachusetts) using a custom-built program.

ccDSA Method

A commercially available ccDSA method (syngo iFlow, Siemens Healthineers) was used to calculate time-to-peak (TTP) in the embolized vessel. A region-of-interest

(ROI) was placed in the proximal segment of the vessel with diameter equal to the width of the vessel in order to estimate a TTP (Figure 1c). The segment of vessel analyzed was the same as that used for the qDSA analysis.

Image Analysis

A post-hoc analysis of all DSA images was performed using both the qDSA and ccDSA methods. A decrease in qDSA calculated BFV and an increase in ccDSA calculated TTP was the expected result in response to a blood flow reduction due to embolization. qDSA calculations were performed on a laptop computer with 16 GB of RAM. ccDSA calculations were performed on the angiography suite workstation (Artis zee; Siemens Healthineers, Forcheim, Germany).

Statistical Analysis

To compare the reduction in hepatic arterial BFV between hepatic lobes that were embolized to sub-stasis versus those that were embolized to partial-stasis, a linear mixed model was fit to the data using the 'lme4' package, where the individual animal was modeled as a random intercept [15]. To assess the correlation between embolization and reduction in BFV (relative to baseline [%]), a similar linear mixed model was estimated. All mixed model p-values were calculated using Satterthwaite's approximation.

To assess the correlation between qDSA and embolization, seven linear models were fit to the data for each individual animal, where qDSA was modeled as the response variable. From each model, the Pearson's correlation coefficient (r) the mean-squared error (MSE), and coefficient of determination (R2) were calculated. Similar models and metrics were calculated to assess the association between ccDSA and embolization. To test if the MSE for the qDSA models was less than the MSE for the ccDSA models, a one-sided, paired, Wilcoxon-rank sum test was used. The same test was used to test if the R2 for the qDSA models was greater than the ccDSA models. To determine if the absolute correlation between qDSA and embolization was stronger than that of ccDSA and embolization, the paired, overlapping, correlation coefficients were tested at the animal level [16].

For this analysis, a p-value less than 0.05 was considered statistically significant. Given the exploratory nature of this study, no corrections for multiple testing were applied to resulting p-values. All statistical analyses were done using R (V 3.6.1) [17].

2.3.2 Results

Embolization Endpoints

Hepatic lobes that were embolized to sub-stasis angiographic endpoints had statistically significant greater reductions ($p < 0.01$) in hepatic arterial blood flow velocity when compared with those embolized to partial-stasis endpoints as calculated using qDSA (Figure 2). There was no statistically significant difference between sub-stasis and partial-stasis angiographic endpoints with regards to time-to-peaks calculated using ccDSA ($p = 0.56$). Lobes embolized to partial-stasis angiographic endpoints had a mean calculated BFV of 45.2%±5.1% and a mean TTP of 120.3%±9.5% (n=4) expressed as a percentage of the baseline value. Lobes that were embolized to sub-stasis angiographic endpoints had a mean calculated BFV of 22.4%%±12.2% and a mean TTP of 113.2%±19.4% (n = 6) as a percentage of the baseline.

Blood Flow Velocity Reduction During Embolization

In embolizations during which images were acquired throughout the procedure, there was a negative linear relationship between qDSA calculated BFVs and the volume of embolic particles delivered in all 7 hepatic lobes. There was a positive linear relationship between ccDSA calculated TTP and the volume of embolic particles delivered in 5 out of 7 lobes. qDSA calculated BFVs were compared to ccDSA calculated TTPs with

correlation, MSE, and R2. The values are reported for qDSA and ccDSA in each animal in Table 3. The average correlation was -0.86 for qDSA and 0.36 for ccDSA. The average MSE for qDSA was 0.22, which was significantly smaller ($p < 0.01$) than the MSE for ccDSA, 0.62. The average R2 for qDSA (0.75) was significantly larger ($p < 0.01$) than the R2 for ccDSA (0.30). A representative embolization from Animal 1 is presented in Figure 3. qDSA calculated blood velocities and ccDSA calculated TTPs for all animals are presented in Figure 5.

2.3.3 Tables

Table 1: Embolization and imaging parameters for all in vivo studies

Animal	Artery Embolized	Angiographic Endpoint	Projection Angle	Contrast Injection Rate	Contrast Volume
1	LMHA*	Sub-Stasis	0 degrees	2.5 mL/s	15 mL
2	LMHA*	Sub-Stasis	0 degrees	2.5 mL/s	15 mL
3	LMHA*	Partial-Stasis	30 degrees LAO	2.5 mL/s	15 mL
3	RLHA	Sub-Stasis	30 degrees LAO	2.5 mL/s	15 mL
4	LMHA*	Partial-Stasis	50 degrees LAO	3.0 mL/s	18 mL
5	LMHA*	Sub-Stasis	0 degrees	2.5 mL/s	15 mL
5	RMHA	Partial-Stasis	0 degrees	2.5 mL/s	15 mL
6	LMHA*	Sub-Stasis	0 degrees	2.0 mL/s	16 mL
7	LMHA*	Partial-Stasis	0 degrees	2.0 mL/s	16 mL
8	LMHA	Sub-Stasis	0 degrees	2.5 mL/s	15 mL

LHMA: left medial hepatic artery, RLHA: right lateral hepatic artery, RMHA: right medial hepatic artery, LAO: left anterior oblique, DSA: digital subtraction angiography

*additional DSA images acquired throughout embolization to generate BFV reduction-embolization curves

Table 2: Modified subjective angiographic embolization endpoint scale

Grade	Stasis Endpoint	Antegrade Flow	Parenchymal Enhancement
1	No stasis	Normal	Normal
2	Partial-stasis	Reduced	Reduced
3	Sub-stasis	Minimal	Minimal
4	Complete stasis	None	None

Table 3: Linear model analysis of degree of embolization and qDSA or ccDSA

Animal	Correlation		Mean Squared Error		R^2	
	qDSA	ccDSA	qDSA	ccDSA	qDSA	ccDSA
1	-0.96	0.70	0.08	0.46	0.92	0.49
2	-0.60	0.42	0.61	0.78	0.36	0.18
3	-0.87	-0.14	0.20	0.82	0.76	0.02
4	-0.85	0.59	0.23	0.55	0.72	0.34
5	-0.80	0.50	0.33	0.62	0.64	0.25
6	-0.98	-0.38	0.03	0.76	0.97	0.14
7	-0.94	0.82	0.10	0.28	0.89	0.68

qDSA: quantitative digital subtraction angiography, ccDSA: color-coded digital subtraction angiography, R2: coefficient of determination

2.3.4 Figures

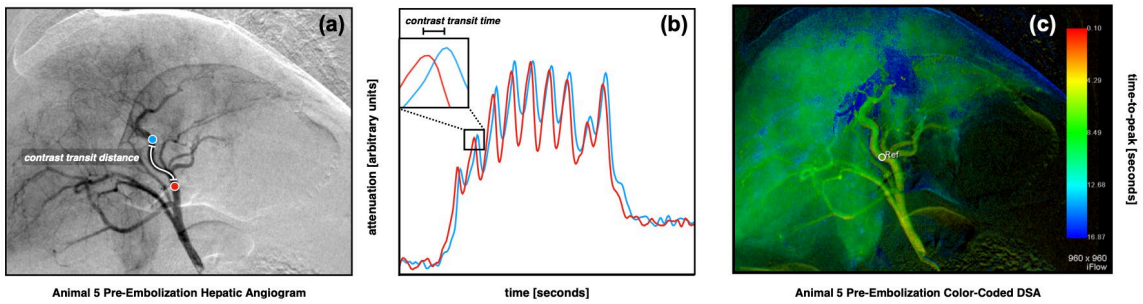

Figure 1: Example qDSA and ccDSA in an in vivo porcine liver model

Quantitative digital subtraction angiography (qDSA) in an in vivo porcine model. A pre-embolization common hepatic arteriogram (a) was acquired. Proximal (red) and distal (blue) points along the left medial hepatic artery were analyzed. The time-attenuation curves (TAC) from the two points are superimposed (b), illustrating a visible temporal shift. The temporal shift represents the transit time of transient contrast boluses developed from contrast pulsatility. A manual spatial and temporal segmentation was completed to ensure adequate centerlines and strong contrast signal pulsatility. A shifted-least squares approach was used to iteratively calculate temporal shifts in the TACs between all pairs of points along the centerline in order to calculate the spatially-averaged blood velocity for the segmented vessel. A color-coded DSA (ccDSA) from the same sequence (c) shows the baseline time-to-peaks (TTP) in the hepatic vasculature. A region-

of-interest in the at the site of embolization (white circle) with diameter equal to the vessel diameter is selected for assessment.

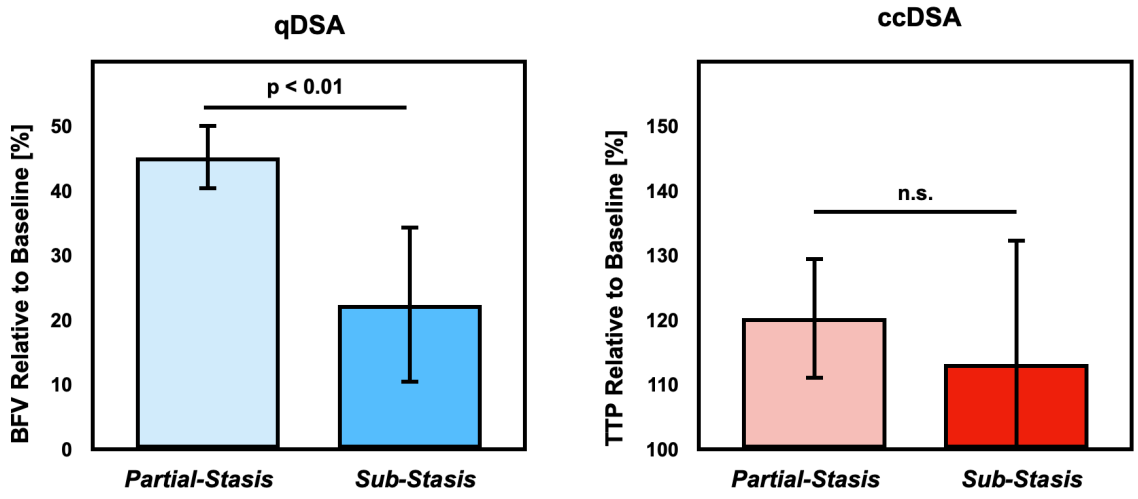

Figure 2: Transarterial embolization angiographic endpoints quantified using qDSA and ccDSA

Post-embolization qDSA calculated blood flow velocities (BFV) and ccDSA calculated time-to-peaks (TTP), relative to baseline, from embolizations performed to partial-stasis and sub-stasis endpoints. There was a statistically significant greater reduction in mean blood velocity relative to baseline for sub-stasis embolizations compared to partial stasis embolizations. There was no significant difference between stasis endpoints when using ccDSA.

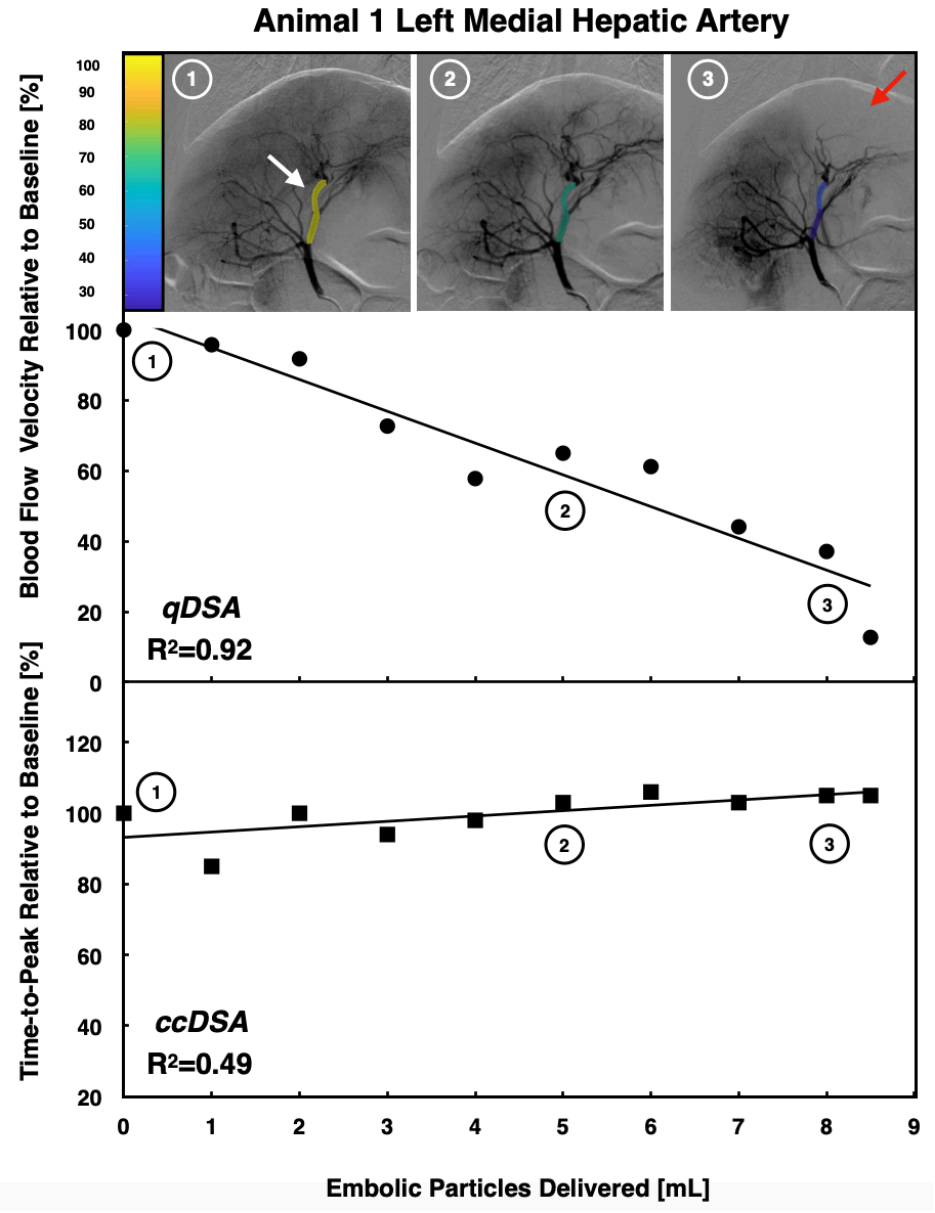

Figure 3: Representative in vivo velocity reduction-embolization curve

A representative velocity reduction-embolization curve from an incremental embolization performed in the left medial hepatic artery (white arrow) in a porcine model. There is a strong negative correlation between the qDSA calculated blood

velocities and the volume of embolic particles delivered. There is a weak positive correlation between ccDSA calculated TTP and the volume of embolic particles delivered. The reduction in qDSA calculated blood velocities from baseline (1, yellow highlight) to partial stasis (2, green highlight) to sub-stasis (3, blue highlight) agrees with a qualitative angiographic assessment of increasing perfusion defect in the embolized region (red arrow). The relative change from baseline is larger in qDSA (9.0% reduction in blood velocity per mL of embolic particles delivered) than in ccDSA (1.5% increase in TTP per mL of embolic particles delivered).

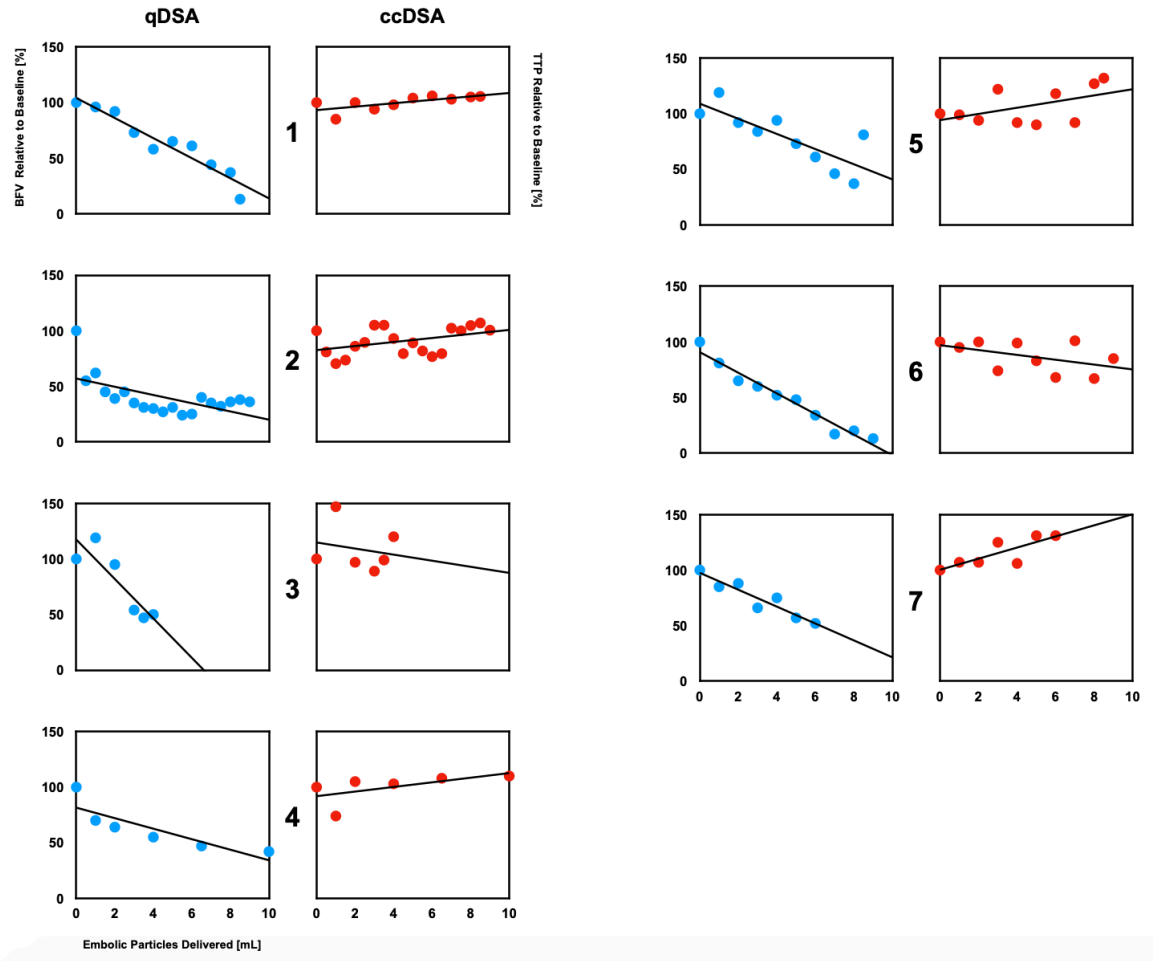

Figure 4: Complete in vivo velocity reduction-embolization curve data

Intraprocedural qDSA (blue) and ccDSA (red) measurements from all embolizations performed incrementally (n=7). qDSA measurements are expressed as blood velocity (BV) as a percentage relative to baseline. ccDSA measurements are expressed as time-to-peak (TTP) as a percentage relative to baseline.

2.4 Characterization of Tissue-Perfusion Changes in Response to Transarterial Embolization of the Liver Using qDSA

2.4.1 Materials and Methods

All procedures were approved by the institutional research animal care and use committee and were compliant with regulatory guidelines. Transarterial embolization was performed in the livers of five swine (mean weight, 47.8 ± 10 kg). Subjects were sedated with an intramuscular administration of 7 mg/kg of tiletamine hydrochloride-zolazepam hydrochloride (Xyla-Ject; Phoenix Pharmaceutical, St. Joseph, Missouri), endotracheally intubated, and then underwent anesthesia induction and maintenance with 2% inhaled isoflurane (Halocarbon Laboratories, River Edge, New Jersey).

Transarterial Embolization

All procedures were performed in an angiography suite (Artis zee; Siemens Healthineers, Forcheim, Germany). Femoral arterial access was obtained and the common hepatic artery selected with a 4 Fr angled glide catheter. A 3D-DSA was acquired to delineate hepatic arterial anatomy and determine an optimal projection angle. Prior to embolization, a 30 frames per second (fps) 2D-DSA of the common hepatic

artery was acquired using an injection of iohexol 300 mg/mL (Omnipaque 300; GE Healthcare, Waukesha, Wisconsin). All DSA images were acquired with breath holds.

Transarterial Embolization Pathology Analysis

In each animal (n=3), up to two (of four) hepatic lobes were selected for embolization. Bland embolizations were performed given that the primary objective of the study was to characterize reductions in blood flow velocity. A 0.014" guidewire was used to select a second-order hepatic artery branch supplying the target lobe, after which a 2.8 Fr microcatheter was advanced into the vessel. Once the microcatheter was correctly positioned, an embolization was performed using 100-300 um microspheres (Embosphere Microsphere; Merit Medical Systems, South Jordan, Utah) diluted in 10 mL of ioxhexol 300 mg/mL. Embolizations were performed to partial- or sub-stasis based on a version of the SACE scale modified for normal liver tissue

Swine were euthanized after a 3-hour standby period to allow for acute ischemic changes to occur. Following euthanasia, the liver was immediately procured and sampled liver lobes were placed in 10% neutral buffered formalin and submitted for histopathology. Tissues were serially sectioned at approximately 1–1.5 cm intervals prior to complete fixation and examined grossly for changes such as congestion and hemorrhage. One to two affected regions (if present) were sampled from each submitted

tissue. Samples were placed in standard histology cassettes in 10% neutral buffered formalin until fully fixed, then underwent routine tissue processing and paraffin embedding. Histologic sections were made at a thickness of 5 um and subsequently stained with hematoxylin and eosin. Slides were examined for changes such as congestion, hemorrhage, and necrosis as well as the presence of intravascular embolic beads. Embolic bead density was also calculated.

Transarterial Embolization PET/MR Analysis

In each animal (n=2), the left hepatic lobes were embolized. Bland embolizations were performed given that the primary objective of the study was to characterize reductions in blood flow velocity. A 0.014" guidewire was used to select the left hepatic artery, after which a 2.8 Fr microcatheter was advanced into the vessel. Once the microcatheter was correctly positioned, an embolization was performed using 100-300 um microspheres (Embosphere Microsphere; Merit Medical Systems, South Jordan, Utah) diluted in 10 mL of ioxhexol 300 mg/mL Intra-procedural qDSAs were performed to calculate the percent reduction in blood velocity in the left hepatic artery. One animal was embolized to a quantitative partial stasis endpoint (~40-50%). The other animal was embolized to a quantitative sub-stasis endpoint (~70-80%). Following embolization, 10 Mbq/kg of 18F-FMISO was administered and PET/contrast-enhanced MR images were

acquired. PET/MR images were analyzed retrospectively to determine the peak SUVs in hypoxic regions of the treated liver as well as in regions of non-treated liver(right lateral lobe). Images were also analyzed to determine the percent volume of hypoxic tissue relative to the total liver.

2.4.2 Results

Pathology analysis

Embolized lobes submitted for pathologic assessment (n = 4) were grossly mottled with purple-black discolorations in a multifocal coalescing pattern (Figure 1). Discolored patches were more frequently peripheral to major vessels of individual hepatic lobules. Lobes that were embolized to sub-stasis endpoints had greater extent of patchy discolorations than those lobes embolized to partial stasis.

On histopathologic evaluation, sections taken from embolized lobes contained multifocal intra-arteriolar globular material consistent with embolic particles (Figures 2a & 2b). The particles occluded anywhere from 10% to 90% of the vascular lumen. There was a moderate, positive correlation ($p < 0.01$) between the number of embolic particles in a section of tissue and the degree of embolization as quantified by the reduction in calculated BFV using the qDSA method (Figure 3). Sections taken from lobes that were not embolized (n=3) did not contain visible particles.

All embolized lobes showed evidence of acute ischemic changes (Figures 2c & 2d). These changes included moderate-to-severe hepatocyte dissociation with moderate-to-severe multifocal intralobular, interlobular, septal, periportal, central, and capsular hemorrhage. Additionally, there was moderate-to-severe septal and periportal

neutrophilic inflammation. Hepatocyte degeneration and necrosis were low-to-moderate, but more significant in central regions of the liver compared to those at the periphery. Sections taken from lobes that were not embolized showed minimal hepatocyte loss and low numbers of neutrophilic and lymphocytic infiltration. There was minimal evidence to suggest ischemic changes in non-embolized lobes.

F18-MISO PET/MR Analysis

Post-embolization DSA images showed significant decrease in parenchymal enhancement and antegrade arterial flow in the left hemi-liver. On qDSA, left hepatic arterial blood velocity decreased by 45% and 77% when treated to partial and sub-stasis, respectively.

On PET/MR, there was decreased arterial phase enhancement of the left hemi-liver and the distribution of FMISO avid regions was heterogeneous, particularly in the central liver and left medial lobe. Regions of high hypoxic signal surrounded regions of low signal (indicating central necrosis). In the animal treated to partial-stasis, peak SUV was 5.03 in the region of strong hypoxia and 1.69 in the untreated liver. The volume of hypoxic tissue (90 cc) was 8% of the total liver (1112 cc). In the animal treated to sub-stasis, peak SUV was 5.22 in the region of strong hypoxia and 1.60 in the untreated liver. The volume of hypoxic tissue (302 cc) was 23% of the total liver (1325 cc).

2.4.3 Figures

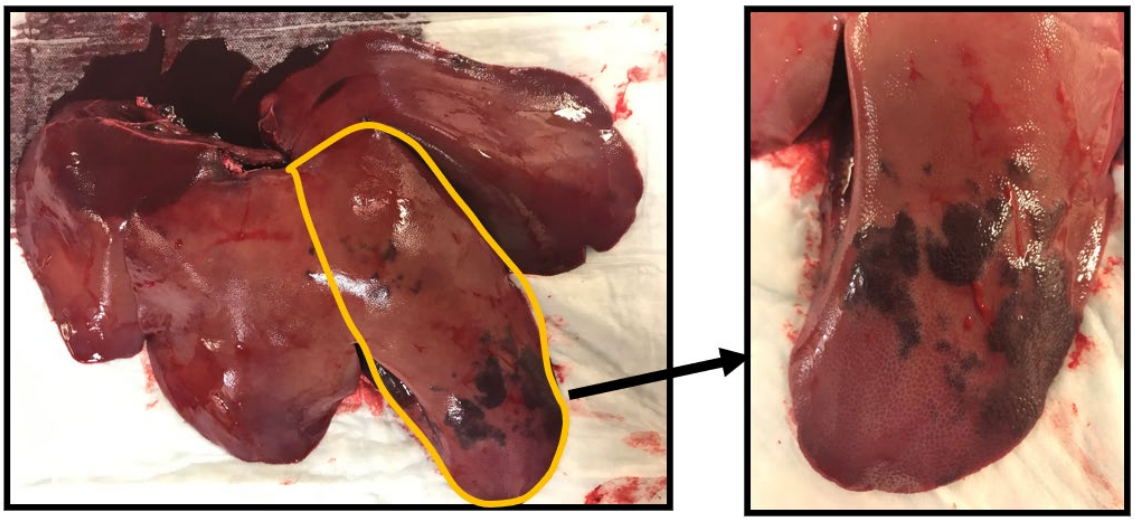

Figure 1: Representative gross pathology of embolized liver lobe

A representative example of the gross acute appearance of the liver following transarterial embolization. Following embolization of the left medial hepatic artery, the left medial lobe (yellow) exhibits patchy discoloration indicative of infarctions. The other three lobes (right lateral, right medial, and left lateral lobe) appear largely normal.

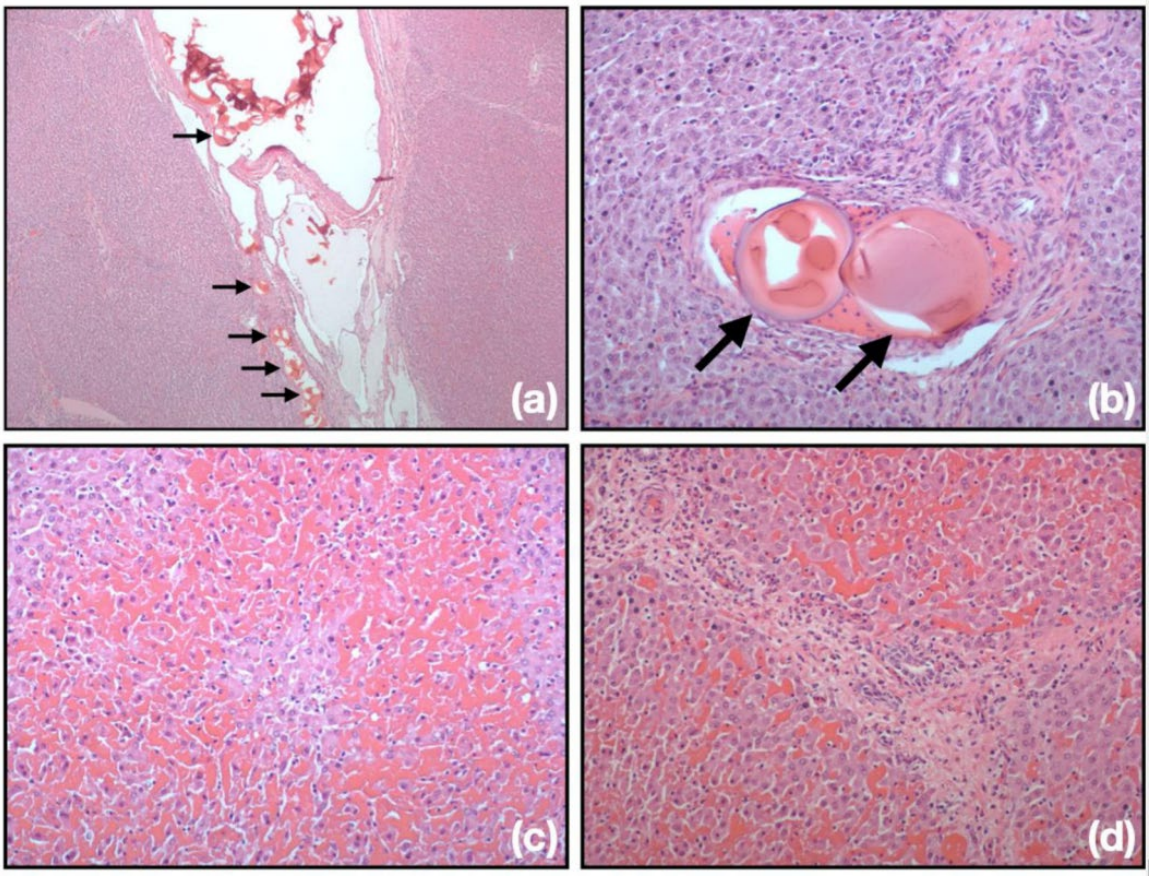

Figure 2: Representative histopathology of embolized liver lobe

Representative histology slides from embolizations performed in the livers of a porcine model. Globular material consistent with embolic particles (black arrows) can be seen occluding the lumen of blood vessels to varying degrees at low (a) and high (b) magnifications. Typical acute ischemic changes observed in the embolized lobes included moderate-to-severe hepatocyte dissociation with moderate-to-severe multifocal intralobular,

interlobular, septal, periportal, central, and capsular hemorrhage (c). Sampled tissue from embolized lobes also included moderate-to-severe septal and periportal neutrophilic inflammation (d).

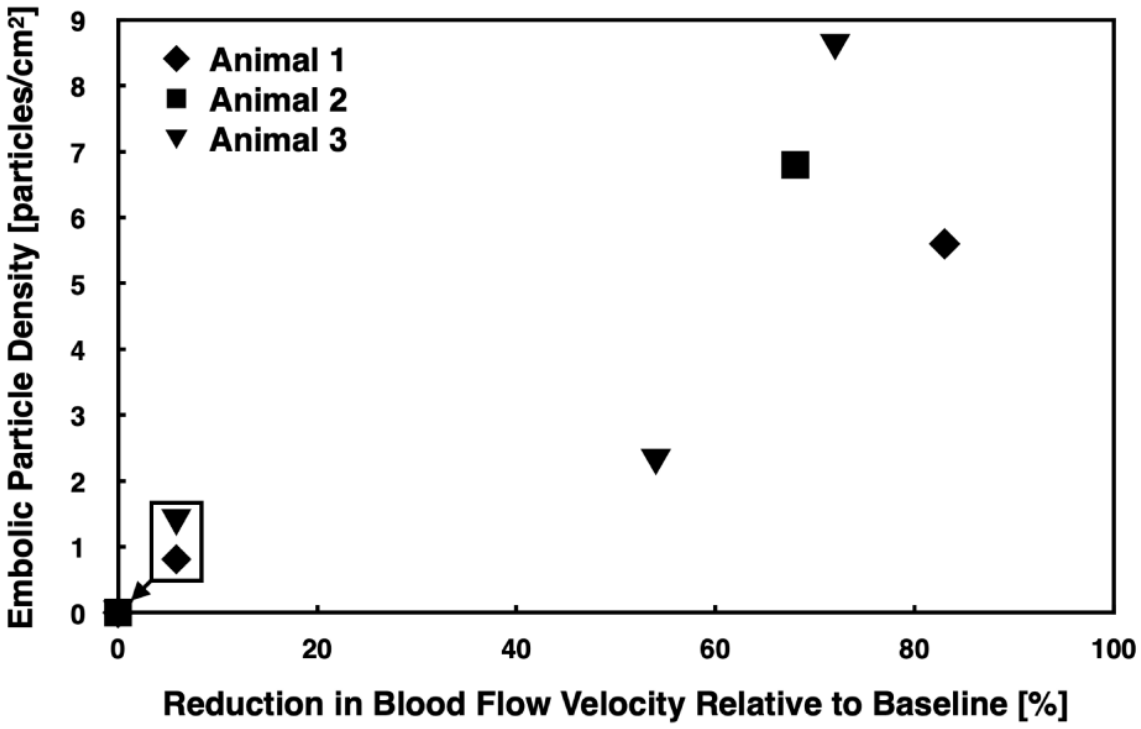

Figure 3: qDSA blood flow velocity reduction correlation with tissue embolic particle density

An embolic density-blood velocity plot illustrating the number of embolic particles observed in sampled tissue relative to the qDSA calculated reduction in blood velocity. The data provided evidence of a moderate, positive correlation between the density of embolic particles in embolized tissue and the degree of blood velocity reduction achieved via embolization ($p<0.01$).

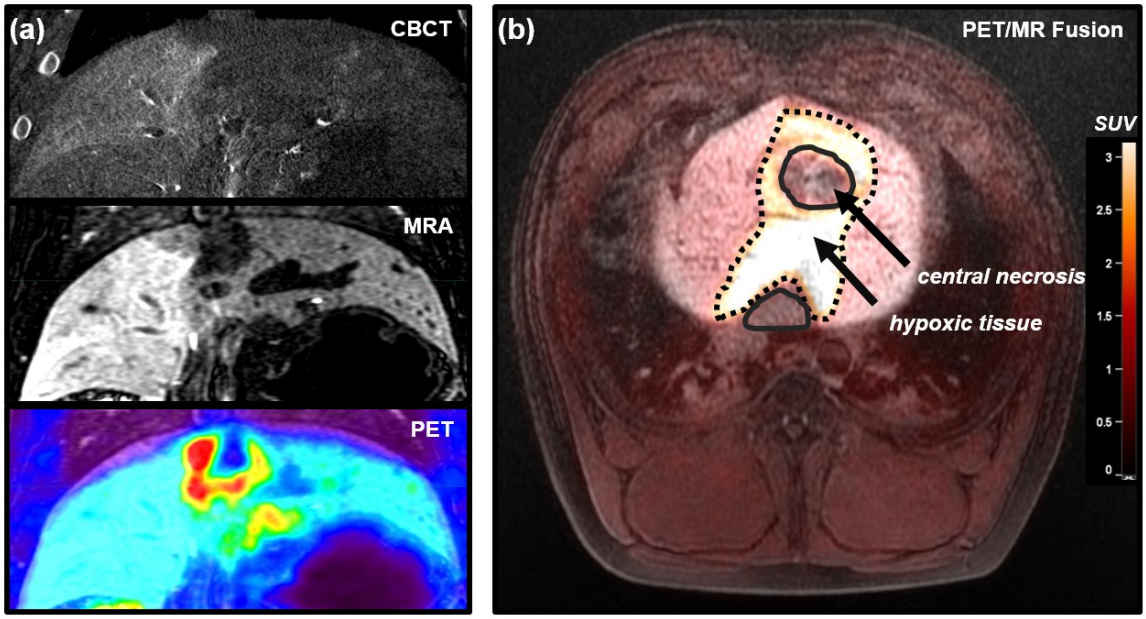

Figure 4: Representative F18-MISO PET/MR images

Multimodal (a) coronal images of the liver shows correlation of decreased contrast-enhancement in the left hemi-liver on cone-beam CT (CBCT) and MR angiography (MRA). On corresponding PET imaging, the hypoxia signal is strongest in the upper portion of the left medial lobe. PET/MR fusion of an axial image (b) illustrates a region of strong FMISO avidity (hypoxic tissue) with a central "cold-spot" (central necrosis).

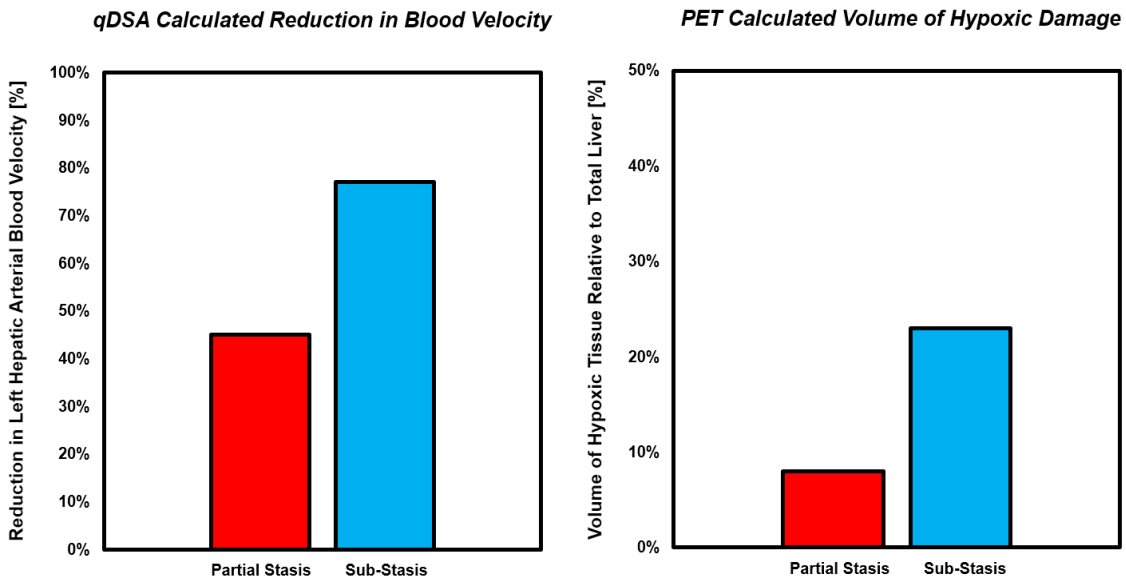

Figure 5: qDSA-calculated blood velocity reduction correlation with F18-MISO PET degree of hypoxia

Arteries embolized to a greater degree of blood flow stasis showed an increase in the degree of qDSA-calculated reduction in blood velocity. In the livers treated to a greater degree of stasis, there is an increase in the extent of hypoxic damage, determined by regions demonstrating post-embolization 18F-FMISO avidity, relative to the total volume of the liver .

2.5 Discussion

The results indicate that qDSA is a more effective quantitative technique for determining treatment endpoints than the commercially available ccDSA technique (H1). Embolizations performed to greater degrees of stasis on angiography had correspondingly greater reductions in BFV as calculated by the qDSA method. Although the ccDSA method did calculate increased TTP after embolization, it was not able to significantly discriminate between stasis endpoints. Such a predictable relationship between velocity reduction on qDSA and degree of embolization is critical for determining in real-time, not only if additional embolic particles are needed to achieve sub-stasis, but approximately how many. qDSA may facilitate achieving standardized, reproducible, and objective endpoints during liver embolization given these results.

In a controlled setting, qDSA demonstrated a stronger correlation with the degree of embolization than a commercially available color-coded technique (ccDSA) that calculates TTP (H2). Techniques such as ccDSA use information in a limited spatial region of a vessel segment and may be more susceptible to variations in imaging parameters (29-31). Additionally, image artifacts, such as those caused by respiratory motion, can introduce error in TTP calculations. Although ccDSA is capable of detecting

a large change in flow, it is less suitable for intra-procedural guidance of an embolization. In contrast, the qDSA technique measures a physiologic variable, blood velocity, which is spatially and temporally-averaged over a selected vessel segment, making it less susceptible to changes in imaging parameters. Additionally, temporal segmentation used in the qDSA calculation (removing frames corrupted by motion) makes the technique more robust and immune to motion artifacts present in a DSA sequence. The granularity achieved in measurements using qDSA may permit titration of an embolization in a way that is otherwise not achievable with currently available quantitative methods. Although DSA images were acquired in regular intervals for the purpose of this study, this technique may not be necessary clinically; instead the measurements may be used intermittently to quantitatively confirm progress of an embolization where a subjective angiographic assessment may otherwise be used.

On pathologic and functional imaging analysis, qDSA demonstrated a correlation with tissue level perfusion changes (H3). In functional imaging assessment, F-18 fluoromisonidazole (FMISO), a well characterized hypoxia PET radiotracer, was used to measure post-embolization acute hypoxia in the liver (34-36). In livers embolized to a higher degree of qDSA-determined blood flow stasis, there was a larger volume of hypoxic damage relative to the total liver on F-FMISO PET/MR imaging. In gross

assessment, the extent of ischemic damage inflicted on the liver parenchyma corresponded with embolizations performed to greater degrees of stasis as characterized by qDSA. Additionally, the reduction in velocity on qDSA had a moderate to strong correlation with embolic particle density of ischemic regions within the embolized lobe. This relationship between qDSA and pathology and functional imaging is important in confirming that the flow-based changes detected by the technique are an appropriate surrogate for tissue-level perfusion changes, the primary endpoint of interest for an embolization procedure.

Other attempts have been made to develop an objective embolization endpoint using volumetric imaging. One, quantitative 4D transcatheter intra-arterial perfusion MRI, showed promise, however, lacks feasibility as it requires a complex and costly hybrid angiography/MR suite only available at select institutions (22,23). A recent study demonstrated the feasibility of using quantitative 4D-DSA to depict changes in hepatic arterial blood velocity during transarterial embolization in a swine model, but the method requires lengthy data acquisition times and greater amounts of iodinated contrast (32,33). The 2D qDSA technique described here could be easily translated to intra-procedural clinical workflows given that it would only require modification to image acquisition parameters. Our qDSA calculations were performed in 1–2 minutes using a laptop

computer; integration into an imaging system with high computing power would permit near-real time calculations (on the order of seconds).

It should be noted that, in its current form, qDSA does require additional radiation dose from additional DSA scans. Previous studies have shown the utility of quantitative fluoroscopy, although those techniques suffer from many of the same limitations as ccDSA. qDSA may feasibly be performed using fluoroscopy, as long as there is sufficient signal in the image to identify peaks in the TAC and there is sufficient temporal resolution to sample the signal. This would significantly decrease radiation exposure compared to subtracted images.

This feasibility study had several limitations. TAE was performed in the livers of non-tumor bearing swine, a model which does not entirely represent the hemodynamics of a human liver with HCC. The qDSA method also has certain technical limitations including the calculation of blood flow velocity rather than flow, as it lacks the cross-sectional area measurement necessary to calculate volumetric flow. The results from this study, however, indicate that changes in relative velocity can be used as an appropriate surrogate for changes in flow. The shifted-least squares approach used in qDSA relies on adequate sampling of a time-varying pulsatile signal, which limits the ability to resolve vessels with very high blood velocities or the very low velocities observed at complete

stasis (due to turbulent, retrograde flow disrupting the pulsatility). The qDSA method, however, does resolve most velocities within the normal range and those encountered routinely during interventions (including sub-stasis).

In conclusion, qDSA was able to quantify embolization endpoints using calculated blood velocity reductions. The velocity reductions were linear with respect to the baseline value and correlated radiologically and pathologically with markers of perfusion changes, including, tissue hypoxia, tissue embolic particle density and extent of ischemic damage.

2.6 References

1. Villanueva, A. Hepatocellular Carcinoma. New England Journal of Medicine 380, 1450–1462 (2019). PMID: 30970190

2. Bray, F. et al. Global cancer statistics 2018: GLOBOCAN estimates of incidence and mortality worldwide for 36 cancers in 185 countries. CA: A Cancer Journal for Clinicians 68, 394–424 (2018). PMID: 30207593

3. Delis, S. G. & Dervenis, C. Selection criteria for liver resection in patients with hepatocellular carcinoma and chronic liver disease. World Journal of Gastroenterology 14, 3452–3460 (2008). PMCID: PMC2716604

4. Forner, A., Reig, M. & Bruix, J. Hepatocellular carcinoma. The Lancet (2018). doi:10.1016/s0140-6736(18)30010-2. PMID: 29307467

5. Cabrera, R. & Nelson, D. R. Review article: the management of hepatocellular carcinoma. Alimentary Pharmacology & Therapeutics 31, 461–476 (2010). PMID: 19925500

6. Murata, S. et al. Interventional treatment for unresectable hepatocellular carcinoma. World Journal of Gastroenterology 20, 13453–13465 (2014). PMCID: PMC4188897

7. Lo, C. et al. Randomized controlled trial of transarterial lipiodol chemoembolization for unresectable hepatocellular carcinoma. Hepatology 35, 1164–1171 (2002). PMID: 11981766

8. Llovet, J. M. et al. Arterial embolisation or chemoembolisation versus symptomatic treatment in patients with unresectable hepatocellular carcinoma: a randomised controlled trial. The Lancet 359, 1734–1739 (2002). PMID: 12049862

9. Manini, M. A. et al. Transarterial chemoembolization with drug-eluting beads is effective for the maintenance of the Milan-in status in patients with a small hepatocellular carcinoma. Liver Transplantation 21, 1259–1269 (2015). PMID: 26074360

10. Bouchard-Fortier, A., Lapointe, R., Perreault, P., Bouchard, L. & Pomier-Layrargues, G. Transcatheter Arterial Chemoembolization of Hepatocellular Carcinoma as a Bridge to Liver Transplantation: A Retrospective Study. International Journal of Hepatology 2011, 974514 (2011). PMCID: PMC3170864

11. Heckman, J. T. et al. Bridging Locoregional Therapy for Hepatocellular Carcinoma Prior to Liver Transplantation. Annals of Surgical Oncology 15, 3169–3177 (2008). PMID: 18696158

12. Jin, B. et al. Chemoembolization endpoints: effect on survival among patients with hepatocellular carcinoma. AJR. American journal of roentgenology 196, 919–28 (2011). PMCID: PMC3157291

13. Geschwind, J.-F. H. et al. Transcatheter Arterial Chemoembolization of Liver Tumors: Effects of Embolization Protocol on Injectable Volume of Chemotherapy and Subsequent Arterial Patency. CardioVascular and Interventional Radiology 26, 111–117 (2003). PMID: 12616414

14. Rhee, T. K. et al. Effect of Transcatheter Arterial Embolization on Levels of Hypoxia-inducible Factor-1α in Rabbit VX2 Liver Tumors. Journal of Vascular and Interventional Radiology 18, 639–645 (2007). PMID: 17494846

15. Shim, J. H. et al. Association between increment of serum VEGF level and prognosis after transcatheter arterial chemoembolization in hepatocellular carcinoma patients. Cancer Science 99, 2037–2044 (2008). PMID: 19016764

16. Kobayashi, N. et al. Co-expression of Bcl-2 protein and vascular endothelial growth factor in hepatocellular carcinomas treated by chemoembolization. Liver 19, 25–31 (1999). PMID: 9928762

17. Sergio, A. et al. Transcatheter Arterial Chemoembolization (TACE) in Hepatocellular Carcinoma (HCC): The Role of Angiogenesis and Invasiveness. The American Journal of Gastroenterology 103, ajg200850181 (2008). PMID: 18177453

18. Iwazawa, J. et al. Identifying Feeding Arteries During TACE of Hepatic Tumors: Comparison of C-Arm CT and Digital Subtraction Angiography. American Journal of Roentgenology 192, 1057–1063 (2009). PMID: 19304714

19. Flannigan, B. D., Gomes, A. S., Stambuk, E. C., Lois, J. F. & Pais, S. O. Intra-arterial digital subtraction angiography: comparison with conventional hepatic arteriography. Radiology 148, 17–21 (1983). PMID: 6856829

20. Waite, S. et al. Interpretive Error in Radiology. American Journal of Roentgenology 1–11 (2016). doi:10.2214/ajr.16.16963. PMID: 28026210

21. Lewandowski, R. J. et al. A Comparison of Chemoembolization Endpoints Using Angiographic versus Transcatheter Intraarterial Perfusion/MR Imaging Monitoring. Journal of Vascular and Interventional Radiology 18, 1249–1257 (2007). PMID: 17911515

22. Gaba, R. C. et al. Four-dimensional Transcatheter Intraarterial Perfusion MR Imaging for Monitoring Chemoembolization of Hepatocellular Carcinoma: Preliminary Results. Journal of Vascular and Interventional Radiology 19, 1589–1595 (2008). PMCID: PMC2603479

23. Larson, A. C. et al. Transcatheter Intraarterial Perfusion: MR Monitoring of Chemoembolization for Hepatocellular Carcinoma—Feasibility of Initial Clinical Translation. Radiology 246, 964–971 (2008). PMID: 18309018

24. Wang, D. et al. Quantitative 4D transcatheter intraarterial perfusion MRI for monitoring chemoembolization of hepatocellular carcinoma. Journal of Magnetic Resonance Imaging 31, 1106–1116 (2010). PMCID: PMC2885358

25. Marquez, H. P. et al. Computed tomography perfusion imaging for monitoring transarterial chemoembolization of hepatocellular carcinoma. European Journal of Radiology 91, 160–167 (2017). PMID: 28629564

26. Wimmer, T. et al. Computed Tomography Perfusion Following Transarterial Chemoembolization of Hepatocellular Carcinoma. Journal of Computer Assisted Tomography 41, 708–712 (2017). PMID: 28296685

27. Taouli, B. et al. Hepatocellular carcinoma: perfusion quantification with dynamic contrast-enhanced MRI. AJR. American journal of roentgenology 201, 795–800 (2013). PMCID: PMC4144815

28. Lin EY, et al. Three-Dimensional Quantitative Color-Coding Analysis of Hepatic Arterial Flow Change during Chemoembolization of Hepatocellular Carcinoma. J Vasc Interv Radiol. 2018 Oct;29(10):1362-1368. doi: 10.1016/j.jvir.2018.04.012. Epub 2018 Aug 28. PMID: 30170947.

29. Ionita CN, et al. Effect of injection technique on temporal parametric imaging derived from digital subtraction angiography in patient specific phantoms. Proc SPIE Int Soc Opt Eng. 2014 Mar 13;9038:90380L. doi: 10.1117/12.2041347. PMID: 25302010; PMCID: PMC4187403.

30. Shpilfoygel SD, et al. X-ray videodensitometric methods for blood flow and velocity measurement: a critical review of literature. Med Phys. 2000 Sep;27(9):2008-23. doi: 10.1118/1.1288669. PMID: 11011728.

31. Kennedy AS et al. Computer modeling of yttrium-90-microsphere transport in the hepatic arterial tree to improve clinical outcomes. Int J Radiat Oncol Biol Phys. 2010 Feb 1;76(2):631-7. doi: 10.1016/j.ijrobp.2009.06.069. Epub 2009 Nov 10. PMID: 19910131.

32. Wu Y, et al. Quantification of Blood Velocity with 4D Digital Subtraction Angiography Using the Shifted Least-Squares Method. AJNR Am J Neuroradiol. 2018 Oct;39(10):1871-1877. doi: 10.3174/ajnr.A5793. Epub 2018 Sep 13. PMID: 30213811; PMCID: PMC6177311.

33. Meram, Ece et al. "Optimization of quantitative time-resolved 3D (4D) digital subtraction angiography in a porcine liver model." European radiology experimental vol. 4,1 37. 2 Jul. 2020, doi:10.1186/s41747-020-00164-3

34. Shah, Rajesh P et al. "Limitations of Fluorine 18 Fluoromisonidazole in Assessing Treatment-induced Tissue Hypoxia after Transcatheter Arterial Embolization of Hepatocellular Carcinoma: A Prospective Pilot Study." Radiology. Imaging cancer vol. 4,3 (2022): e210094. doi:10.1148/rycan.210094

35. Piert, M et al. “Dependency of the [18F]fluoromisonidazole uptake on oxygen delivery and tissue oxygenation in the porcine liver.” Nuclear medicine and biology vol. 27,8 (2000): 693-700. doi:10.1016/s0969-8051(00)00151-7

36. Piert, M et al. “Introducing fluorine-18 fluoromisonidazole positron emission tomography for the localisation and quantification of pig liver hypoxia.” European journal of nuclear medicine vol. 26,2 (1999): 95-109. doi:10.1007/s002590050365

Chapter 3: Quantitative Digital Subtraction Angiography (qDSA): Advanced Techniques

Portions of this chapter were presented at the following scientific meetings:

Periyasamy S, Wagner M, Speidel M, Yadav P, Laeseke PF. Characterization of Respiratory Motion in the Hepatic Vasculature Using a 3D Elastic Registration Technique. SIR 2020. Virtual. March 2020. Poster

Periyasamy S, Kleedehn M, Eifler A, Woods M, Ozkan O, Laeseke PF. A Review of Cone-Beam CT, Its Role in Interventional Oncology. CIRSE 2020. Virtual Summit. September 2020. Poster

Periyasamy S, Whitehead J, Speidel M, Wagner M, Laeseke P. Evaluation of an Intra-Acquisition Motion-Correction Algorithm for 3D-DSAs of the Hepatic Vasculature Using a Digital Liver Phantom. SIR 2021. Virtual. March 2021. Poster

Periyasamy S, Pieper AA, Oberstar E, Whitehead J, Hoffman CA, Speidel M, Laeseke PF. Super-Selective Quantitative Digital Subtraction Angiography for Hepatic Arterial Interventions: Feasibility Study in a Swine Model. SIO 2022. San Francisco, CA. March 2022. Poster

Periyasamy S, Hoffman CA, Wagner M, Whitehead J, Speidel M, Laeseke PF. A 2D-3D Quantitative Angiography Technique for Calculating Volumetric Reduction in Blood Flow During Hepatic Transarterial Embolization. Submitted to CIRSE 2022. Barcelona, Spain. September 2022.

or co-authored and published in the following conference proceedings:

Whitehead J, Nikolau E, **Periyasamy S**, Torres L, Laeseke PF, Speidel M, Wagner M, "Simulation of hepatic arteries and synthesis of 2D fluoroscopic images for interventional imaging studies," Proc. SPIE 11312, Medical Imaging 2020: Physics of Medical Imaging, 113121W (16 March 2020); https://doi.org/10.1117/12.2549570

3.1 Introduction

Following successful demonstration of the feasibility of performing qDSA during liver embolizations, its improvement over current techniques, and its correlation with tissue-level changes, we sought to optimize the technique in order to improve its robustness and clinical translatability. This chapter explores *advanced* qDSA techniques including the ability to perform super-selective blood velocity quantification, incorporation of pre-procedure 3D imaging to enable volumetric blood flow quantification, and motion-compensation strategies to permit higher-quality 3D imaging.

3.2 Motivation

The technical practice of transarterial embolization (TAE) transarterial embolization and transarterial chemoembolization (TACE) has evolved significantly since it became standard of care for intermediate-stage primary liver cancer (1). These advances have not only improved the procedural workflow but increased the diagnostic and therapeutic capabilities of the procedures. Many of these advances have been driven by the difficulties of intervention in the liver. These include the complex geometry and vascular anatomy, and the proximity of the organ to the diaphragm, which introduces significant respiratory motion artifacts into x-ray-based imaging techniques.

One procedural technique which has become increasingly common is super-selective angiography and embolization (2-4). Rather than injecting into larger, more proximal arteries, super-selective catheterization involves advancement of a microcatheter into smaller, sub-segmental branches. This targeted approach mitigates risk of collateral embolization by directly embolizing the tumor, and has been shown to improve outcomes over lobar approaches (5-8).

Cone-beam CT (CBCT), another major advance in imaging technology, permitted the use of single-rotation intra-procedural volumetric imaging with high spatial

resolution for planning and guiding embolization procedures (9). CBCT has been shown to significantly increase detection of tumors and tumor supplying arteries in comparison to traditional DSA for TACE procedures (10,11). CBCT has also been shown to detect tumor findings not found on DSA or 99mTc MAA imaging for Y90 radioembolization procedures (12). Additionally, 3D CBCT images can be co-registered with 3D pre-procedure imaging (CT, MR) or 2D intra-procedural imaging (fluoroscopy, ultrasound) for improved real-time navigation (13-16).

The increased use of 3D CBCT imaging during embolization procedures has demanded new techniques for motion-compensation strategies to improve image quality. The long rotation time for many C-arm based CBCT acquisitions can lead to unintended respiratory motion and subsequently, deleterious motion artifacts, particularly in DSA scans where there are consecutive acquisitions. Motion artifacts are seen in 50% of CBCT hepatic arteriograms with moderate or severe motion artifacts present in 30% of studies (17,18). Several techniques have emerged over the last few decades to address these limitations. These include 3D elastic (deformable) registration, 2D-3D registration approaches, and novel reconstruction techniques which require fewer projections (leading to shorter scans and/or limited rotations) (19-23).

The objective of this study was to incorporate many of the modern imaging andprocedural techniques used in current embolization practice into qDSA in order to expand the capabilities of the technique and help make it more translatable. Specifically, the aim was to (I) validate qDSA performance in a super-selective approach compared to conventional non-selective qDSA, (II) develop a volumetric qDSA (vqDSA) technique which incorporates pre-procedure 3D imaging with intra-procedural qDSA, and (III) characterize complex intra-hepatic motion to develop and validate motion-compensation strategies for 3D acquisitions (which may be used in vqDSA).

3.3 Validating a Super-Selective qDSA (ss-qDSA) Technique in Distal Hepatic Arterial Branches

3.3.1 Materials and Methods

All procedures were approved by the institutional research animal care and use committee and were compliant with regulatory guidelines. Hepatic angiography was performed in the liver of one swine (50 kg). The subject was sedated with an intramuscular administration of 7 mg/kg of tiletamine hydrochloride-zolazepam hydrochloride (Xyla-Ject; Phoenix Pharmaceutical, St. Joseph, Missouri), endotracheally intubated, and then underwent anesthesia induction and maintenance with 2% inhaled isoflurane (Halocarbon Laboratories, River Edge, New Jersey).

Hepatic Angiography

All procedures were performed in an angiography suite (Artis zee; Siemens Healthineers, Forcheim, Germany). Femoral arterial access was obtained and the common hepatic artery selected with a 5 Fr angled glide catheter (Teruomo, Tokyo , Japan). Conventional qDSA images were acquired through the common hepatic artery using an injection of iohexol 300 mg/mL (Omnipaque 300; GE Healthcare, Waukesha, Wisconsin). Contrast was injected at a rate of 2.0 mL/s for a total of 16.0 mL. Triplicate

images were acquired. After conventional images were acquired, a 2.8 Fr high-flow microcatheter (Boston Scientific, Marlborough, MA) was then used to select distal hepatic arterial branches including a sub-segmental left medial branch ("distal left") and a sub-segmental right lateral branch ("distal right"). Super-selective qDSA (ss-qDSA) images were acquired using the same injection parameters as the conventional qDSA images.

Image Analysis

A post-hoc analysis of all DSA images was performed using both the qDSA and ss-qDSA acquisitions. Blood velocity was calculated using a custom-built MATLAB tool. Mean branch arterial blood velocities were calculated, as were the standard deviations in repeated measures (n = 6) to assess consistency of calculations. Although flow pulsatility is not a requirement for qDSA, sufficient variations in the time-oscillating contrast signal are necessary for calculation. Time-attenuation curves from both sets of images were assessed for pulsatility by calculating a peak-to-trough metric (PTM) using the time-oscillating contrast signal in the regions of interest (n = 6) in the distal left and distal right hepatic arteries.

$$PTM = 100\left(\frac{Peak_{\ intensity}}{Trough_{\ intensity}} - 1\right)$$

3.3.2 Results

Contrast Signal Assessment

In the distal left hepatic artery, the super-selective approach resulted in a two-fold increase in PTM (ss-qDSA: 24.1 ± 5.4, qDSA: 11.6 ± 3.6, p = 0.01) (Figure 1). In the distal right hepatic artery, the super-selective approach also resulted in a two-fold increase in PTM (ss-qDSA: 82.4 ± 28.9, qDSA: 35.3 ± 18.7, p = 0.05). Contrast pulsatility maps assessing the time-oscillating signal in the time-attenuation curves showed higher PTM in the distal hepatic arteries using the ss-qDSA technique compared to the conventional qDSA technique (Figure 2).

Blood Velocity Assessment

In the distal left hepatic artery, the super-selective approach resulted in a reduction in standard deviation for repeated velocity calculations (ss-qDSA: 30.1 ± 4.23 cm/s, qDSA: 45.27 ± 8.56 cm/s) (Figure 3). In the distal right hepatic artery, the super-selective approach also resulted in a reduction in standard deviation for repeated velocity calculations (ss-qDSA: 36.8 ± 3.5 cm/s, qDSA: 38.9 ± 15.6 cm/s).

3.3.3 Figures

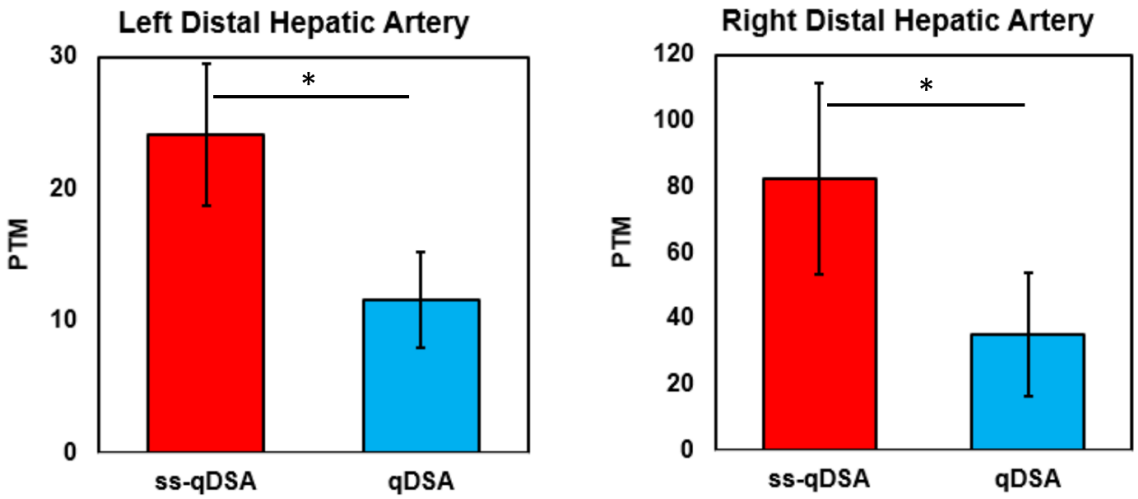

Figure 1: Comparison of pulsatility using conventional qDSA and ss-qDSA

Super-selective qDSA (ss-qDSA) results in significantly more contrast signal time-oscillation in the image time-attenuation curves than conventional qDSA protocols in the distal hepatic arteries.

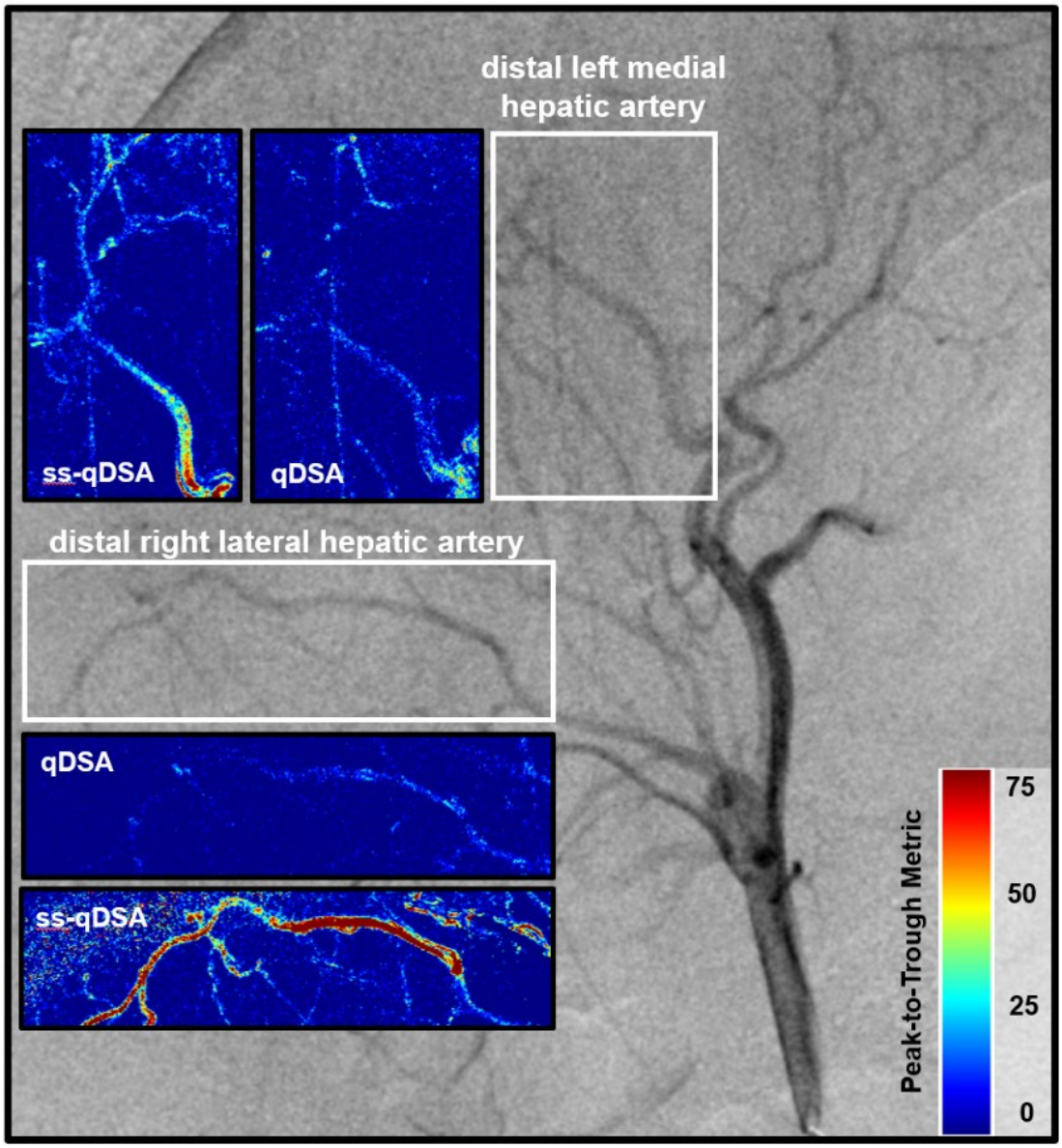

Figure 2: Contrast pulsatility maps comparing conventional qDSA with ss-qDSA

Hepatic arteriogram in a swine using both a conventional qDSA protocol and a super-selective qDSA (ss-qDSA) protocol. Pulsatility maps show a significant visible increase in time-oscillatory contrast signals in the distal hepatic arteries.

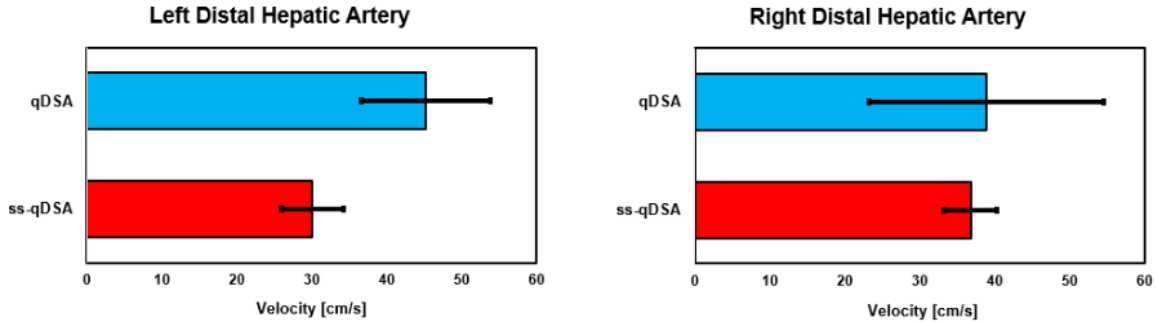

Figure 3: Blood velocity measurements comparing conventional qDSA with ss-qDSA

Super-selective qDSA (ss-qDSA) results in more consistent blood velocity calculations than conventional qDSA protocols in the distal hepatic arteries.

3.4 Characterization of Volumetric Reduction in Blood Flow During Hepatic Transarterial Embolization Using a 2D-3D qDSA Technique

3.4.1 Materials and Methods

All procedures were approved by the Institutional Research Animal Care and Use Committee and were compliant with regulatory guidelines. Transarterial embolization was performed in the livers of five swine (mean weight, 49.4 ± 3.1 kg kg). Subjects were sedated with an intramuscular administration of 7 mg/kg of tiletamine hydrochloride-zolazepam hydrochloride (Xyla-Ject; Phoenix Pharmaceutical, St. Joseph, Missouri), endotracheally intubated, and then underwent anesthesia induction and maintenance with 2% inhaled isoflurane (Halocarbon Laboratories, River Edge, New Jersey).

Transarterial Embolization

All procedures were performed in an angiography suite (Artis zee; Siemens Healthineers, Forcheim, Germany). Femoral arterial access was obtained and the common hepatic artery was selected with a 4 Fr angled glide catheter. A Baseline 3D-CBCT of the hepatic arterial anatomy was acquired using an injection of iohexol 300 mg/mL (Omnipaque 300; GE Healthcare, Waukesha, Wisconsin). Prior to embolization,

a baseline 30 frames per second (fps) 2D-DSA of the common hepatic artery was acquired (2 mL/s for 16.0 mL total). All images were acquired with breath holds.

In each animal, the left medial hepatic artery was selected for embolization. Bland embolizations were performed given that the primary objective of the study was to characterize reductions in blood flow. A 0.014″ guidewire was used to select the left medial hepatic artery supplying the left medial lobe, after which a 2.8 Fr microcatheter was advanced into the vessel. Once the microcatheter was correctly positioned, an embolization was performed using 100–300 μm microspheres (Embosphere Microsphere; Merit Medical Systems, South Jordan, Utah) diluted in 10 mL of iohexol 300 mg/mL. A total of 10 mL of embolic particles, delivered in 2 mL aliquots) were delivered. After delivery of each aliquot, the microcatheter was withdrawn, and 2D-DSAs were acquired via the stationary base catheter positioned in the common hepatic artery. In some animals (n=2), a 3D CBCT was acquired mid-way through the procedure The target vessel was then reselected with the microcatheter and the embolization resumed. In these embolizations, there was a minimum of 2 min between microcatheter withdrawal and subsequent imaging in order to minimize any effects of transient arterial spasm. Following complete delivery of the embolic particles, post-embolization 2D-DSAs and 3D CBCTs were acquired.

Volumetric qDSA

The volumetric qDSA (vqDSA) method combines three dimensional vascular anatomic information from a pre-procedure 3D-CBCT with time-attenuation data from intra-procedural 2D-DSAs (Figure 1). Vessel centerlines extracted from pre-procedure images which were then registered and projected onto the 2D-DSA for flow calculation using the qDSA method (Figure 2). The 2D-3D registration was performed using previously described methods (24). Cross-sectional area was calculated at each centerline point along the length of the vessel and averaged for a spatially-averaged vessel cross sectional-area. Cross-sectional area measurements were made at pre-, mid-, and post-embolization time points in order to assess for potential intra-procedural changes in vessel size as a result of embolization. A full-width half-max technique was used to segment vessel cross-sections and calculate area.

3.4.2 Results

Volumetric Blood Flow Reduction During Embolization

There was a large reduction in calculated blood flow in all animals following embolization to a sub-stasis endpoint (65 ± 10.7 % reduction in blood flow from baseline) (Figure 3). The number of particles delivered for a sub-stasis endpoint was consistent (6.5 ± 0.9 mL embolic particles delivered per animal). There were strong linear decreases (R^2 = 0.80, 0.88, 0.78, 0.79) in calculated average blood flow seen in the treated left medial hepatic arteries (0.4, 1.3, 2.1, 0.4 mL/s reduction in flow per mL of embolic particles delivered, respectively) until the sub-stasis endpoint was achieved.

Cross-Sectional Area During Embolization

In animal 1, the cross-sectional area in the left medial hepatic artery at pre-, mid-, and post-embolization time-points was 16.3, 16.7, and 14.7 mm^2. The mean cross-sectional area was 15.9 ± 0.9 mm^2 with a percent deviation of 5.7%. In animal 2, the cross-sectional area in the medial branch of the left medial hepatic artery at pre-, mid-, and post-embolization time-points was 11.4, 12.7, and 13.0 mm^2. The mean cross-sectional area was 12.4 ± 0.7 mm^2 with a percent deviation of 5.6%. Results are presented in Table 1.

3.4.3 Tables

Table 1: Intra-procedural cross-sectional area measurements

Animal	Hepatic Artery	Time-Point	Cross-Sectional Area (mm^2)	Measurement Deviation (%)
1	Left Medial	Pre-Embolization	16.3	5.7
		Mid-Embolization	16.7	
		Post-Embolization	14.3	
2	Left Medial	Pre-Embolization	11.4	5.6
		Mid-Embolization	12.7	
		Post-Embolization	13	

3.4.4 Figures

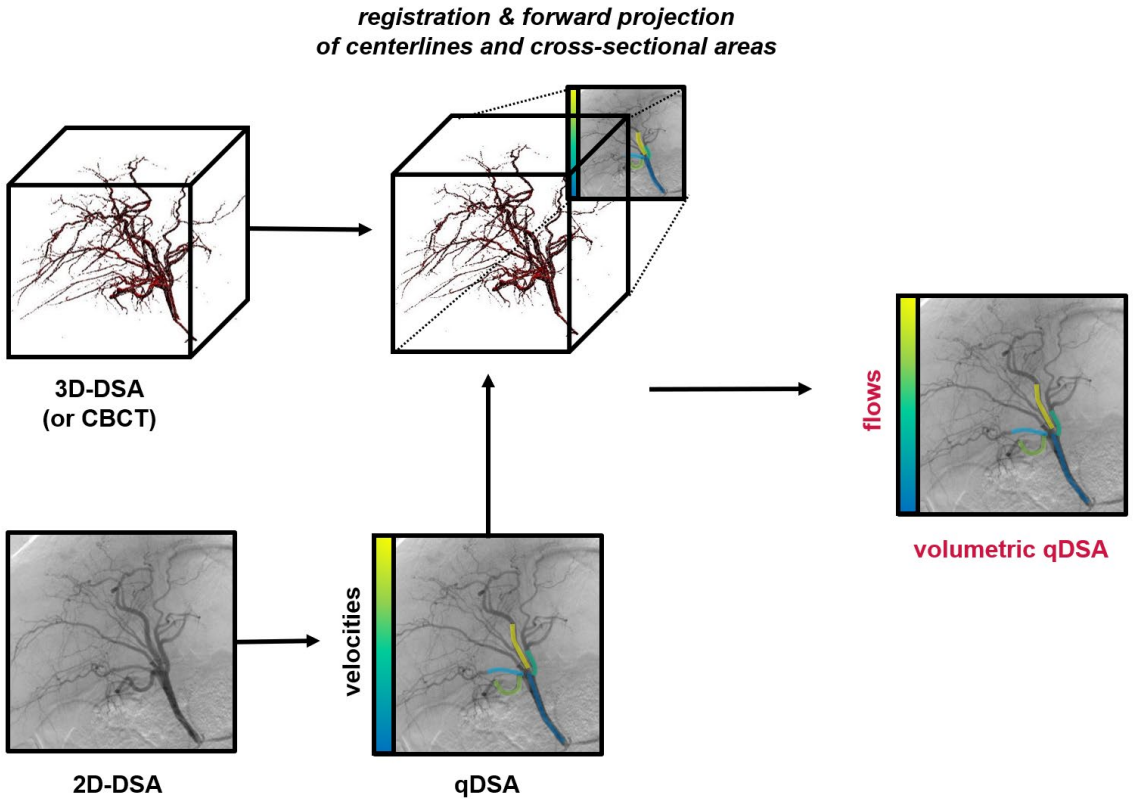

Figure 1: Volumetric qDSA algorithm using 2D and 3D images

An illustration of the volumetric qDSA (vqDSA) technique using pre-procedure 3D imaging (either 3D-DSAs or contrast-enhanced cone beam CTs) and intra-procedural 2D-DSAs. Centerlines and cross-sectional areas are registered and forward-projected onto intra-procedural 2D images to calculate volumetric blood flow.

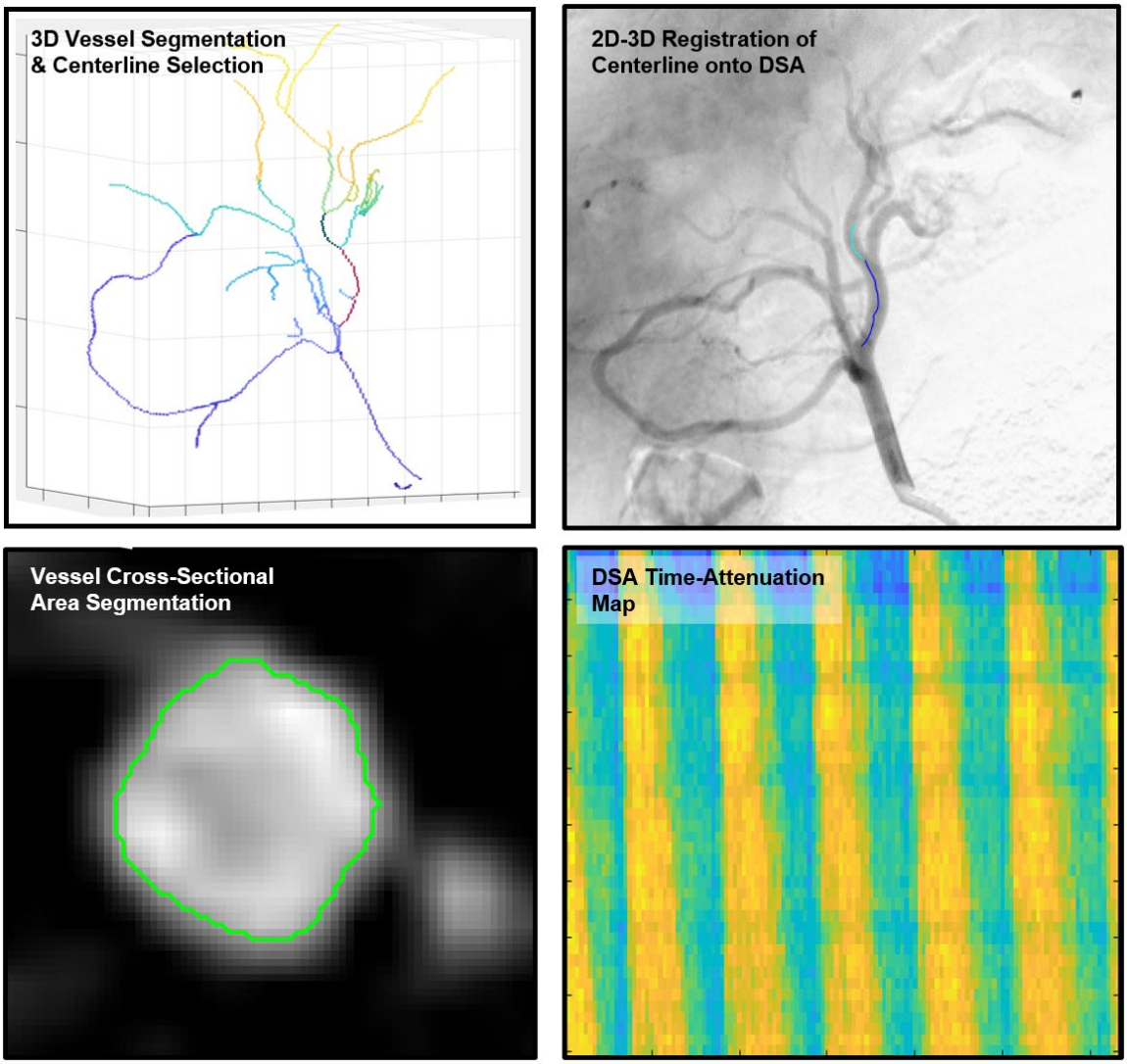

Figure 2: Representative in vivo vqDSA image processing

Representative imaging from an in vivo study using the vqDSA technique. A pre-procedure 3D-DSA is segmented and centerlines are generated for all vessel branches. Vessels are color-coded by branches. This segmentation is registered to all intra-procedural 2D DSA images and the target vessel is overlaid on to the images. The vessel

cross-sectional area is segmented from the 3D images and an average area is calculated across the length of the vessel. Time-attenuation maps from the 2D images are used to perform conventional blood velocity calculations to be combined with the centerline and cross-sectional area information for volumetric flow quantification.

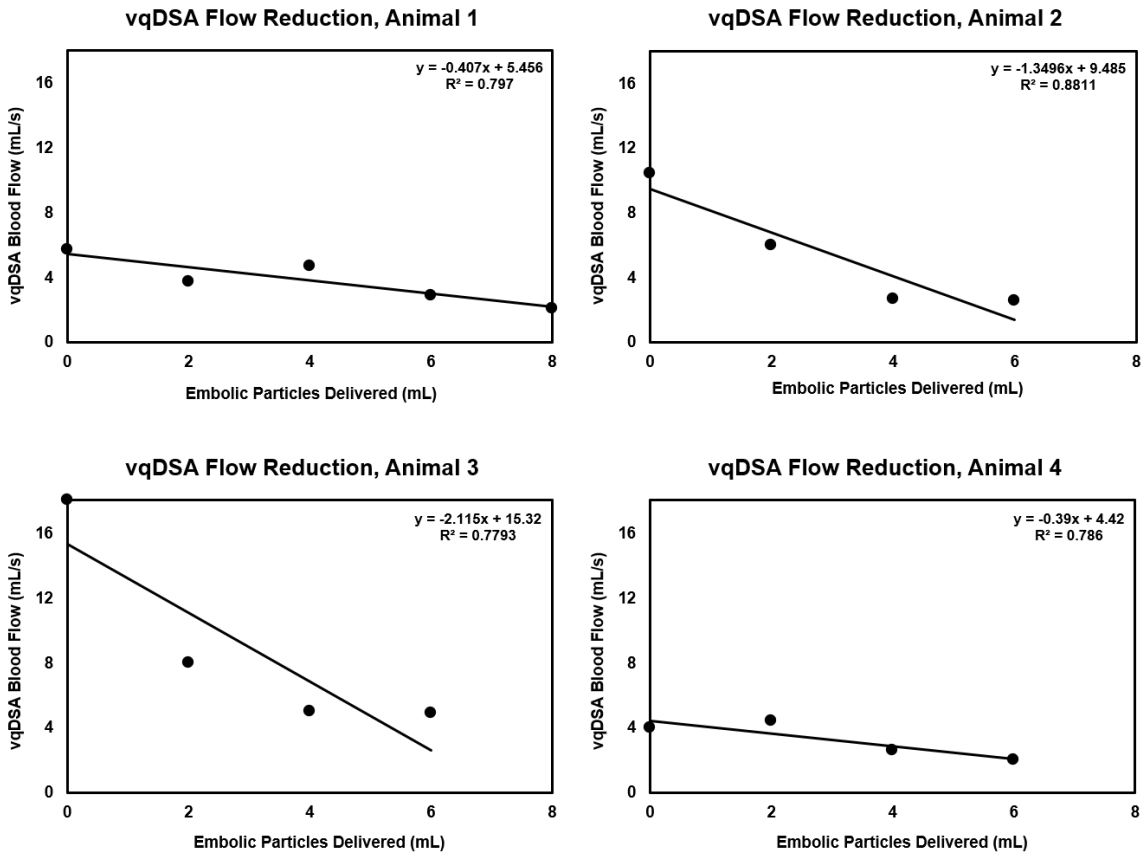

Figure 3: Complete vqDSA blood flow reduction curves

All transarterial embolizations exhibited linear decreases in blood flow relative to baseline as the embolization progressed. The was strong linear correlations between vqDSA blood flow and embolic particles delivered with variable rate of blood flow decrease.

3.5 Characterization of Respiratory Motion in the Hepatic Vasculature

3.5.1 Materials and Methods

All analysis was approved by the institutional review board (IRB) and studies were compliant with regulatory guidelines.

Non-contrast 4D CTs from 10 radiation oncology patients with abdominal malignancies were retrospectively analyzed. In each case, a 3D elastic grid registration technique (diffeomorphic demons) was applied to CT acquisitions from an inspiratory and expiratory phase to produce a displacement field (Figure 1). A volume of interest (VOI) within the displacement field (3x3x3 voxels) was selected for two peripheral and two central locations within the liver: hepatic dome, right lateral lobe, porta hepatis, and left portal vein (Figure 2). In each VOI, the average magnitudes of the superoinferior component, transverse-plane component (anteroposterior and mediolateral), and total displacement vectors were computed.

3.5.2 Results

The mean total displacements (± standard deviation) in the hepatic dome, right lateral lobe, porta hepatis, and left portal vein were, 11.21 (± 4.93), 7.9143 (± 3.26), 9.87 (± 5.17), and 11.09 (± 4.27), respectively (Figure 3). The mean superoinferior displacements were 10.98 (± 4.88), 7.17 (± 3.50), 8.84 (± 5.21), and 10.18 (± 4.23). The mean transverse-plane displacements were 2.02 (± 1.25), 2.79 (± 1.47), 4.02 (± 1.70), and 4.16 (± 1.60).

The primary effect of respiratory motion on the liver is superoinferior translation, but there is significant transverse-plane deformation as well. Centrally within the liver, near the hepatic vasculature, there was a statistically significant increase in transverse-plane deformation relative to more peripheral regions ($p<0.01$).

3.5.3 Figures

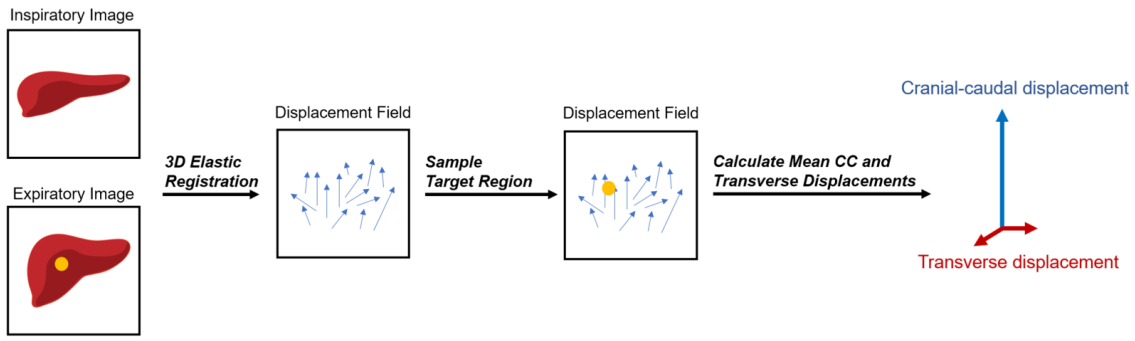

Figure 1: Hepatic motion characterization algorithm

Motion characterization algorithm utilizing a 3D elastic registration technique. The displacement field produced when registering inspiratory and expiratory phase images is analyzed in volumes of interest to determine the character of motion.

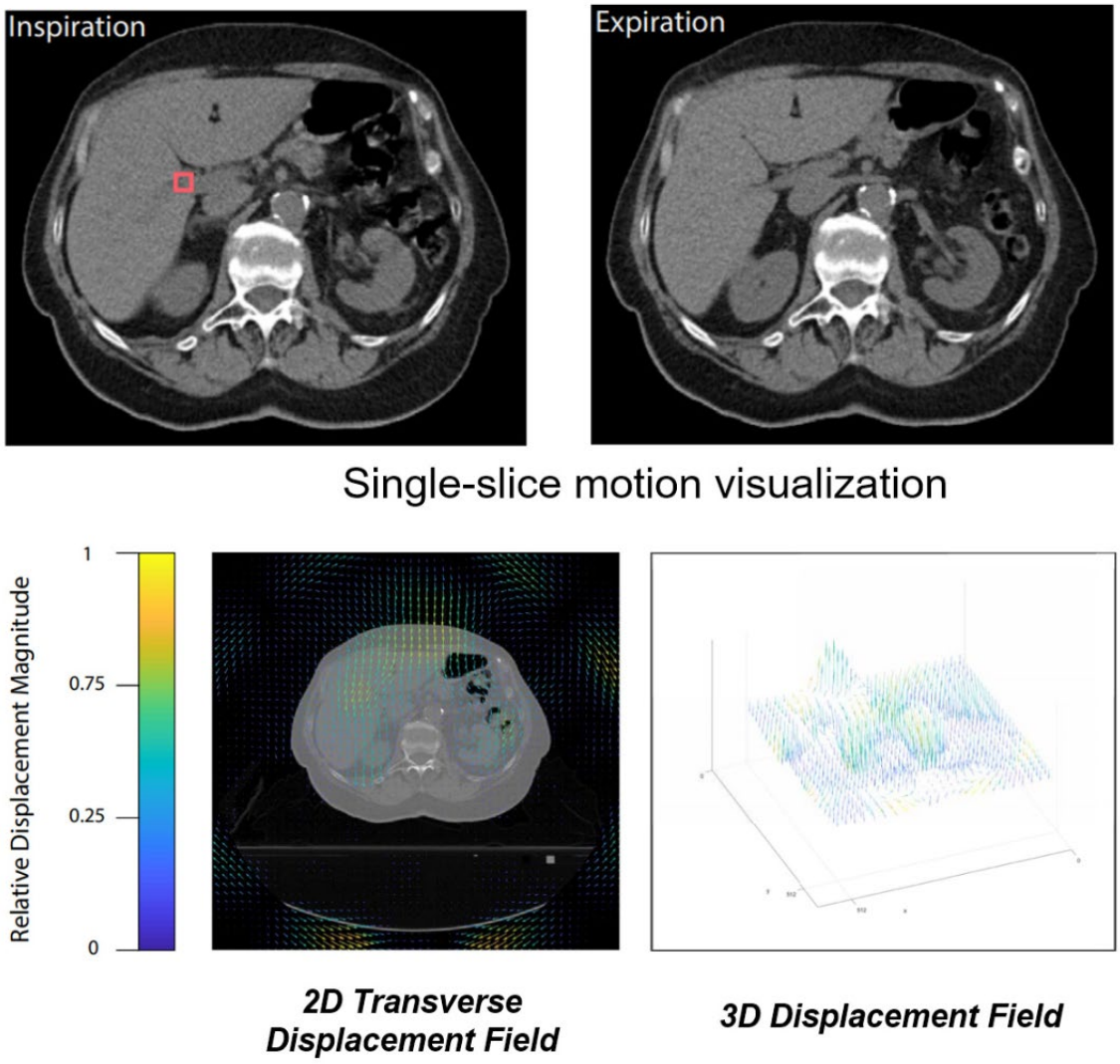

Figure 2: Representative motion displacement field images

Representative slices from one case showing an inspiratory and expiratory phase with the porta hepatis VOI highlighted (pink) in the inspiratory-phase. A 2D Vector map showing the transverse-plane deformation as well as a 3D vector map showing 3D displacement for the representative slice is shown.

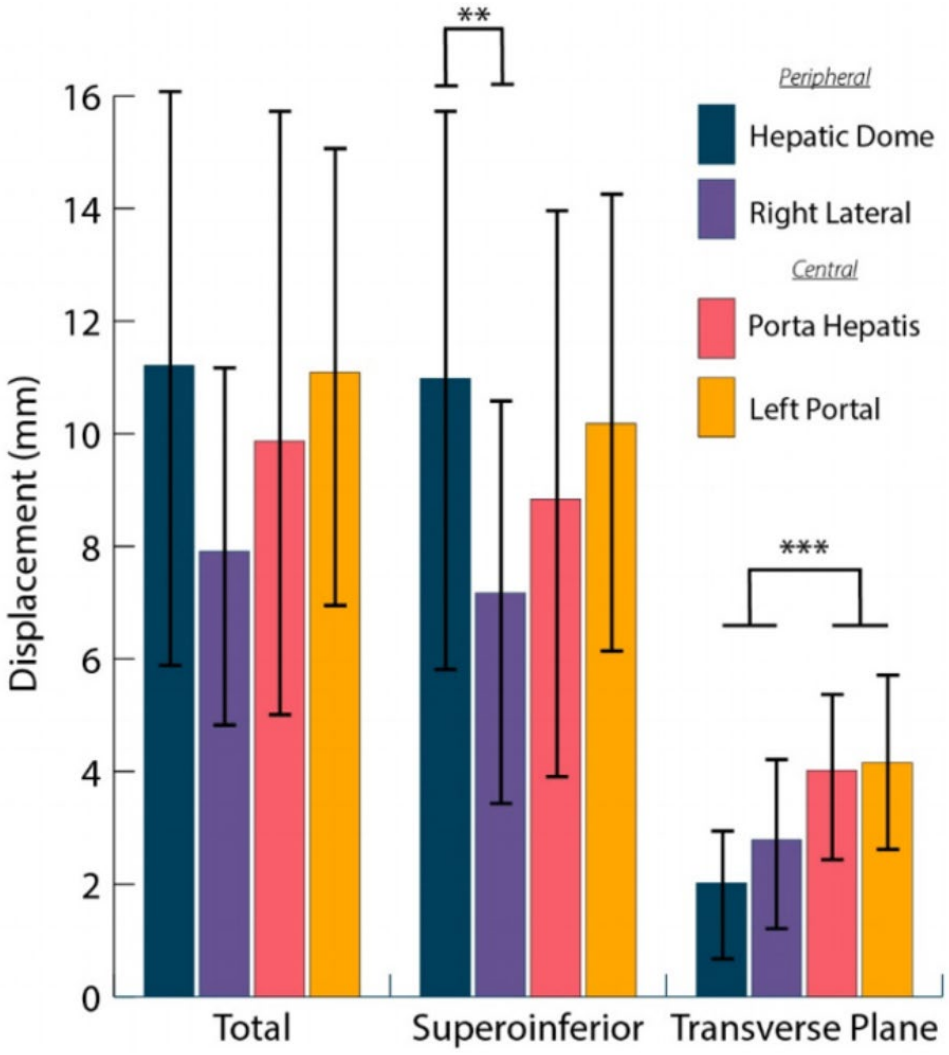

Figure 3: Magnitude of intra-hepatic motion stratified by location

Analysis of the mean total, superoinferior, and transverse-plane displacements in different VOIs. There is a significant increase in transverse-plane deformation in central regions relative to peripheral regions. There is also a significant decrease in superoinferior translation as distance to the diaphragm increases.

3.6 Validation of a Motion-Compensation Technique for Intra-Acquisition Respiratory Motion During 3D DSA

3.6.1 Materials and Methods

Digital Phantom Liver Study

6 digital liver phantoms (3 male, 3 female) were created by generating synthetic hepatic arterial trees and superimposing the vasculature onto a digital phantom of the background anatomy (XCAT, version 2.0, Durham, NC) (Figure 1). To simulate motion-corrupted acquisitions, motion due to a single respiratory cycle (simulated respiratory rate) was simulated and introduced during a random point during the simulated image acquisition. Full x-ray system imaging, geometry and rotational parameters are described by Whitehead et al. (24). Motion-corrupted, and motion-corrected reconstructions were compared to stationary volumes, respectively, using a Dice similarity coefficient (25).

In Vivo Porcine Liver Study

All procedures were approved by the institutional research animal care and use committee and were compliant with regulatory guidelines. Hepatic angiography was performed in the liver of one swine (50 kg). The subject was sedated with an intramuscular administration of 7 mg/kg of tiletamine hydrochloride-zolazepam

hydrochloride (Xyla-Ject; Phoenix Pharmaceutical, St. Joseph, Missouri), endotracheally intubated, and then underwent anesthesia induction and maintenance with 2% inhaled isoflurane (Halocarbon Laboratories, River Edge, New Jersey).

All procedures were performed in an angiography suite (Artis zee; Siemens Healthineers, Forcheim, Germany). Femoral arterial access was obtained and the common hepatic artery selected with a 5 Fr angled glide catheter. A series of 5 hepatic 3D-DSAs (2.5 mL/s iodinated contrast injection, 12 second rotations) were acquired: 4 with respiratory motion(4-6 respiratory cycles each) in the scan (ventilated-mask, free breathing-mask, ventilated-fill, free breathing-fill) and 1 breath-held scan. All motion-corrupted acquisitions were reconstructed with and without the motion-correction algorithm and compared to a breath-held reconstruction using a Dice similarity coefficient.

Motion-Compensation Technique

The motion-correction algorithm (Figure 2) wasimplemented in custom-built MATLAB program (ver. 2021b) (Figure 3). The algorithm was adapted from a previously described approach for 4D-DSA intra-acquisition motion-compensation (26). First, the algorithm performs a 2D-deformable (elastic) registration to align corresponding mask and fill projections using the diffeomorphic demons approach (21). This method

estimates a smooth vector field of translation vectors for each pixel in the corresponding mask and fill images frames. The mask frame is then transformed and subtracted from the corresponding fill frame to remove anatomical background. The corrected projections are subtracted and subsequently filtered using a Gaussian filter to remove excess image noise and minimize registration artifacts. A center of mass calculation in the projection images tracks the cranial-caudal position of the liver in order to select subsets of projections acquired during similar respiratory states. A weighted average of the intensity in the y-direction can be to calculate center of mass over consecutive time frames. The peaks representing the time frames of maximum inspiration are identified by extracting all local maxima with a prominence larger than a threshold. The minima between two peaks represent maximum expiration frames. The 3D constraint volume is reconstructed from a subset of subtracted projection images acquired in a similar respiratory state (typically the pre-inspiratory pause. An iterative compressed sensing reconstruction (multiplicative algebraic reconstruction) is used to perform the 3D reconstruction from a reduced set of projection images excluding motion-corrupted projections (Figure 4) (27). It iteratively adjusts an initial guess to minimize the projection error between the forward projection of the estimated solution and the subtracted projection images.

3.6.2 Results

Digital Phantom Liver Study

The Dice coefficients for motion-corrected and motion-corrupted images were 0.64± .19 and 0.26 ± 0.07 respectively ($p = 0.01$) (Figure 4). The motion correction algorithm resulted in images with fewer motion artifacts and improved visualization of distal hepatic artery branches when compared to motion-corrupted images.

In Vivo Porcine Liver Study

When maximal respiratory motion occurred during either the mask or fill, the Dice coefficients for motion-corrected and uncorrected images were 0.30 ± .11 and 0.08± 0.12 respectively ($p = 0.01$) (Figures 5, 6). The motion compensation algorithm resulted in higher Dice coefficients when motion occurred during the mask, 0.40 ± 0.03, than when motion occurred during the fill, 0.20 ± 0.04 ($p = 0.02$).

3.6.3 Figures

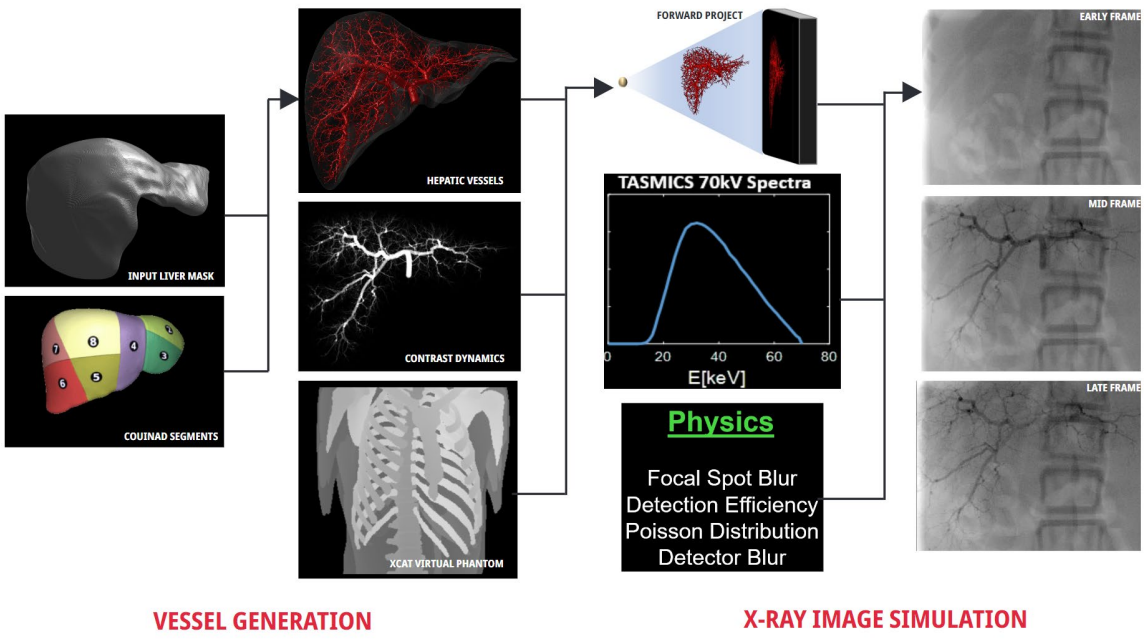

Figure 1: Digital hepatic vasculature phantom generation algorithm

Generation of the digital liver phantom. Hepatic arteries are formed through the connection of points (within Couinad segments) chosen within the liver mask and connected via the minimization of a physiological based cost function. Contrast dynamics are simulated and the vessels are then combined with the XCAT virtual phantom for anatomical background. The phantom is forward projected (with approximated X-ray acquisition parameters) to generate simulated fluoroscopic image sequences of contrast enhanced hepatic arteries (adapted from J. Whitehead, Medical Imaging SPIE 2020).

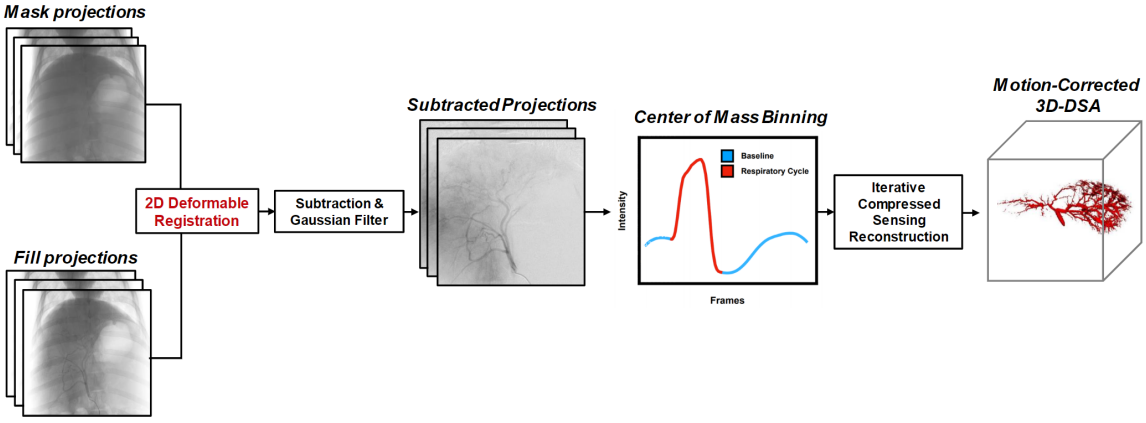

Figure 2: Intra-acquisition motion compensation algorithm

Algorithm for performing intra-acquisition motion compensation during 3D-DSA acquisitions. Mask and fill projection images are registered using a deformable 2D registration. After subsequent subtraction and filtering a center of mass calculation is used to exclude projection images acquired during respiration from the iterative reconstruction.

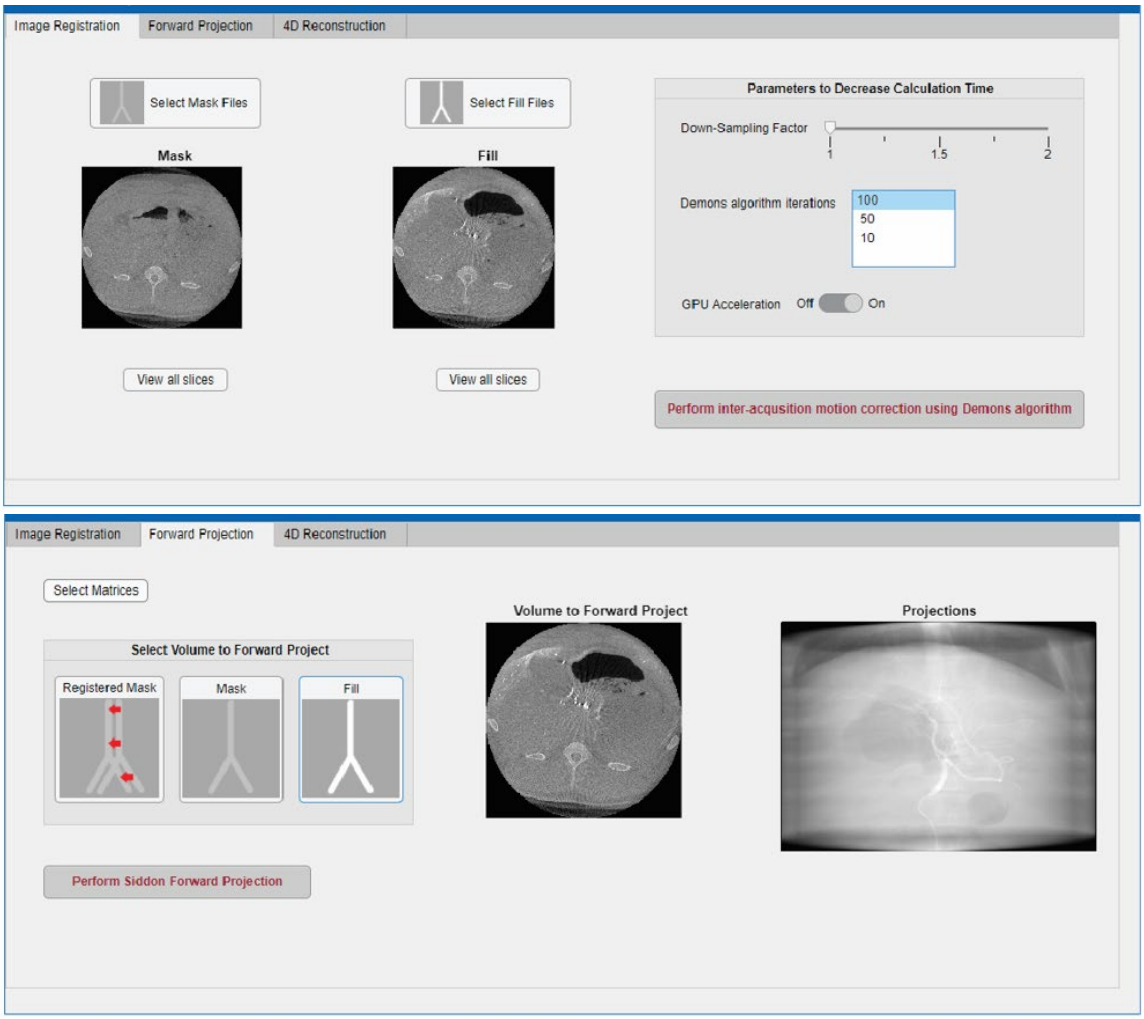

Figure 3: Custom-built MATLAB tool for performing motion-compensation and reconstructions

An in-house developed MATLAB application for performing inter- and intra-acquisition motion correction. The tool has multiple tabs including registration, projection, and reconstruction tabs for each stage in the motion compensation method. In the image registration tab, the user can select (and view) the mask and fill volumes. Before

performing 2D or 3D registration, the user can select different parameters (down-sample the image, decrease the iterations in the registration, use GPU processing) to decrease the time for registration. In the projection tab, the user can select the matrices from the acquisition, select the volume to perform forward projection on, and visualize the volume before and after forward projection. The reconstruction tab includes the ability to calculate the constraint volume and perform a time-resolved reconstruction.

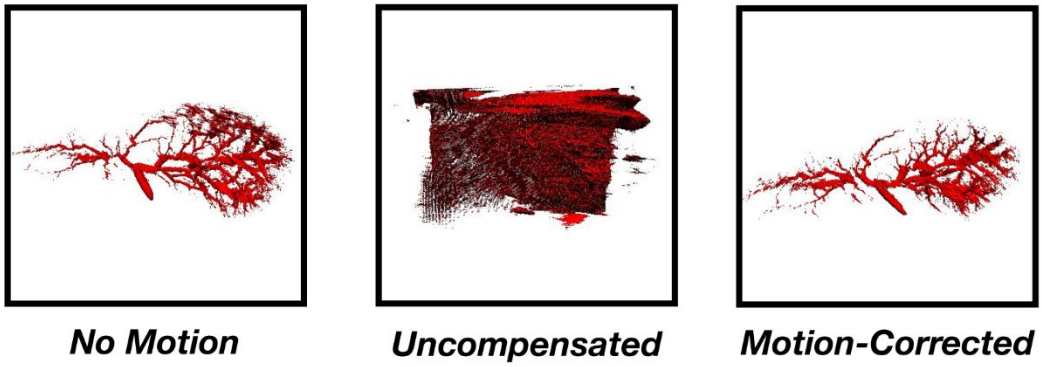

Figure 4: Representative images of motion-compensation in a digital liver phantom

Intra-acquisition motion correction performed in a digital liver phantom. Motion-corrected 3D-DSAs (bottom) resulted in significant reduction of artifacts and increased preservation of distal vessel anatomy.

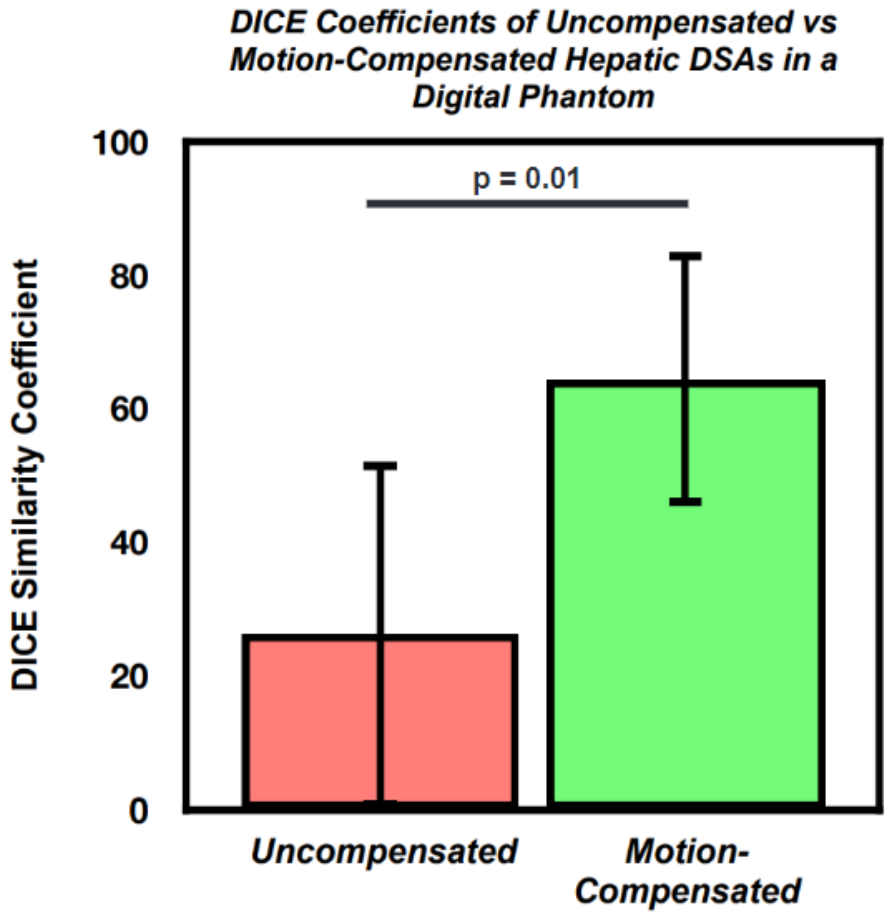

Figure 5: DICE similarity of uncompensated and motion-compensated 3D-DSAs

Motion-corrupted 3D-DSAS of the hepatic vasculature in digital liver phantoms had significantly larger DICE similarity coefficients to stationary images when the motion-correction algorithm was applied compared to those that were uncompensated.

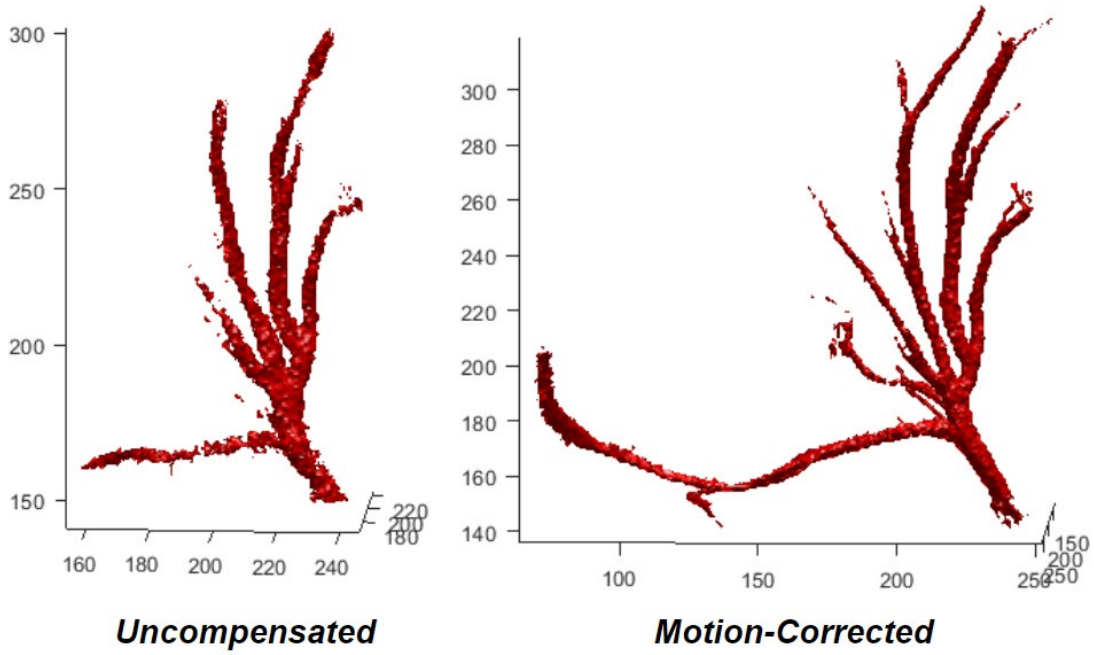

Figure 6: Representative images of in vivo motion compensation

Motion-corrupted 3D-DSAS of the hepatic vasculature in an in vivo porcine liver model had significantly larger DICE similarity coefficients to breath-held images when the motion-correction algorithm was applied compared to those that were uncompensated. Motion-compensated images have increased resolution of distal arteries and fewer subtraction artifacts compared to uncompensated images.

3.7 Discussion

Several advanced qDSA techniques were investigated in order to integrate qDSA into the modern imaging and procedural workflow.

Super-selective qDSA (ss-qDSA) in the distal hepatic arteries is feasible and there is a two-fold increase in the strength of contrast signal time oscillations (the signal which is used for qDSA calculations). The increase in the strength of contrast signal time oscillations in ss-qDSA may improve accuracy and reproducibility of blood velocity calculations in smaller vessels such as tumor-feeding arteries. The superior ability to measure pulsatility in smaller arteries using ss-qDSA may improve the clinical translatability of qDSA as it permits the use of microcatheter injections rather than injections through a base catheter. This feasibility study was only investigated with one injection flow rate. Future investigations may explore alternative injection protocols, including temporally-modulated injections, in order to further optimize velocity quantification in smaller arteries.

Volumetric qDSA (vqDSA) was able to characterize linear intra-procedural reductions in hepatic arterial blood flow during embolization. Vessel cross-sectional area remained relatively consistent throughout the procedure, suggesting that a single-pre

procedure 3D image (either a 3D-DSA or a contrast-enhanced CBCT) can be used in combination with conventional intra-procedural qDSA acquisitions to calculate reductions in blood flow during transarterial embolization. Importantly, the use of 3D geometry improves the accuracy of vqDSA over conventional qDSA as it is less susceptible to errors due to distance, magnification, and foreshortening which are more difficult to estimate with 2D imaging. Ultimately the ability to calculate flow rather than velocity gives a more complete characterization of the hemodynamic changes occurring embolization.

In characterizing respiratory motion within the liver, the primary effect of respiratory motion on the liver is superoinferior translation, but there is a significant transverse-plane deformation component as well. The degree of superoinferior translation is correlated with the distance from the diaphragm; as the distance from the diaphragm increases, the amount of superoinferior translation decreases. Centrally within the liver, near the hepatic vasculature, there was a statistically significant increase in transverse-plane deformation relative to more peripheral regions.. These findings suggest the value of incorporating non-rigid correction in the development of advanced motion-compensation techniques for hepatic angiography.

Based on the significant deformation component in intra-hepatic motion, a deformable registration technique was incorporated into the motion-compensation method. The digital liver phantoms were able to simulate clinically relevant 3D-DSAs of the liver in both stationery and motion-corrupted acquisitions. When an intra-acquisition motion-correction algorithm was applied to 3D-DSAs acquired in a digital liver phantom with simulated motion, motion-corrected images had a significantly larger Dice similarity coefficient compared to images corrupted by motion. In an in vivo model, when maximal respiratory motion occurred during either the mask or fill run of a 3D-DSA, the motion corrected images were more similar to the breath-held images than those uncorrected. Furthermore, the performance of the motion correction algorithm was better if motion occurred during the mask rather than the fill. This suggests that motion mitigation strategies (e.g. breath-holds) may be better focused on fill acquisitions in order to improve image quality. The combination of simulated and animal data indicate that proposed motion correction algorithm is feasible.

In conclusion, advanced qDSA techniques are feasible. These technique may improve the accuracy and consistency of the technique in addition to making them more clinically translatable.

3.8 References

1. Llovet JM, Real MI, Montaña X, Planas R, Coll S, Aponte J, Ayuso C, Sala M, Muchart J, Solà R, Rodés J, Bruix J; Barcelona Liver Cancer Group. Arterial embolisation or chemoembolisation versus symptomatic treatment in patients with unresectable hepatocellular carcinoma: a randomised controlled trial. Lancet. 2002 May 18;359(9319):1734-9. doi: 10.1016/S0140-6736(02)08649-X. PMID: 12049862.

2. Wang C, Mao Q, Tan F, Shen B. Superselective renal artery embolization in the treatment of renal hemorrhage. Ir J Med Sci. 2014 Mar;183(1):59-63. doi: 10.1007/s11845-013-0972-4. Epub 2013 Jun 4. PMID: 23733504.

3. Tanaka M, Valavanis A. Role of superselective angiography in the detection and endovascular treatment of ruptured occult arteriovenous malformations. Interv Neuroradiol. 2001 Dec 22;7(4):303-11. doi: 10.1177/159101990100700404. Epub 2002 Jan 10. PMID: 20663362; PMCID: PMC3621043.

4. Chuang VP, Soo CS, Carrasco CH, Wallace S. Superselective catheterization technique in hepatic angiography. AJR Am J Roentgenol. 1983 Oct;141(4):803-11. doi: 10.2214/ajr.141.4.803. PMID: 6604435.

5. Itsubo M, Koike K, Tsuno S, Osada M, Komuro O, Shimada N, Okuda J, Fukada H, Okuaki Y, Kawabe T, Toda G. Subsegmental transcatheter arterial embolization for small hepatocellular carcinoma. Hepatogastroenterology. 2002 May-Jun;49(45):735-9. PMID: 12063981.

6. Matsui O, Kadoya M, Yoshikawa J, Gabata T, Takashima T, Demachi H. Subsegmental transcatheter arterial embolization for small hepatocellular carcinomas: local therapeutic effect and 5-year survival rate. Cancer Chemother Pharmacol. 1994;33 Suppl:S84-8. doi: 10.1007/BF00686674. PMID: 8137490.

7. Matsui O, Kadoya M, Yoshikawa J, Gabata T, Arai K, Demachi H, Miyayama S, Takashima T, Unoura M, Kogayashi K. Small hepatocellular carcinoma: treatment with

subsegmental transcatheter arterial embolization. Radiology. 1993 Jul;188(1):79-83. doi: 10.1148/radiology.188.1.8390073. PMID: 8390073.

8. Park JH, Han JK, Chung JW, Choi BI, Han MC, Kim YI. Superselective transcatheter arterial embolization with ethanol and iodized oil for hepatocellular carcinoma. J Vasc Interv Radiol. 1993 May-Jun;4(3):333-9. doi: 10.1016/s1051-0443(93)71869-2. PMID: 8390316.

9. A.C. Miracle, S.K. Cone beam CT of the Head and Neck, Part 1: Physical Principles Mukherji.American Journal of Neuroradiology Jun 2009, 30 (6) 1088-1095;

10. Pung L, Ahmad M, Mueller K, Rosenberg J, Stave C, Hwang GL, Shah R, Kothary N. The Role of Cone-Beam CT in Transcatheter Arterial Chemoembolization for Hepatocellular Carcinoma: A Systematic Review and Meta-analysis. J Vasc Interv Radiol. 2017 Mar;28(3):334-341. doi: 10.1016/j.jvir.2016.11.037. Epub 2017 Jan 18. PMID: 28109724.

11. Gonzalez-Aguirre, Adrian, J.; Petre, Elena, N.; Hsu, Meier, S.; Moskowitz, Chaya, B.; Solomon, Stephen, C.; Durack, Jeremy, C.CardioVascular and Interventional Radiology, 2018, Vol.41(6), pp.898-904

12. Louie JD, Kothary N, Kuo WT, Hwang GL, Hofmann LV, Goris ML, Iagaru AH, Sze DY. Incorporating cone-beam CT into the treatment planning for yttrium-90 radioembolization. J Vasc Interv Radiol. 2009 May;20(5):606-13. doi: 10.1016/j.jvir.2009.01.021. Epub 2009 Apr 5. PMID: 19345589.

13. Liu WP, Otake Y, Azizian M, Wagner OJ, Sorger JM, Armand M, Taylor RH. 2D-3D radiograph to cone-beam computed tomography (CBCT) registration for C-arm image-guided robotic surgery. Int J Comput Assist Radiol Surg. 2015 Aug;10(8):1239-52. doi: 10.1007/s11548-014-1132-7. Epub 2014 Dec 12. PMID: 25503592; PMCID: PMC4476946.

14. Frysch R, Pfeiffer T, Rose G. A novel approach to 2D/3D registration of X-ray images using Grangeat's relation. Med Image Anal. 2021 Jan;67:101815. doi: 10.1016/j.media.2020.101815. Epub 2020 Sep 30. PMID: 33065470.

15. Lorenzo Monfardini, Franco Orsi, Rosalba Caserta, Claudio Sallemi, Paolo Della Vigna, Guido Bonomo, Gianluca Varano, Luigi Solbiati & Giovanni Mauri (2018)

Ultrasound and cone beam CT fusion for liver ablation: technical note, International Journal of Hyperthermia, 35:1, 500-504

16. Yabo Fu, Yang Lei, Yingzi Liu, Tonghe Wang, Walter J. Curran, Tian Liu, Pretesh Patel, and Xiaofeng Yang "Cone-beam Computed Tomography (CBCT) and CT image registration aided by CBCT-based synthetic CT", Proc. SPIE 11313, Medical Imaging 2020: Image Processing, 113132U (10 March 2020); https://doi.org/10.1117/12.2549095

17. Lee IJ, Chung JW, Yin YH, Kim H-C, Kim YI, Jae HJ, et al. Cone-Beam Computed Tomography (CBCT) Hepatic Arteriography in Chemoembolization for Hepatocellular Carcinoma: Performance Depicting Tumors and Tumor Feeders. Cardiovasc Intervent Radiol. 2015 Oct;38(5):1218–30. 29.

18. Lee IJ, Chung JW, Yin YH, Kim H-C, Kim YI, Jae HJ, et al. Cone-beam CT hepatic arteriography in chemoembolization for hepatocellular carcinoma: angiographic image quality and its determining factors. J Vasc Interv Radiol. 2014 Sep;25(9):1369–79–quiz1379–.e1.

19. Dandekar O, Walimbe V, Shekhar R. Hardware implementation of hierarchical volume subdivision-based elastic registration. Conf Proc IEEE Eng Med Biol Soc. IEEE; 2006;1:1425–8. 31.

20. Siddon RL. Fast calculation of the exact radiological path for a three-dimensional CT array. Med Phys. 1985 Mar;12(2):252–5. 32.

21. Vercauteren T, Pennec X, Perchant A, Ayache N. Diffeomorphic demons: efficient non-parametric image registration. Neuroimage. 2009 Mar;45(1 Suppl):S61–72. 33.

22. Byrne C. Choosing parameters in block-iterative or ordered subset reconstruction algorithms. IEEE Trans Image Process. 2005 Mar;14(3):321–7.

23. Chen GH, Tang J, Leng S. Prior image constrained compressed sensing (PICCS): a method to accurately reconstruct dynamic CT images from highly undersampled projection data sets. Med Phys. 2008;35(2):660-663.

24. Joseph F. Whitehead, Ethan P. Nikolau, Sarvesh Periyasamy, Luis A. Torres, Paul F. Laeseke, Michael A. Speidel, and Martin G. Wagner "Simulation of hepatic arteries and

synthesis of 2D fluoroscopic images for interventional imaging studies", Proc. SPIE 11312, Medical Imaging 2020: Physics of Medical Imaging, 113121W (16 March 2020); https://doi.org/10.1117/12.2549570

25. Zou KH, Warfield SK, Bharatha A, Tempany CM, Kaus MR, Haker SJ, Wells WM 3rd, Jolesz FA, Kikinis R. Statistical validation of image segmentation quality based on a spatial overlap index. Acad Radiol. 2004 Feb;11(2):178-89. doi: 10.1016/s1076-6332(03)00671-8. PMID: 14974593; PMCID: PMC1415224.

26. Martin Wagner, Paul Laeseke, Colin Harari, Sebastian Schafer, Michael Speidel, and Charles Mistretta "Feasibility of intra-acquisition motion correction for 4D DSA reconstruction for applications in the thorax and abdomen", Proc. SPIE 10574, Medical Imaging 2018: Image Processing, 1057415 (2 March 2018); https://doi.org/10.1117/12.2293812

27. Byrne, C., "Choosing parameters in block-iterative or ordered subset reconstruction algorithms," IEEE Trans. Image Process, 14 (3), 321 –327 (2005). https://doi.org/10.1109/TIP.2004.841193

Chapter 4: Quantitative Digital Subtraction Angiography (qDSA): Non-Oncologic Application

Portions of this chapter were submitted to or presented at the following scientific meetings:

Periyasamy S, Hoffman CA, Schefelker G, Speidel M, Laeseke PF. A Quantitative Angiography Technique Using Time-Resolved 2D-DSA for Determining Treatment Endpoints in Partial Splenic Embolization. SIR 2020. Virtual. March 2020. Poster

Periyasamy S, Kutlu A, Pieper AA, Whitehead J, Hoffman CA, Speidel M, Laeseke PF. Using a Quantitative Digital Subtraction Angiography Technique to Determine Treatment Endpoints in Partial Splenic Artery Embolization: Feasibility in an In Vivo Porcine Model. Submitted to RSNA 2022. Chicago, IL. November 2022.

4.1 Introduction

Following successful demonstration of qDSA for application in cancer therapy, we sought to determine how qDSA could be used for non-oncologic applications. One application which would benefit from quantitative treatment endpoints is partial splenic artery embolization. This chapter explores the feasibility of performing intra-procedural splenic qDSA, how it correlates with other measures of splenic and portal venous hemodynamics, and how the flow dynamics may differ through the use of different size embolic particles.

4.2 Motivation

Cirrhosis is the 8th leading cause of death in the United States and the 13th worldwide (1,2). A major consequence of cirrhosis is portal hypertension (PHT) which can lead to a number of complications including variceal hemorrhage, ascites, and hepatic encephalopathy (3). Splenomegaly and hypersplenism are also major secondary complications resulting from portal congestion which can increase morbidity and mortality due to bleeding risk from thrombocytopenia (among other cytopenias) (4-7). TIPS is the preferred interventional therapy for PHT, but carries a number of absolute and relative contraindications (8). Splenectomy is another option for treating the splenic effects of PHT, but there is a significant risk of surgical complications including abscess formation (9,10). Partial splenic artery embolization (PSE) is a promising method for treating PHT and associated splenomegaly or hypersplenism, and it may be an effective alternative to TIPS or splenectomy (11,12).

PSE is most commonly performed by targeting distal splenic artery branches in order to embolize splenic segments to sub- or complete-stasis (13). Alternatively, embolization may be performed at a proximal segment of the splenic artery to induce diffuse infarcts. In both techniques, the typical aim is to embolize a significant (30-70%)

percentage of the splenic parenchymal volume in order to achieve the treatment effect. This often necessitates the induction of significant ischemia, which increases the rate of infarction-related complications such as abscess formation. It has been demonstrated that the extent of embolization has a direct relationship with the severity of post-PSE complications, but intra-procedural determination of that extent is largely based on subjective angiographic assessments (14,15). In TACE and balloon angioplasty, visual assessments of digital subtraction angiography (DSA) were shown to be poorly reproducible and poorly correlated with outcomes (16,17). A flow-based metric, which quantifies global reduction in blood flow to the spleen, would help complications. It would allow incremental reduction of splenic arterial flow to a degree which avoids ischemia and infarction-related effects whilst still achieving the desired therapuetic effect. Such an objective metric would standardize procedures and allow for the identification of optimal PSE endpoints.

Prior attempts in developing intra-procedural embolization endpoints include volumetric techniques such as quantitative 4D transcatheter intra-arterial perfusion MRI and quantitative 4D-DSA(18-20); the techniques, however, required specialized infrastructure or complex, lengthy imaging protocols. Peri-procedural perfusion imaging (e.g. MRI or CT) has been shown to aid in treatment assessment, but lack the ability to

provide intra-procedural guidance (21-23). Other methods with promise include commercially available 2D techniques. One such technique is 2D-parametric parenchymal blood flow (2D-PPBF), which measures wash-in-time (WIT), time-to-peak (TTP), and area-under-the-curve (AUC) from the time-attenuation curves (TAC) of a region of interest within the target tissue (24-26). Another is quantitative color-coded DSA (QCC-DSA), which similarly uses WIT and TTP to estimate blood flow within a selected vessel (27,28). Although preliminary investigation using these techniques show feasibility, they suffer from limitations. Both techniques rely heavily on contrast arrival dynamics, which is a surrogate that approaches, but does not truly represent, hemodynamics (29,30). Contrast arrival metrics are susceptible to significant variability due to factors such as motion artifact, catheter position, vessel size, turbulent flow (from tortuosity), contrast concentration (due to viscosity) and vessel/tissue overlap.

We propose a flow-based partial splenic embolization technique incorporating a novel quantitative angiography technique (qDSA) which utilizes time-resolved 2D-DSA sequences to calculate blood velocity within a segment of a blood vessel (31). The qDSA method measures the velocity of transient contrast boluses that are developed from cardiac pulsatility within an artery (32,33). The major advantage of this over 2D-PPBF and QCC-DSA is that this produces a physiologic parameter, blood velocity, which is

closer to the true variable of interest in an embolization procedure: changes in blood flow. Additionally, this technique is spatially-averaged over the entire length of the blood vessel which makes it more robust than other 2D techniques, which generally compare signals from single pixels or regions of interest at different points within the vessel (34). This technique is not computationally-intensive and calculations can be performed within seconds-to-minutes of image acquisition, permitting near real-time assessment of blood flow changes and feasible integration into current interventional imaging systems. Perhaps most importantly, this method utilizes DSA and would therefore be minimally-intrusive to current PSE workflow, requiring only slight modifications to imaging protocols. We believe qDSA will improve the efficacy of PSE procedures by allowing for the intra-procedural identification of flow-based treatment endpoints. Furthermore, we believe qDSA can improve the safety of PSE by helping to avoid endpoints in which significant ischemia/infarction occur, which increases risk of complications.

The objective of this study was to demonstrate that (I) qDSA is a feasible technique for calculating reductions in splenic arterial blood flow velocity (BFV) during PSE, (II) qDSA-calculated reductions in splenic arterial blood velocity correlate with changes in splenic arterial, splenic venous, and portal venous blood flow during PSE, and

(III) qDSA is able to characterize differential reductions in splenic arterial blood flow depending on the embolization technique employed (i.e. different particle sizes).

4.3 Characterizing Reductions in Splenic and Portal Venous Blood Flow During Splenic Arterial Embolization Using qDSA

4.3.1 Materials and Methods

All procedures were approved by the institutional research animal care and use committee and were compliant with regulatory guidelines. Proximal splenic artery embolization was performed in the spleens of two swine (mean weight, 49.1 ± 2.4 kg). Subjects were sedated with an intramuscular administration of 7 mg/kg of tiletamine hydrochloride-zolazepam hydrochloride (Xyla-Ject; Phoenix Pharmaceutical, St. Joseph, Missouri), endotracheally intubated, and then underwent anesthesia induction and maintenance with 2% inhaled isoflurane (Halocarbon Laboratories, River Edge, New Jersey).

Splenic Arterial Embolization

All procedures were performed in an angiography suite (Artis zee; Siemens Healthineers, Forcheim, Germany). Femoral arterial access was obtained and the splenic

artery selected with a 5 or 4 Fr angled glide catheter. A 3D-DSA was acquired to delineate splenic arterial anatomy and determine an optimal projection angle. Prior to embolization, a 30 frames per second (fps) 2D-DSA of the splenic artery was acquired using an injection of iohexol 300 mg/mL (Omnipaque 300; GE Healthcare, Waukesha, Wisconsin. All DSA images were acquired with paralytic-induced (vecuronium) breath holds.

In each animal, bland embolizations (n=2) were performed given that the primary objective of the study was to characterize reductions in blood flow velocity. An embolization was performed using 100-300 um microspheres (Embosphere Microsphere; Merit Medical Systems, South Jordan, Utah) diluted in 10 mL of ioxhexol 300 mg/mL. After each delivery of 1 mL aliquots, a DSA image (See Table 1 for imaging parameters) was acquired via stationary base catheter in the proximal splenic artery in order to generate blood velocity reduction-embolization curves to better characterize changes in velocity throughout embolization. In these embolizations, there was a minimum of two minutes between microcatheter withdrawal and subsequent imaging in order to minimize any effects of transient arterial spasm. Embolizations were performed till a complete stasis endpoint was achieved.

In one animal intra-procedural changes in splenic hemodynamics were assessed with indwelling intravascular Doppler wires (Phillips Volcano, San Diego, CA). One Doppler wire was left indwelling in the splenic artery, through the base catheter, several centimeters distal to the site of embolization. Transabdominal percutaneous access to the splenic vein was acquired and a second Doppler wire was left indwelling in the proximal splenic vein. Doppler ultrasound blood velocity measurements were made at the same time points as DSA image acquisitions.

In one animal, 4D-Flow MRI (using a PC VIPR technique) were acquired before and after embolization for multi-modal blood velocity reduction characterization (see Table 1 for imaging parameters). A semi-automated workflow for the 4D flow MRI analysis was developed in MATLAB 2018a. Angiograms were segmented using an adaptive region growing technique on the complex difference data. A 3D centerline path was generated to aid in the automatic placement of cross-sectional planes. Automatic segmentation of vessels was completed using a local thresholding technique and reported velocities were an average of all points along the vessel centerline.

qDSA Method

The qDSA method uses inherent oscillations in the image contrast caused by arterial flow pulsatility as a trackable marker of BFV in the artery. The oscillatory image

signal is measured in the time-attenuation curves (TAC) of pixels along the centerline of a vessel. When two TACs from two pixels along the centerline of the vessel (separated by a distance) are superimposed, the temporal shift between the two functions represents the time of contrast transit along the vessel. An in vivo example of the TAC shift in a porcine spleen model is illustrated in Figure 1. Distances and temporal shifts (using a shifted-least squares approach, (35)) can be found for all pairs of points along the centerline of a vessel in order to calculate a spatially-averaged BFV in the vessel of interest. An algorithm employing the qDSA method was implemented in MATLAB (MATLAB R2018b version 9.5, MathWorks, Natick, Massachusetts) using a custom-built program.

ccDSA Method

A commercially available ccDSA method (syngo iFlow, Siemens Healthineers) was used to calculate time-to-peak (TTP) in the embolized vessel. A region-of-interest (ROI) was placed in the proximal segment of the vessel with diameter equal to the width of the vessel in order to estimate a TTP (Figure 1c). The segment of vessel analyzed was the same as that used for the qDSA analysis.

Image Analysis

A post-hoc analysis of all DSA images was performed using qDSA and ccDSA methods. A decrease in qDSA calculated BFV and an increase in ccDSA calculated TTP

was the expected result in response to a blood flow reduction due to embolization. qDSA calculations were performed on a laptop computer with 16 GB of RAM. ccDSA calculations were performed on the angiography suite workstation (Artis zee; Siemens Healthineers, Forcheim, Germany). 4D Flow MRI images were analyzed to quantify blood velocity in the splenic artery as well as cross-sectional area in the portal vein.

Statistical Analysis

To assess the correlation between qDSA and embolization, linear models were fit to the data for each animal, where qDSA was modeled as the response variable. From each model, the Pearson's correlation coefficient (r) and coefficient of determination (R2) were calculated. For assessment of the difference in pre- and post-embolization velocities on qDSA and MRI, paired sample t-tests were used. A p-value < 0.05 was considered statistically significant.

4.3.2 Results

Blood Flow Velocity Reduction During Embolization

In the embolization in which images and measurements were acquired throughout the procedure, there is a linear decrease in splenic arterial blood velocity as calculated by qDSA (Figure 2). There was a 7.4% reduction in blood velocity (from baseline) per 1 mL of embolic particles delivered. The correlation between qDSA-calculated blood velocity and amount of embolic particles delivered had a very strong correlation and coefficient of determination ($R = 0.95$, $R^2 = 0.90$). Indwelling intravascular Doppler wires in the splenic artery and vein showed congruent decreases in blood velocity of 11.0% ($R = 0.99$, $R^2 = 0.98$) and 9.7% ($R = 0.97$, $R^2 = 0.94$) reductions in velocities per 1 mL of particles delivered respectively.

Multi-Modal Comparison of Blood Velocity Reduction

In multimodal comparison, qDSA-calculated splenic arterial blood velocity showed a reduction of 54.3 ± 5.8 cm/s at baseline to 32.4 ± 2.5 cm/s post-embolization (Figure 3). This corresponded to a 40.3% reduction in velocity at the complete stasis endpoint. On 4D Flow MRI using PC VIPR and 100 VENC, maximum splenic arterial velocity was 31.5 cm/s at baseline (mean velocity: 16.4 cm/s) and 11.2 cm/s post embolization (mean velocity: 5.9 cm/s). This corresponded to a 64.1% reduction in

velocity at the complete stasis endpoint. Cross-sectional area in the portal vein, immediately distal to the junction of the splenic vein, was 207.8 mm^2 at baseline and 159.5 mm^2 post-embolization (Figure 4). This corresponded to a 23.2% reduction in portal vein cross-sectional area at the complete stasis endpoint. There was a slight decrease in portal vein flow from 14.6 mL/s to 13.8 mL/s near the splenic vein junction, although portal flow was maintained from other mesenteric veins.

4.3.3 Tables

Table 1: DSA and MR imaging parameters for blood velocity quantification

DSA Vessel	Injection Rate	Injection Time	Injection Volume	Frame Rate
Splenic Artery	2 mL/s	8 s	16 mL	30 FPS
MRI Vessel	Spatial Resolution	Scan Time	VENC	Time Frames
Splenic Artery	1 x 1 x 1 mm	18 s	100 cm/s	14

4.3.4 Figures

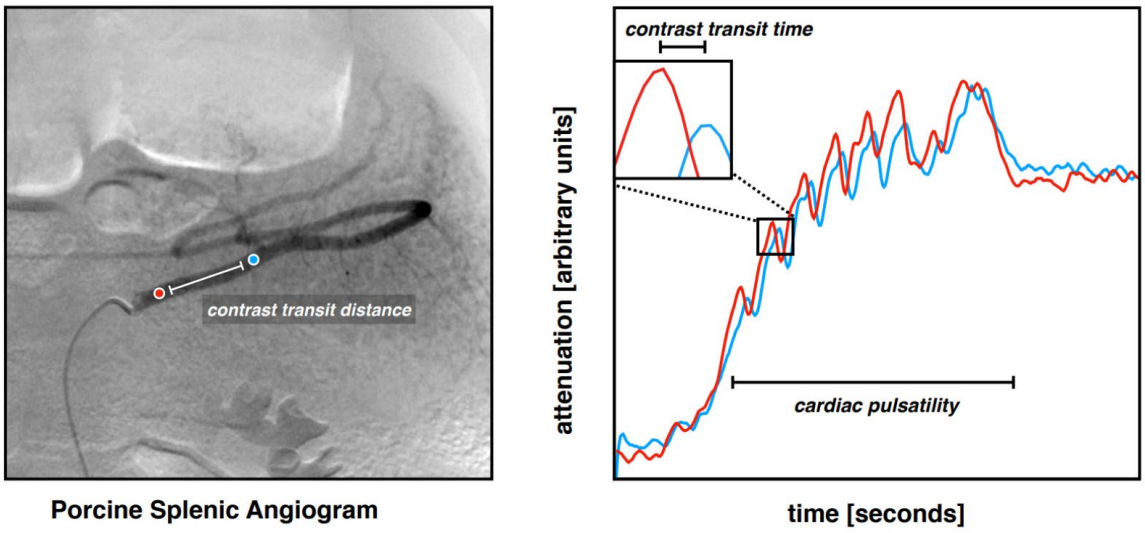

Figure 1: Example qDSA in an in vivo porcine spleen model

Within a vessel, a proximal (red) and distal point (blue) is analyzed. The time-attenuation curves (TAC) from the points are superimposed (right), illustrating a visible temporal shift. Using the distance between the points and a calculated temporal shift, a spatially-averaged blood velocity can be determined.

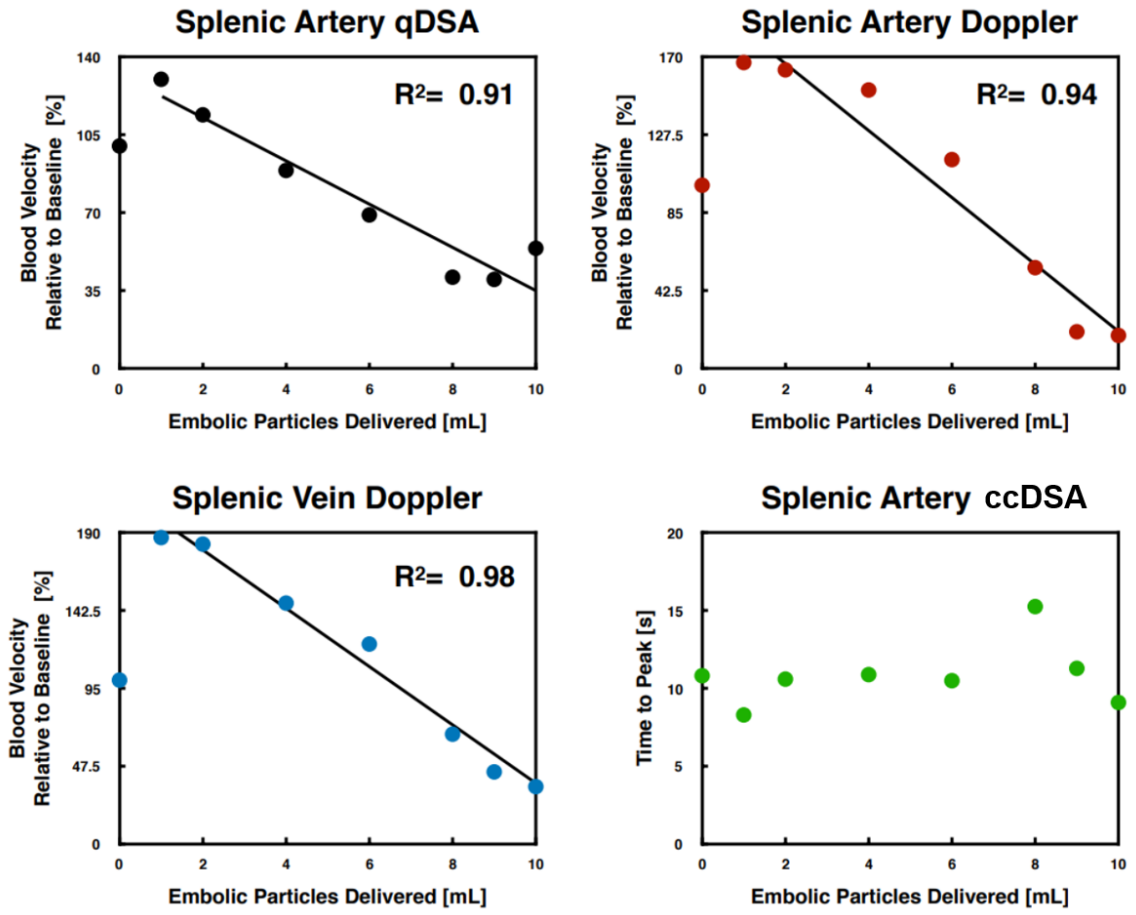

Figure 2: In vivo correlation of qDSA with intravascular Doppler and ccDSA

Splenic arterial blood velocity calculated via qDSA decreased linearly as embolic particles were delivered with a very strong correlation between qDSA-calculated blood velocity and embolic particles delivered. This linear decrease was congruent with measurements made in the splenic artery and vein using an intravascular Doppler wire, both of which also exhibited very strong linear correlations. A commercially available color-coded DSA technique had poor relationships with the amount of embolic particles delivered.

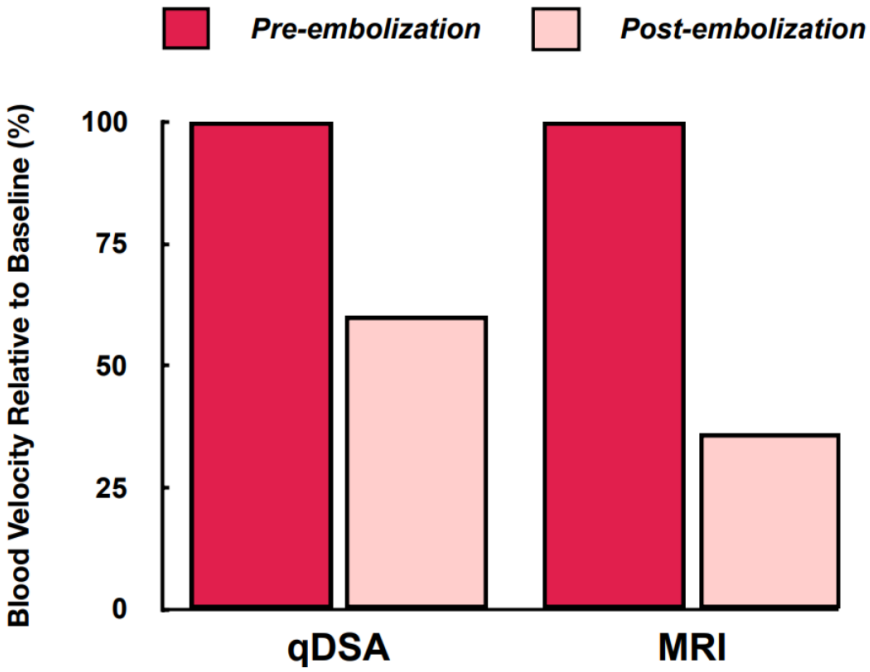

Figure 3: qDSA and MRI blood velocity reductions measured post-embolization

The velocity reduction in the splenic artery calculated using qDSA (40%) is comparable to the velocity reduction calculated using 4D Flow MRI PC VIPR technique (64%). Pre- and post-4D Flow MRIs showed a significant decrease in flow in the splenic vein as well.

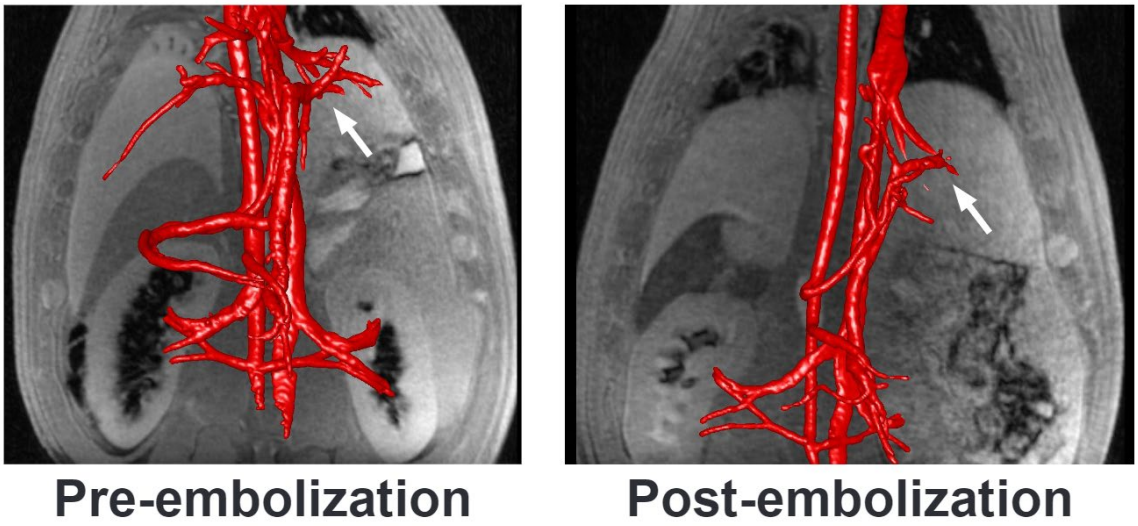

Figure 4: Pre- and post-embolization MRI images of the hepatic and splenic vasculature

Pre- and post-splenic embolization MR angiograms in a porcine model. There is decreased visualization of the splenic artery (arrow), splenic vein, and portal venous vasculature following embolization. Calculations of blood velocity using 4D Flow MRI (PC VIPR) show a 64.1% decrease in splenic arterial blood velocity following embolization. Measurements made in the portal vein indicate a 23.2% decrease in cross-sectional area following embolization which may be due to decreased total portal venous inflow .

4.4 Characterizing The Velocity Reduction in Splenic Arterial Embolization Using Embolic Particles of Varying Sizes

4.4.1 Materials and Methods

All procedures were approved by the institutional research animal care and use committee and were compliant with regulatory guidelines. Proximal splenic artery embolization was performed in the spleens of five swine (mean weight, 48.2 ± 3.3 kg). Subjects were sedated with an intramuscular administration of 7 mg/kg of tiletamine hydrochloride-zolazepam hydrochloride (Xyla-Ject; Phoenix Pharmaceutical, St. Joseph, Missouri), endotracheally intubated, and then underwent anesthesia induction and maintenance with 2% inhaled isoflurane (Halocarbon Laboratories, River Edge, New Jersey).

Splenic Arterial Embolization

All procedures were performed in an angiography suite (Artis zee; Siemens Healthineers, Forcheim, Germany). Femoral arterial access was obtained and the splenic artery selected with a 5 or 4 Fr angled glide catheter. A 3D-DSA was acquired to delineate splenic arterial anatomy and determine an optimal projection angle. Prior to embolization, a 30 frames per second (fps) 2D-DSA of the splenic artery was acquired

using an injection of iohexol 300 mg/mL (Omnipaque 300; GE Healthcare, Waukesha, Wisconsin. All DSA images were acquired with paralytic-induced (vecuronium) breath holds.

In each animal, bland embolizations (n=5) were performed given that the primary objective of the study was to characterize reductions in blood flow velocity. An embolization was performed using microspheres (Embosphere Microsphere; Merit Medical Systems, South Jordan, Utah) diluted in 10 mL of ioxhexol 300 mg/mL. Microspheres sizes used during embolization included 100-300 μm, 300-500 μm, and 500-700 μm particles. After each delivery of 1 mL aliquots, a DSA image (See Table 1 for imaging parameters) was acquired via stationary base catheter in the proximal splenic artery in order to generate blood velocity reduction-embolization curves to better characterize changes in velocity throughout embolization. In these embolizations, there was a minimum of two minutes between microcatheter withdrawal and subsequent imaging in order to minimize any effects of transient arterial spasm. Embolizations were performed to till a complete stasis angiographic endpoint was achieved. Image acquisition times were extended in order to capture portal venous filling of the liver. A field of view was selected to ensure visibility of portal vein and the splenic artery in the same acquisition.

Image Analysis

A post-hoc analysis of all DSA images was performed using qDSA and ccDSA methods. A decrease in qDSA calculated BFV was the expected result. A region of interest was selected in the visible portal vein in order to calculated time-to-peak using ccDSA. An increase in ccDSA calculated TTP was the expected result in response to a blood flow reduction due to embolization. qDSA calculations were performed on a desktop computer with 32 GB of RAM. ccDSA calculations were performed on the angiography suite workstation (Artis zee; Siemens Healthineers, Forcheim, Germany).

4.4.2 Results

Blood Flow Velocity Reduction During Embolization

In embolizations during which images were acquired throughout the procedure, there was a negative linear relationship between qDSA calculated blood velocities and the volume of embolic particles delivered in all five animals. The mean reduction in blood velocity from baseline was 28.3 ± 10.0% per mL of embolic particles delivered. There was a strong linear correlation and coefficient of determination between qDSA-calculated blood velocity and amount of embolic particles delivered (mean R = -0.97 ± 0.02, mean R2 = 0.94 ± 0.04). Embolizations performed with larger particles had larger overall post-embolization blood velocity reductions (300-500 μm: 88%, 500-700 μm: 90%, 82%) compared to embolizations performed with smaller particles (100-300 μm: 71%, 70%).

Portal Vein Time-to-Peak Increase During Embolization

There was a positive linear relationship between ccDSA calculated TTP contrast signal in the portal vein and the volume of embolic particles delivered in all five animals. There was a strong linear correlation and coefficient of determination between ccDSA-calculated TTP in the portal vein and amount of embolic particles delivered (mean R = 0.95 ± 0.02, mean R2 = 0.90 ± 0.05).

4.4.3 Tables

Table 1: DSA imaging parameters for blood velocity quantification

Embolic Particle Size	Injection Rate	Injection Time	Injection Volume	Acquisition Time	Frame Rate
100-300 (I)	2 mL/s	7 s	14 mL	20 s	30 FPS
100-300 (II)	2.5 mL/s	7 s	17.5 mL	20 s	30 FPS
300-500	2.5 mL/s	7 s	17.5 mL	20 s	30 FPS
500-700 (I)	2 mL/s	7 s	14 mL	20 s	30 FPS
500-700 (II)	2.5 mL/s	7 s	17.5 mL	20 s	30 FPS

4.4.4 Figures

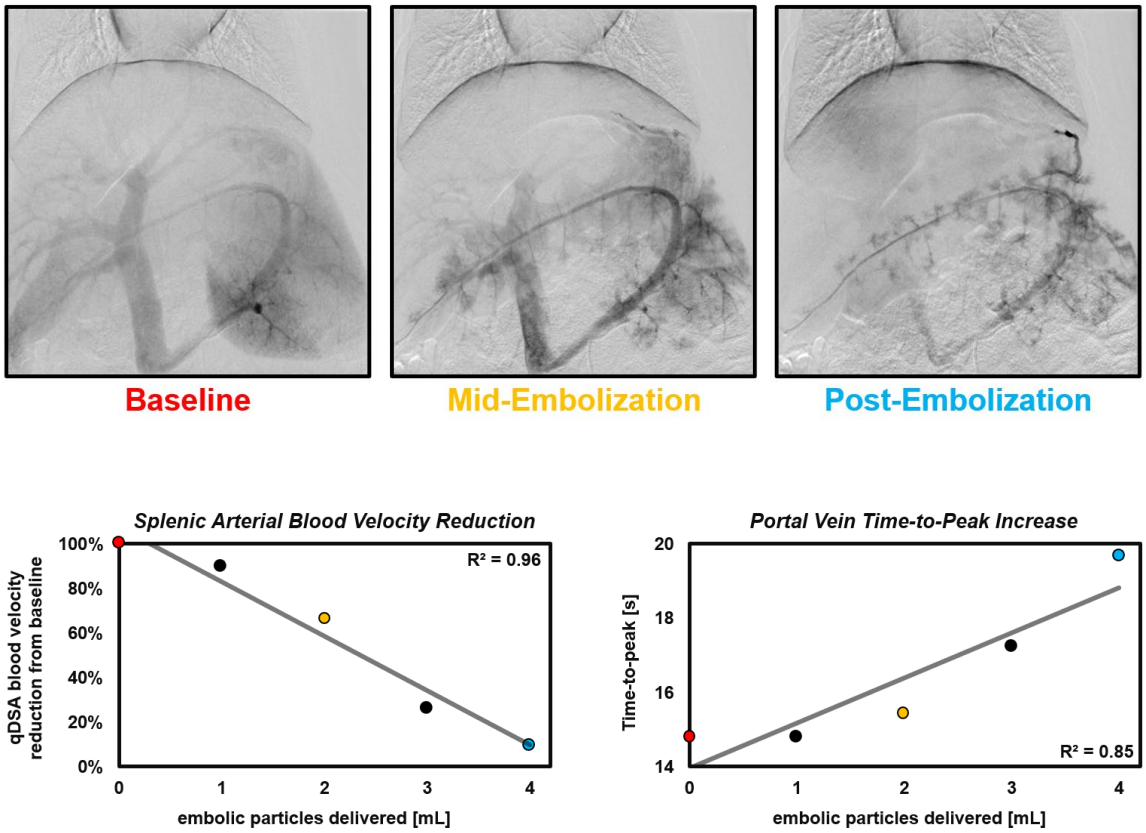

Figure 1: Representative splenic arterial embolization with qDSA and ccDSA

A representative splenic arterial embolization performed in a porcine model, using 500-700 μm embolic particles, demonstrates linear decrease in splenic arterial blood velocity and an increase in portal vein time-to-peak signal until a complete stasis endpoint is achieved. Angiographic images acquired at sequence matched time-points show patchy decreases in splenic parenchymal enhancement and progressive decrease in portal venous enhancement corresponding with increased delivery of embolic particles.

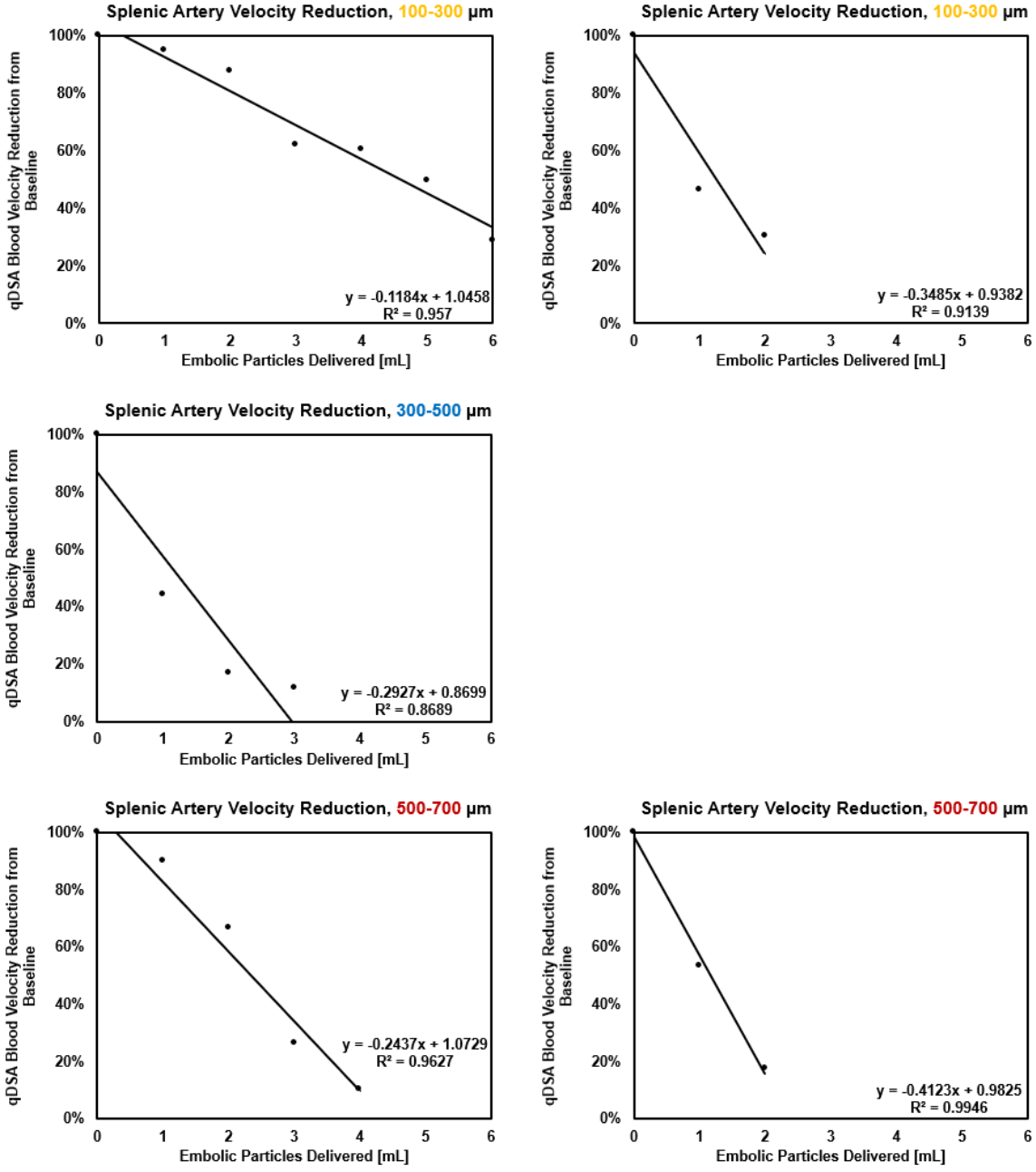

Figure 2: Complete qDSA blood velocity reduction curves from splenic artery embolizations stratified by embolic particle size

All splenic artery embolizations exhibited linear decreases in blood velocity relative to baseline as the embolization progressed. The was strong linear correlations between qDSA blood velocity and embolic particles delivered. Embolizations performed using larger particles (>300 μm) to complete stasis angiographic endpoints had larger overall blood velocity reductions compared to embolizations performed using small particles (100-300 μm).

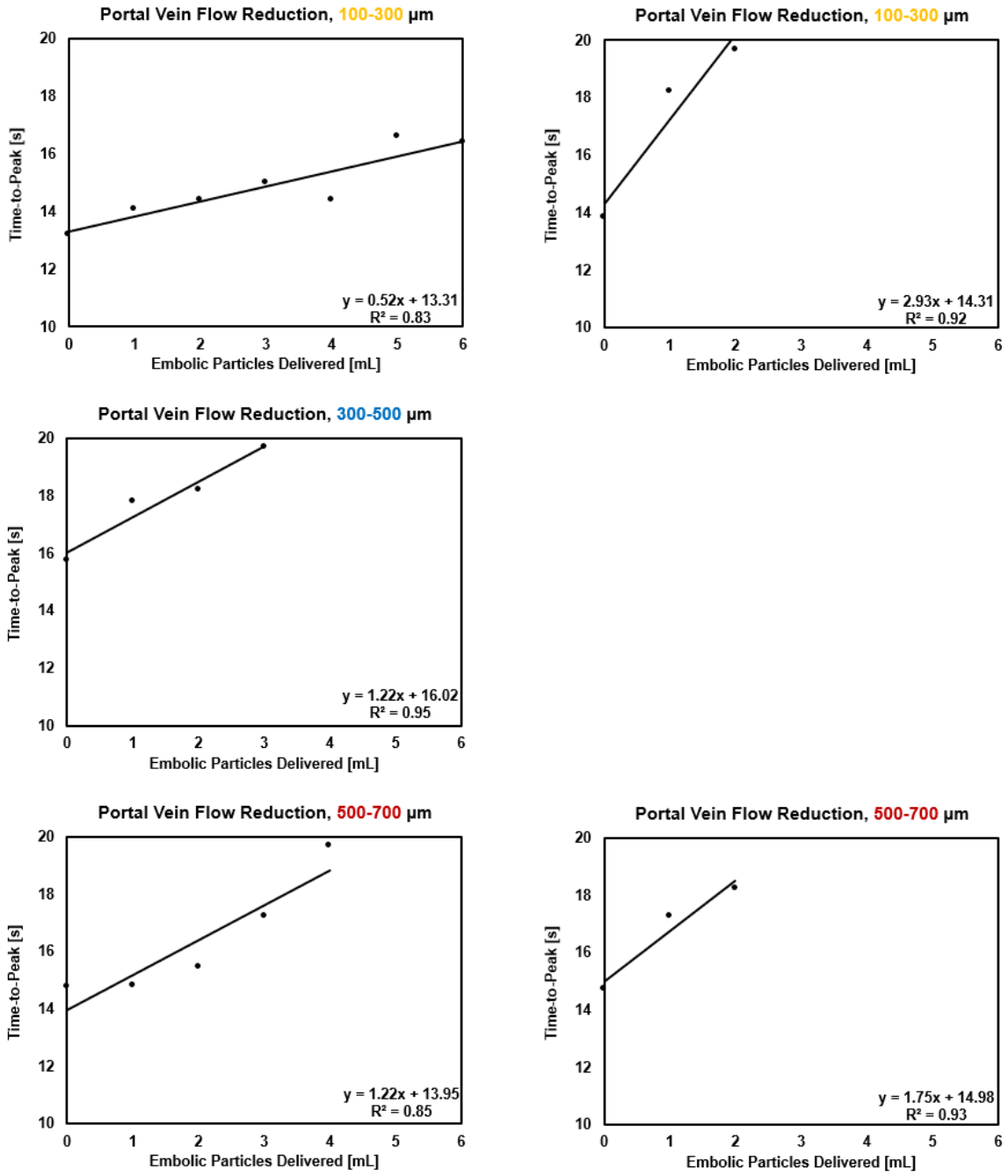

Figure 3: Complete ccDSA time-to-peaks curves from splenic artery embolizations stratified by embolic particle size

All splenic artery embolizations exhibited linear increases in portal vein time-to-peak (TTP) contrast signal relative to baseline as the embolization progressed. There was a strong linear correlations between portal vein TTP and embolic particles delivered. Increases in TTPs appeared to correlate with decreases in splenic arterial blood velocity as characterized by qDSA.

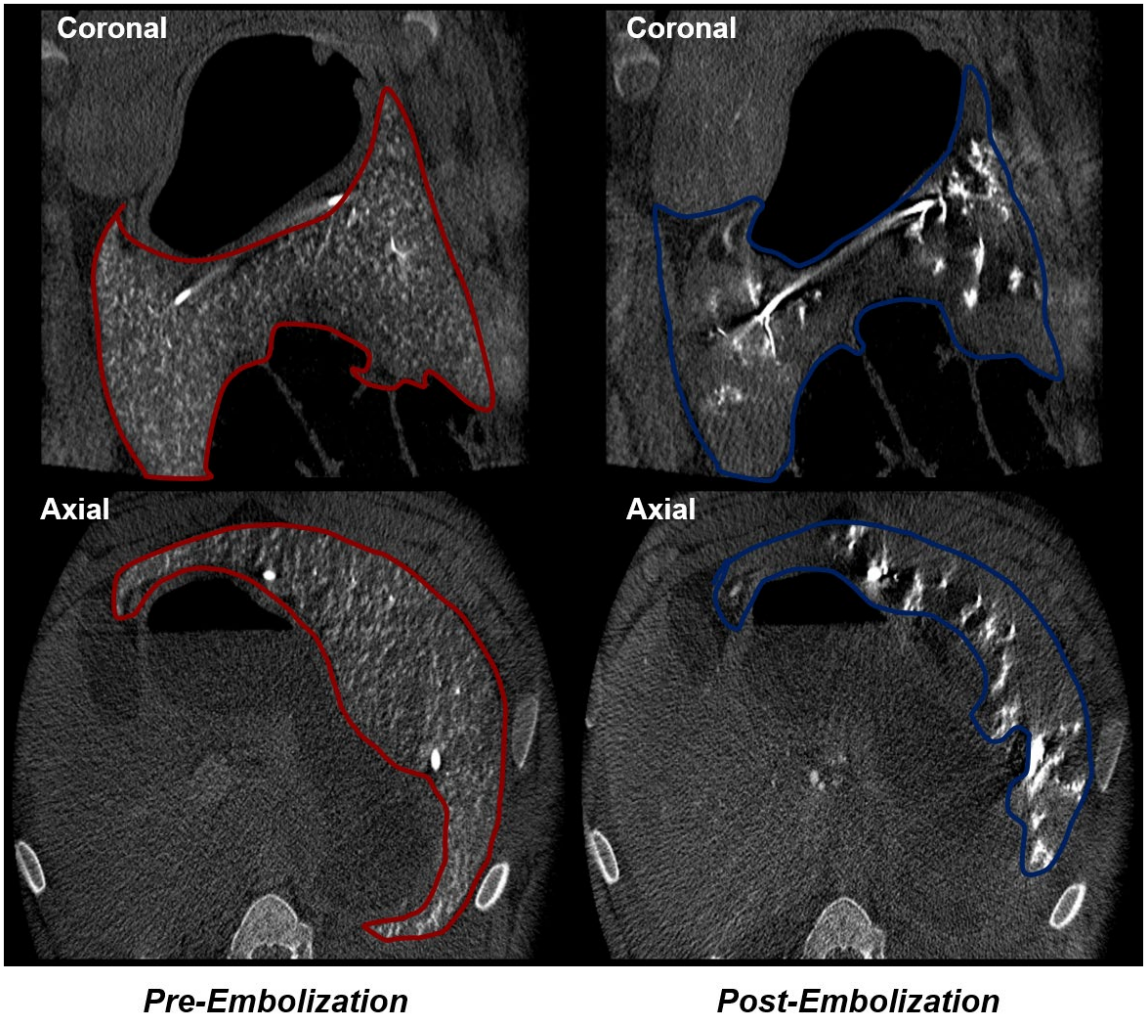

Figure 4: Representative Cone-Beam CTs from splenic arterial embolization

3D Cone beam CTs (CBCTs) acquired prior to (red) and after (blue) splenic arterial embolization. Prior to embolization, there is more homogeneous parenchymal enhancement of the spleen, which stretches across the left-anterior abdomen of the animal. Following embolization, there is significantly reduced parenchymal enhancement and significant contrast stasis in the splenic artery and larger arterioles.

4.5 Discussion

In a feasibility study, splenic arterial embolizations performed in an incremental fashion exhibited linear decreases in qDSA-calculated blood velocities which were strongly correlated with Doppler ultrasound measurements made in the splenic artery and splenic vein. A commercially-available color-coded DSA method for determining contrast time-to-peak within a vessel had poor correlation with the degree of embolization. Reduction in splenic arterial velocity calculated via qDSA corresponded with the reduction in blood velocity found using 4D-Flow MRI and the cross-sectional area of the portal vein. In a study characterizing the splenic arterial blood velocity reduction with different size embolic particles, qDSA calculated blood velocities decreased in all particle sizes. There was a correlative increase in portal vein contrast signal time-to-peak which corresponded to decreased portal venous flow. Embolizations performed with larger particles had larger overall blood velocity reductions compared to embolizations performed with smaller particles.

qDSA demonstrated strong correlation with several modalities measuring changes in splenic and hepatopetal hemodynamics following embolization. Direct intra-procedural measurements of splenic artery and splenic vein blood velocity confirmed that

qDSA was able to characterize progressive decreases in near-real time. Additionally, the magnitude of blood velocity change detected was on the order of 10-20%. This allows for more precise titration of the embolization and enables the determination of a more optimal endpoint than currently achievable. Both 4D Flow MRI and ccDSA indicated reduction in portal venous flow corresponding to the qDSA-calculated reduction in splenic arterial blood velocity. Importantly, the primary objective of many PSE procedures is to reduce portal venous flow in order to relieve PTH. This indicates that the changes in splenic arterial blood velocity detected by qDSA may be useful in controlling portal flow.

Embolizing the splenic artery with different sized particles appeared to have differing effects on the rate at which blood velocity is reduced. Additionally, when embolizations were performed to a complete stasis angiographic endpoint, the quantitative degree of stasis achieved appeared to be different based on the particle size. These results indicate the particle size may have a significant effect on the rate and degree at which stasis is achieved, both factors which may be important in determining safer, more optimal embolization endpoints during PSE. Smaller particles may afford the ability to more gradually decrease flow during the procedure, but may also inhibit perfusion at the level of the microvasculature. Larger particles may decrease flow more rapidly, but

may preserve collateral flow, reducing the risk for necrosis of the splenic tissue whilst still decreasing overall splenic venous blood flow.

This feasibility study had several limitations. Splenic artery embolization was performed in domestic swine, a model that approximates but does not fully recreate the anatomy and physiology of the human spleen. The size and orientation of the porcine spleen is quite different from human spleens, and subsequently, their splenic arterial anatomy and arrangement is also variant. The length and branching pattern of the porcine splenic artery may result in different rates of flow reduction compared to flow reduction in humans. This study was performed in a smaller number of animals; a larger sample size of animals and particle sizes may be necessary to better validate qDSAs ability to guide a splenic embolization. Additionally, all data analysis in this study was performed retrospectively. Intra-procedural qDSA calculation would permit near-real time calculation and selection of quantitative endpoints for improved comparison of outcomes between animals.

In future studies, we aim to characterize changes in ischemia and splenic perfusion in response to qDSA-guided embolization. This includes the use of functional perfusion imaging (CT/MR perfusion) and molecular imaging (F18-MISO PET/MR imaging. Additionally, we plan to use histopathology in order to assess inflammatory and

necrotic changes in the splenic tissue, including the use of immunohistochemistry for markers such as hypoxia-inducible factors (HIF1, HIF2), tumor necrosis factor-alpha factor (TNF-a), among others.

In conclusion, qDSA was able to quantify intra-procedural reductions in splenic arterial blood velocity during splenic artery embolization. These reductions correlated with Doppler US measures in the splenic artery and vein, and also correlated with MR and ccDSA measures of reduced portal flow. This technique may permit the determination of objective treatment endpoints for PSE, improving the safety and efficacy of the procedure.

4.6 References

1. Xu, J., Murphy, S. L., Kochanek, K. D., Bastian, B. & Arias, E. Deaths: Final Data for 2016. National Vital Statistics Reports Centers Dis Control Prev National Cent Heal Statistics National Vital Statistics Syst 67, 1–76 (2018).

2. GBD 2013 Mortality and Causes of Death Collaborators, G. Global, regional, and national age–sex specific all-cause and cause-specific mortality for 240 causes of death, 1990–2013: a systematic analysis for the Global Burden of Disease Study 2013. Lancet 385, 117–171 (2015).

3. Ge, P. S. & Runyon, B. A. Treatment of Patients with Cirrhosis. New Engl J Med 375, 767–777 (2016).

4. Li, L. et al. The spleen in liver cirrhosis: revisiting an old enemy with novel targets. J Transl Med 15, 111 (2017).

5. Bolognesi, M., Merkel, C., Sacerdoti, D., Nava, V. & Gatta, A. Role of spleen enlargement in cirrhosis with portal hypertension. Digest Liver Dis 34, 144–150 (2002).

6. Peck-Radosavljevic, M. Hypersplenism. Eur J Gastroen Hepat 13, 317–323 (2001).

7. Peck-Radosavljevic, M. Thrombocytopenia in Liver Disease. Can J Gastroenterol 14, 60D-66D (2000).

8. Boyer, T. D. & Haskal, Z. J. AASLD practice guidelines the role of transjugular intrahepatic portosystemic shunt (TIPS) in the management of portal hypertension update 2009. Hepatology NA-NA (2009) doi:10.1002/hep.23392 .

9. Zhan, X.-L., Ji, Y. & Wang, Y.-D. Laparoscopic splenectomy for hypersplenism secondary to liver cirrhosis and portal hypertension. World J Gastroentero 20, 5794 (2014).

10. Kedia, S. et al. Splenectomy in cirrhosis with hypersplenism: improvement in cytopenias, child's status and institution of specific treatment for hepatitis C with success. Ann Hepatol 11, 921–929 (2012).

11. Yoshida, H., Mamada, Y., Taniai, N. & Tajiri, T. Partial splenic embolization. Hepatol Res 38, 225–233 (2008).

12. Koconis, K., Singh, H. & Soares, G. Partial Splenic Embolization in the Treatment of Patients with Portal Hypertension: A Review of the English Language Literature. J Vasc Interv Radiol 18, 463–481 (2007).

13. Hadduck, T. A. & McWilliams, J. P. Partial splenic artery embolization in cirrhotic patients. World J Radiology 6, 160–8 (2014).

14. Cai, M. et al. Partial splenic embolization for thrombocytopenia in liver cirrhosis: predictive factors for platelet increment and risk factors for major complications. Eur Radiol 26, 370–80 (2015).

15. Owman, T., Lunderquist, A.,Alwmark, A. & Borjeson, B. Embolization of the Spleen for Treatment of Splenomegaly and Hypersplenism in Patients with Portal Hypertension. Invest Radiol 14, 457–464 (1979).

16. Lewandowski, R. J. et al. A Comparison of Chemoembolization Endpoints Using Angiographic versus Transcatheter Intraarterial Perfusion/MR Imaging Monitoring. J Vasc Interv Radiol 18, 1249–1257 (2007).

17. Gardiner, G. A. et al. Angiographic Assessment of Initial Balloon Angioplasty Results. J Vasc Interv Radiol 15, 1081–1087 (2004).

18. Meram, E. et al. Quantitative 4D-Digital Subtraction Angiography to Assess Changes in Hepatic Arterial Flow during Transarterial Embolization: A Feasibility Study in a Swine Model. J Vasc Interv Radiol (2019) doi:10.1016/j.jvir.2019.01.018 .

19. Shaughnessy, G., Schafer, S., Speidel, M. A., Strother, C. M. & Mistretta, C. A. Measuring blood velocity using 4D-DSA: A feasibility study. Med Phys 45, 4510–4518 (2018).

20. Wang, D. et al. Quantitative 4D transcatheter intraarterial perfusion MRI for monitoring chemoembolization of hepatocellular carcinoma. J Magn Reson Imaging 31, 1106–1116 (2010).

21. Wimmer, T. et al. Computed Tomography Perfusion Following Transarterial Chemoembolization of Hepatocellular Carcinoma. J Comput Assist Tomo 41, 708–712 (2017).

22. Marquez, H. P. et al. Computed tomography perfusion imaging for monitoring transarterial chemoembolization of hepatocellular carcinoma. Eur J Radiol 91, 160–167 (2017).

23. Taouli, B. et al. Hepatocellular carcinoma: perfusion quantification with dynamic contrast-enhanced MRI. Ajr Am J Roentgenol 201, 795–800 (2013).

24. Maschke, S. et al. Evaluation of a newly developed 2D parametric parenchymal blood flow technique with an automated vessel suppression algorithm in patients with chronic thromboembolic pulmonary hypertension undergoing balloon pulmonary angioplasty. Clin Radiol 74, 437–444 (2019).

25. Hinrichs, J. B. et al. Evaluation of a novel 2D perfusion angiography technique independent of pump injections for assessment of interventional treatment of peripheral vascular disease. Int J Cardiovasc Imaging 33, 295–301 (2016).

26. Meine TC, Maschke SK, Kirstein MM, Renne J, Werncke T, Baumgart J, Dewald CA, Wacker FK, Meyer BC, Hinrichs JB. Assessment of angiographic outcome using 2D parametric parenchymal blood flow (2D-PPBF) technique in patients with hypersplenism undergoing partial spleen embolization (PSE). Oral presentation at: Cardiovascular and Interventional Radiological Society of Europe CIRSE Annual Congress; 2019 Sep 9-11; Barcelona, Spain. 2019.

27. Lin, E. et al. Three-Dimensional Quantitative Color-Coding Analysis of Hepatic Arterial Flow Change during Chemoembolization of Hepatocellular Carcinoma. J Vasc Interv Radiol 29, 1362–1368 (2018).

28. Wang, J. et al. Quantitative assessment of angiographic perfusion reduction using color-coded digital subtraction angiography during transarterial chemoembolization. Abdom Radiol 41, 545–552 (2016).

29. Swanson, D. K. et al. Videodensitometric quantitation of mean blood flow. J Surg Res 34, 524–532 (1983).

30. Rosen, L. & Silverman, N. R. Videodensitometric Measurements of Blood Flow Using Crosscorrelation Techniques. Radiology 109, 305–310 (1973).

31. Periyasamy S, Hoffman C, Schefelker G, Laeseke PF. A Quantitative Angiography Technique Using Time-Resolved 2D-DSA for Determining Treatment Endpoints in Partial Splenic Embolization. Poster presented at: Society of Interventional Radiology SIR Annual Scientific Meeting; 2020 Mar 28-Apr 2; Seattle, WA. 2020.

32. Hoffman C, Periyasamy S, Medero R, Laeseke P. Angular dependence of 2D DSA velocity quantification in a carotid artery bifurcation phantom. Poster session presented at: Cardiovascular and Interventional Radiological Society of Europe CIRSE Annual Congress; 2019 Sep 9-11; Barcelona, Spain. (2019).

33. Hoffman C, Periyasamy S, Wu Y, Speidel M, Laeseke P. Quantitative 2D DSA: Metrics for determining treatment endpoints in TAE. Oral presentation at: Radiological Society of North America, RSNA Annual Meeting; 2019 Dec 1-6; Chicago, IL. (2019).

34. Folgado, D. et al. Time Alignment Measurement for Time Series. Pattern Recognition 81, 268–279 (2018).

35. Wu, Y. et al. Quantification of Blood Velocity with 4D Digital Subtraction Angiography Using the Shifted Least-Squares Method. Am J Neuroradiol 39, 1871–1877 (2018).

Chapter 5: Quantitative Digital Subtraction Venography (qDSV)

Portions of this chapter were submitted for review in a peer-reviewed journal:

Periyasamy S, Oberstar E, Kutlu A, Pieper AA, Whitehead J, Hoffman CA, Li G, Speidel MA, Laeseke PF. Quantitative Digital Subtraction Venography for Venous Interventions: Validation in Phantom and In Vivo Porcine Models. **Submitted to *Radiology***. April 2022

and presented at or submitted to the following scientific meetings:

Periyasamy S, Oberstar E, Hoffman CA, Schefelker G, Laeseke PF, Speidel MA. A Quantitative Venography Technique Using Time-Modulated Contrast Injections. SIR 2020. Virtual. March 2020

Periyasamy S, Oberstar E, Pieper AA, Kutlu A, Whitehead J, Hoffman CA, Brace C, Speidel MA, Laeseke PF. Quantifying Blood Velocity during Venous Interventions using Quantitative Digital Subtraction Venography. Submitted to CIRSE 2022. Barcelona, Spain. September 2022

or co-authored and published in the following conference proceedings:

Oberstar E, **Periyasamy S**, Laeseke PF, Speidel MA. "Power injector for angiographic flow analysis using custom contrast density profiles", Proc. SPIE 11312, Medical Imaging 2020: Physics of Medical Imaging, 1131216 (16 March 2020); https://doi.org/10.1117/12.2549656

5.1 Introduction

Following successful demonstration of qDSA in oncologic and non-oncologic applications, we sought to determine whether the technique could be used in other vascular procedures, namely venous interventions. Veins lack many of the physiologic characteristics which permit qDSA to quantify arterial blood velocity. This chapter explores the feasibility of performing quantitative digital subtraction venography (qDSV) using temporally-modulated contrast injections by validating the accuracy of the technique in phantom and in vivo models.

5.2 Motivation

Endovascular therapy is an established method for treating acute and chronic obstructive venous disease(1–5). Venous procedures are currently guided by qualitative angiographic endpoints, including increased visual patency, improved antegrade contrast flow, and/or decreased filling of collateral veins. Subjective angiographic endpoints have high inter-observer variability, poor reproducibility, and can negatively affect patient outcomes (6,7). A recent consensus panel convened by the Society of Interventional Radiology Foundation concluded that quantification of venous flow dynamics is a top research priority for improving outcomes related to deep venous interventions (8).

Current methods for determining endpoints during venous interventions largely provide surrogate measures for venous flow restoration. Trans-stenotic blood pressure gradients may vary based on catheter, and there is no consensus on pre- or post-intervention pressure gradients significant for long term treatment success (9,10). Intravascular ultrasound (IVUS) is an important diagnostic tool for morphologically assessing venous pathology (11,12). It is more sensitive for detecting pathologic venous stenoses and more predictive of clinical outcomes compared to single-plane venography, but it is unclear whether it would be superior to a flow-based endpoint (13–15). Doppler ultrasound is a method for direct blood velocity measurement, but is limited in that deep

iliocaval and femoral veins cannot be visualized due to depth, overlying bone or bowel gas, or requires low frequency transducers with limited spatial resolution (16). Additionally, accurate and consistent measurements may be limited by high inter-observer variability (17).

Quantitative digital subtraction angiography (qDSA) is a newly developed technique that can accurately quantify intra-procedural arterial blood velocity from time-resolved DSA images (18,19). The qDSA algorithm relies on cardiac-pulsatility driven oscillations in the time-attenuation curves of a vessel segment in an image to calculate a spatially- and temporally-averaged blood velocity, using methods previously described for 4D-DSA (20–22). qDSA has not been used for venous interventions because venous flow lacks strong cardiac-driven pulsatility which creates the trackable oscillations in contrast density at the point of injection. We propose a 2D quantitative digital subtraction venography technique (qDSV) which employs a temporally modulated contrast injection, permitting the quantification of blood velocity in a manner similar to qDSA. This technique is minimally-intrusive to the procedural workflow and leverages venographic images that are typically acquired throughout an intervention. The objective of this study was to determine the feasibility of using qDSV in phantom, normal, and stenotic porcine

iliac vein models by correlating qDSV-calculated blood velocity with US-measured blood velocity.

5.3 Validation of qDSV Accuracy in a Phantom and In Vivo Models of Peripheral Venous Blood Flow

5.3.1 Materials and Methods

All procedures were approved by the Institutional Research Animal Care and Use Committee and were compliant with regulatory guidelines.

qDSV Method

The proposed qDSV method uses temporal modulation of the contrast injection to develop transient boluses of contrast medium to calculate blood velocity (Figure 1). An oscillatory signal can be measured in time-attenuation curves (TAC) extracted from pixels within time-resolved 2D DSA images. TACs from points along a vessel centerline, separated by a distance '*d*', will exhibit similar signals but with a temporal shift '*t*', representing the transit time of contrast through the vessel. Distances and temporal shifts are calculated for all pairs of points along a vessel centerline to calculate a spatially- and temporally-averaged blood velocity '*v*'. Distances and temporal shifts were calculated using a previously described shifted-least squares approach (19,21). Given the two-dimensional, projectional nature of venography, calculations are "apparent velocities" and can be used to determine relative changes in velocity. Magnification and foreshortening

corrections can be applied to achieve results closer to "absolute velocity", thereby enabling direct comparison with pulsed wave Doppler ultrasound. All qDSVs were acquired at 30 frames per second and calculations were performed in a custom-built MATLAB tool (MATLAB R2021b version 9.5, MathWorks, Natick, Massachusetts) (19).

Phantom Venous Study

A peristaltic pump (Anko MityFlex, Bradenton, FL) with a water source was connected to a compliance chamber and polyethylene tube phantom to simulate constant rate venous blood flow (Figure 2). Triplicate qDSV images were acquired in a curved section of the phantom using an Artis zee x-ray system (Siemens Healthineers, Forchheim, Germany). An in-line Doppler ultrasound flow sensor (Transonic, Ithaca, NY) was connected to the in-flow of the phantom for non-intrusive and simultaneous measurement of fluid velocity for comparison. Iodinated contrast media (Omnipaque 300, GE Healthcare, Waukesha, WI) was injected through a 6 Fr straight flush catheter positioned proximal to the flow sensor and imaging region. Images were acquired with pump-driven velocity at low (~10-20 cm/s), medium (~20-30 cm/s), and high (~40-50 cm/s) flow rates corresponding to typical venous blood velocities in human iliofemoral veins (23,24).

A custom-built dual-barrel angiographic power injector (DPI) was used to perform temporally-modulated contrast injections (25). The custom DPI offers programmable contrast and saline injection waveforms. Several different contrast injection protocols using square waveforms were evaluated by modifying injection flow rate, duty cycle, and modulating frequency. Additionally, a commercial DPI (Nemoto, Tokyo, Japan) and hand injections via syringe were used to evaluate the feasibility of performing qDSV with currently available contrast injection methods. Contrast injection parameters are included in Table 1 and Table 2.

Porcine Iliac Venous Study

Seven domestic swine (48.6 ± 2.7 kg) were sedated with an intramuscular administration of 7 mg/kg of tiletamine hydrochloride-zolazepam hydrochloride (Xyla-Ject; Phoenix Pharmaceutical, St. Joseph, Missouri), endotracheally intubated, and then underwent anesthesia induction and maintenance with 2% inhaled isoflurane (Halocarbon Laboratories, River Edge, New Jersey). The femoral vein was accessed percutaneously, and a 4 Fr straight flush catheter was positioned in the distal iliac vein. A catheter with radiopaque markers spaced by 1-cm was placed in the iliac vein for magnification and foreshortening correction. Triplicate right or left iliac DSV images were acquired with a temporally-modulated contrast injection using the custom DPI or

commercial DPI using protocols similar to the phantom studies. Immediately following qDSV imaging, triplicate Doppler US blood velocity measurements were made using a Vivid q ultrasound system (GE Healthcare, Waukesha, WI) with a diagnostic linear probe (9L) in the distal portion of the vein that was sonographically visible, typically near the iliofemoral venous junction. Mean velocities were measured over a 5-second scan. To assess different flow states, baseline flow was altered in one animal by occluding the ipsilateral common iliac artery, thereby decreasing both arterial and venous flow in that extremity.

Porcine Iliac Venous Stenosis Study

In three animals (49.3 ± 0.7 kg), an iliac venous stenosis was created. Baseline venograms (2D and 3D), qDSVs, and US measurements of the iliac venous velocity were acquired. Following imaging, a venous stenosis was created using a modified version of a recently described endovenous RF ablation technique (26). Electrical current at 480 kHz was applied through a custom 8F flexible catheter electrode (Figure 8). Electrode temperature and impedance feedback were provided by the RF current generator (Radionics, Inc., Burlington, Massachusetts). With the electrode in the mid-iliac vein, manual compression was applied to improve contact with the vessel wall and reduce heat sinking due to blood flow. Current (0.4-0.6 A) was applied until local temperature

exceeded 90 °C and a commensurate increase in electrical impedance was detected (20 ohm). Total heating time was 15-20 seconds. After withdrawing the electrode, the flush catheter was re-introduced and repeat venography performed to verify the stenosis. Subsequently, venoplasty was performed (up to a 12 mm balloon catheter). Finally, a stent (Animal 1: 12 mm x 60 mm WALLSTENT, Boston Scientific; Animal 2: 10 mm x 68 mm WALLSTENT; Animal 3: 14 mm x 50 mm WALLGRAFT, Boston Scientific) was deployed across the stenosis. Venography and quantitative imaging measurements were acquired at each step: post-stenosis creation, post-venoplasty and post-stenting.

Image Analysis

For all studies, qDSV acquisitions were analyzed using the aforementioned MATLAB tool to calculate a spatially- and temporally-averaged blood velocity in the iliac vein. For phantom studies, real-time US-sensor velocity data was imported into MATLAB and a time-averaged blood velocity was calculated. For in vivo studies, the mean blood velocity over the length of a pulse-wave Doppler US acquisition was measured in the target vein.

Statistical Analysis

Mean qDSV and US velocities were calculated as mean±standard deviation of triplicate acquisitions. For assessment of correlation between qDSV and US velocities in

phantom and in vivo models, linear regression analysis was performed using MATLAB. A Bland-Altman analysis was performed to assess agreement between the two techniques. For assessment of the difference in mean qDSV and US velocities between injection methods, and to compare pre- and post-balloon occlusion velocities, paired sample t-tests were used. A p-value < 0.05 was considered statistically significant. Bland-Altman and t-test analysis were performed in R (version 4.1.2).

5.3.2 Results

Phantom Venous Study

In the phantom study using the custom DPI, a range of blood velocities (13-51 cm/s) were observed (Figure 3). Peaks in US-measured blood velocity and peaks in TACs from the baseline injection protocol and half-frequency protocol were larger than those of the half-rate and half-duty cycle protocols. Linear regression analyses between mean US-measured blood velocity (cm/s) and qDSV-calculated blood velocity (cm/s) ($US_{velocity}$ = slope * $qDSV_{velocity}$ + intercept) are presented in Figure 4. The base injection (slope = 1.28, intercept = -8.31, R2 = 0.99), half-rate (slope = 1.01, intercept = 1.70, R2 = 0.99), half-duty cycle (slope = 1.07, intercept = -0.85, R2 = 0.98), and half-frequency protocols (slope = 1.35, intercept = -4.17, R2 = 0.98) all had very strong linear correlations between qDSV and US velocities. The Bland-Altman analysis of the difference in velocity means (qDSV – US) showed a bias of 0.3 cm/s for the base injection (limits of agreement: [-6.9 to 7.5 cm/s]), -2.1 cm/s for the half-rate (limits of agreement: [-5.7 to 1.6 cm/s]), -1.2 cm/s for the half-duty cycle (limits of agreement: [-5.8 to 3.4 cm/s]), -4.9 cm/s for the half-frequency (limits of agreement: [-14.1 to 4.4 cm/s]) protocols (Figure 5).

In the phantom study comparing different injection methods (Figure 6), there was no statistically significant difference between qDSV and US using the custom injector (qDSV=23.6±0.4 cm/s, US=24.3±0.0 cm/s, p=0.09), commercial injector protocol 3 (qDSV=24.0±2.3 cm/s, US=23.2±0.0 cm/s, p=0.60), multiple-syringe hand injections (qDSV=22.3±2.4 cm/s, US=24.3±0.6 cm/s, p=0.20), or single-syringe hand injections (qDSV=23.4±2.7 cm/s, US=24.5±0.3 cm/s, p=0.52). There was a statistically significant difference between qDSV and US using the commercial injector protocol 1 (qDSV=21.7±0.6 cm/s, US=24.1±0.3 cm/s, p=0.02) with an absolute difference of 2.4 cm/s, and commercial injector protocol 2 (qDSV=22.3±0.9 cm/s, US=24.1±0.3 cm/s, p=0.03) with an absolute difference of 1.8 cm/s.

Porcine Iliac Venous Study

In the in vivo normal porcine iliac vein model, blood velocities were measured over a range of 5-16 cm/s using Doppler US. Linear regression analyses between mean US-measured blood velocity (cm/s) and qDSV-calculated blood velocity (cm/s) ($US_{velocity}$ = slope * $qDSV_{velocity}$ + intercept) are presented in Figure 7. In vivo, there was a strong linear correlation between qDSV and US velocities (slope = 1.22, intercept = -4.32, R2 = 0.90). The Bland-Altman analysis of the difference in velocity means (qDSV – US) showed a bias of 1.4 cm/s (limits of agreement: [-2.4 to 5.2 cm/s]). In the animal where

the venous blood velocity was reduced through ipsilateral iliac arterial occlusion, a statistically significant reduction in velocity was captured by both qDSV (pre-occlusion: 13.5±2.6 cm/s, post-occlusion: 7.6±2.1 cm/s, p =0.03) and US (pre-occlusion: 12.0±2.9 cm/s, post-occlusion: 5.3±0.7 cm/s, p=0.02).

Porcine Iliac Venous Stenosis Study

In the stenosis study, successful creation of an iliac venous stenosis and subsequent treatment with venoplasty and stenting was achieved in all animals (Figures 9 & 10). The diameter and cross-sectional area of the target region in the iliac vein, the US-measured blood velocity, and the qDSV-calculated blood velocity for each of the three animals are presented in Table 3. In Animal 1, both US and qDSV indicated a decrease in velocity following stenosis, subsequent increase in velocity after venoplasty, and further increase in velocity after stenting. In animal 2, both US and qDSV indicated a decrease in velocity following stenosis, subsequent increase in velocity after venoplasty, and minimal change in velocity after stenting. In animal 3, both US and qDSV indicated a high grade stenosis or complete occlusion with no antegrade flow and significant reflux following stenosis creation. There was an increase in both US and qDSV velocity following two rounds of venoplasty and stenting. In all animals, the relative changes in blood velocity were similar between the two modalities at all intra-procedural timepoints.

5.3.4 Tables

Table 1: Contrast injection parameters for the phantom experiment using the custom power injector

Injection Protocol	Contrast Injection Rate (mL/s)	Saline Injection Rate (mL/s)
Base Protocol	6.0 (peak), 0.0 (minimum)	6.0 (peak), 0.0 (min)
Half-Rate	3.0 (peak), 0.0 (minimum)	3.0 (peak), 0.0 (min)
Half-Duty Cycle	6.0 (peak), 0.0 (minimum)	6.0 (peak), 0.0 (min)
Half-Frequency	6.0 (peak), 0.0 (minimum)	6.0 (peak), 0.0 (min)

Cont.

Injection Protocol	Duty Cycle (%)	Frequency (Hz)	Acquisition Time (s)	Contrast Volume (mL)
Base Protocol	10	0.35	20	3.6
Half-Rate	10	0.35	20	1.8
Half-Duty Cycle	5	0.35	20	1.8
Half-Frequency	10	0.17	20	3.6

Table 2: Contrast injection parameters for the phantom experiment comparing different injection methods

Injection Method	Protocol	Injection Parameters	Acquisition Time (s)	Contrast Volume (mL)
Custom Injector	Base Protocol	6.0 (peak), 0.0 (minimum) contrast and saline, 10% duty cycle, 0.35 Hz	20 s	3.6 mL
Conventional Injector	Protocol 1	3-phase injection: 6 mL/s, 0.6 mL, 3 second phase delay	20 s	1.8 mL
Conventional Injector	Protocol 2	3-phase injection: 4 mL/s, 0.4 mL, 3 second phase delay	20 s	1.2 mL
Conventional Injector	Protocol 3	3-phase injection: 2 mL/s, 0.2 mL, 3 second phase delay	20 s	0.6 mL
Hand Injection	Multiple Syringes	4 syringes, 1.2 mL of contrast, injected ~3 seconds apart	20 s	4.8 mL
Hand Injection	Single Syringe	1 syringe, 5 mL of contrast, ~6 injections per acquisition	20 s	5.0 mL

Table 3: Peri-procedural measurements from the porcine iliac venous stenosis study

Animal	Measurement	Baseline	Post-Stenosis	Post-Venoplasty	2nd Post-Venoplasty	Post-Stenting
1	CSA (cm^2)	0.73	0.13	0.36	n/a	1.30
1	Diam. (cm)	1.02	0.78	0.79	n/a	1.19
1	qDSV (cm/s)	15.2 ± 2.5	8.7 ± 0.9	15.8 ± 0.4	n/a	18.0 ± 0.4
1	US (cm/s)	12.8 ± 1.2	4.8 ± 0.1	10.1 ± 3.0	n/a	12.3 ± 1.2
2	CSA (cm^2)	0.76	0.26	0.37	n/a	0.76
2	Diam. (cm)	1.26	0.58	0.62	n/a	0.97
2	qDSV (cm/s)	17.6 ± 1.9	8.4 ± 0.1	11.5 ± 0.8	n/a	11.2 ± 1.7
2	US (cm/s)	20.2 ± 2.6	12.9 ± 0.8	16.6 ± 3.0	n/a	16.3 ± 0.5
3	CSA (cm^2)	0.98	0.37	0.38	0.46	0.97
3	Diam. (cm)	1.17	0.44	0.44	0.67	0.91
3	qDSV (cm/s)	13.1 ± 2.3	~ 0*	3.8 ± 0.4	6.3 ± 0.7	9.8 ± 0.6
3	US (cm/s)	11.6 ± 0.7	~ 0*	3.5 ± 0.4	7.8 ± 1.3	11.9 ± 0.6

CSA: Cross-sectional area, Diam.: Diameter, qDSV: quantitative digital subtraction venography, US: ultrasound

* Denotes qualitative features of complete stasis

5.3.5 Figures

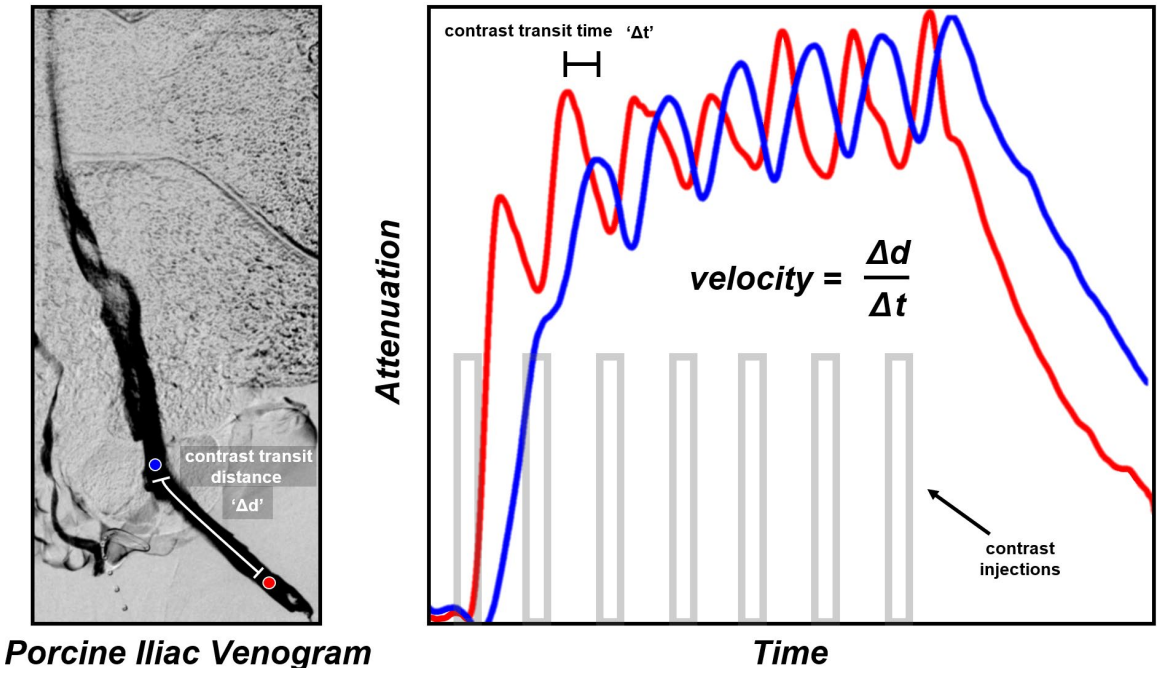

Figure 1: Example qDSV in an in vivo porcine iliac vein model

An example of the qDSV technique in a porcine iliac venogram (left). Within the target vein, a proximal (red) and distal point (blue) is analyzed. The time-attenuation curves (TAC) from the points exhibit contrast peaks developed from temporally-modulated injection of contrast medium. The two TACs are superimposed (right), illustrating a temporal shift. Using the distance between the points and calculated temporal shift, a spatially- and temporally-averaged blood velocity can be determined.

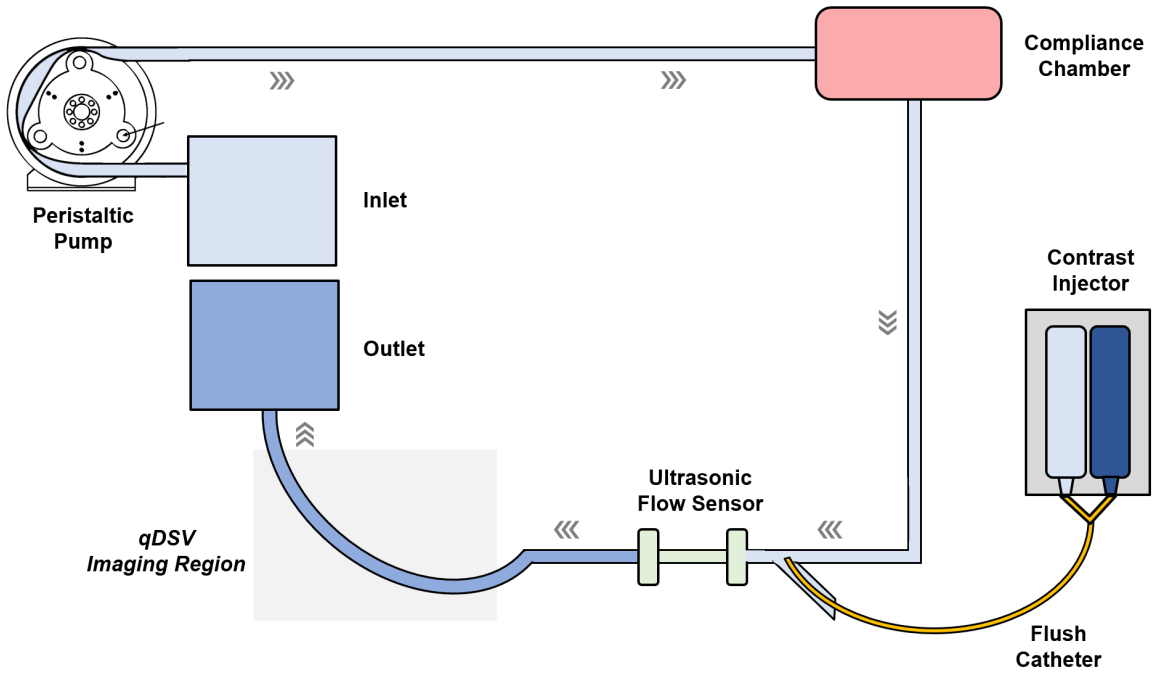

Figure 2: qDSV Phantom Experimental Setup

An illustration of the phantom experimental setup for validating qDSV accuracy. A peristaltic pump was used to generate fluid flow from an inlet water reservoir. A compliance chamber was connected in series to the pump in order to remove any pulsatility from the flow and more accurately mimic constant venous flow rate. Temporally-modulated contrast injections were performed through a flush catheter introduced through a Y-junction. Real-time ultrasound velocities were recorded using an in-line ultrasonic flow sensor immediately proximal to the x-ray imaging region. Angiographic images were acquired in a curved section of ¼" polyethylene tubing that was used to simulate iliac venous anatomy.

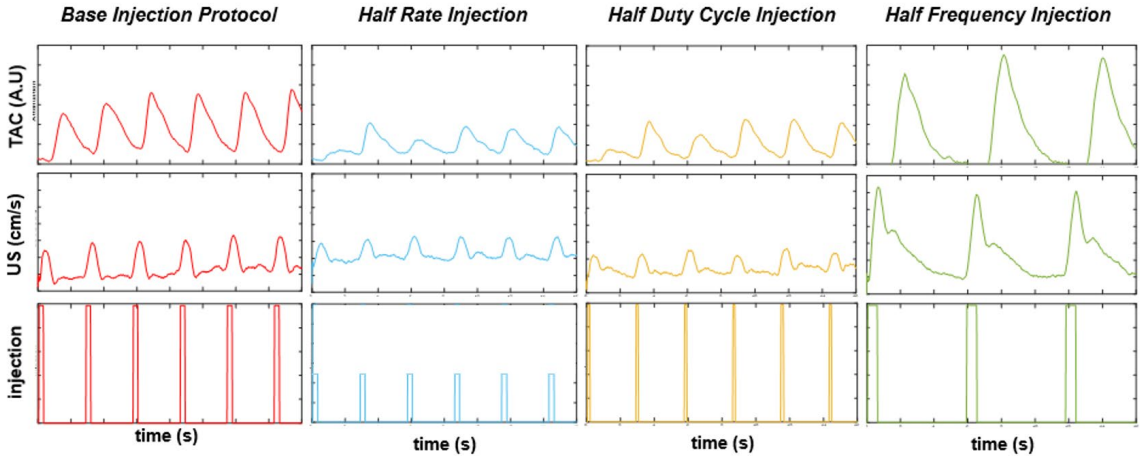

Figure 3: Example time-attenuation curves and US velocities from temporally-modulated contrast injection protocols

Time attenuation curves (TAC, arbitrary units) and real-time ultrasound (US, cm/s) velocities from varied temporally-modulated contrast injection protocols. These include a base injection protocol (red), a protocol in which the peak injection rate is halved (blue), a protocol in which the injection duty cycle is halved (yellow), and a protocol in which the injection frequency is halved (green). Injection protocols with higher effective injection rates (base injection, half frequency) exhibit the largest transient increases in blood velocity and TAC signal. Injection protocols decreased effective injection rates (half rate, half duty cycle) exhibit smaller transient increases in blood velocity and TAC signal.

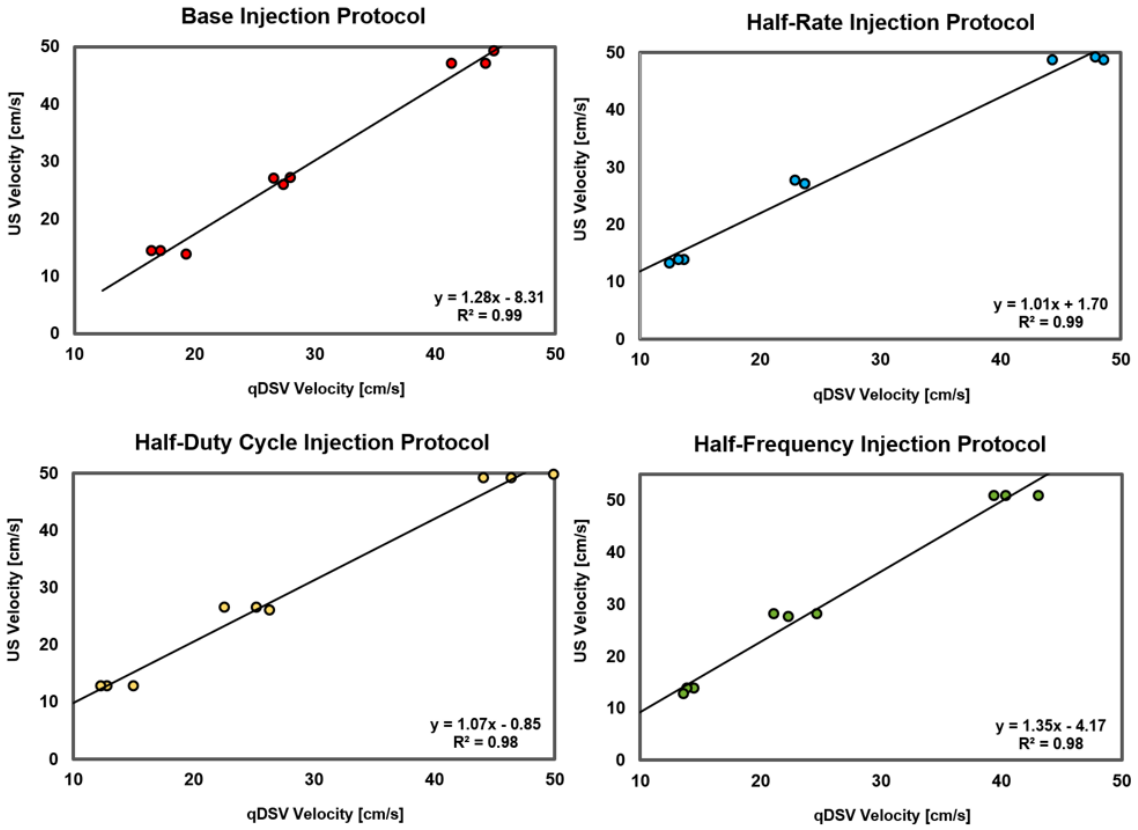

Figure 4: qDSV accuracy in phantom models across different temporally-modulated contrast injection protocols

Correlation of qDSV-calculated velocity with US-measured velocity in a phantom model. Across all injection protocols, there is a very strong correlation between qDSV and US. Injection protocols with higher effective injection rates (base injection, half-frequency) exhibit larger velocity biases towards qDSV compared to injection protocols with decreased effective injection rates (half-rate, half-duty cycle).

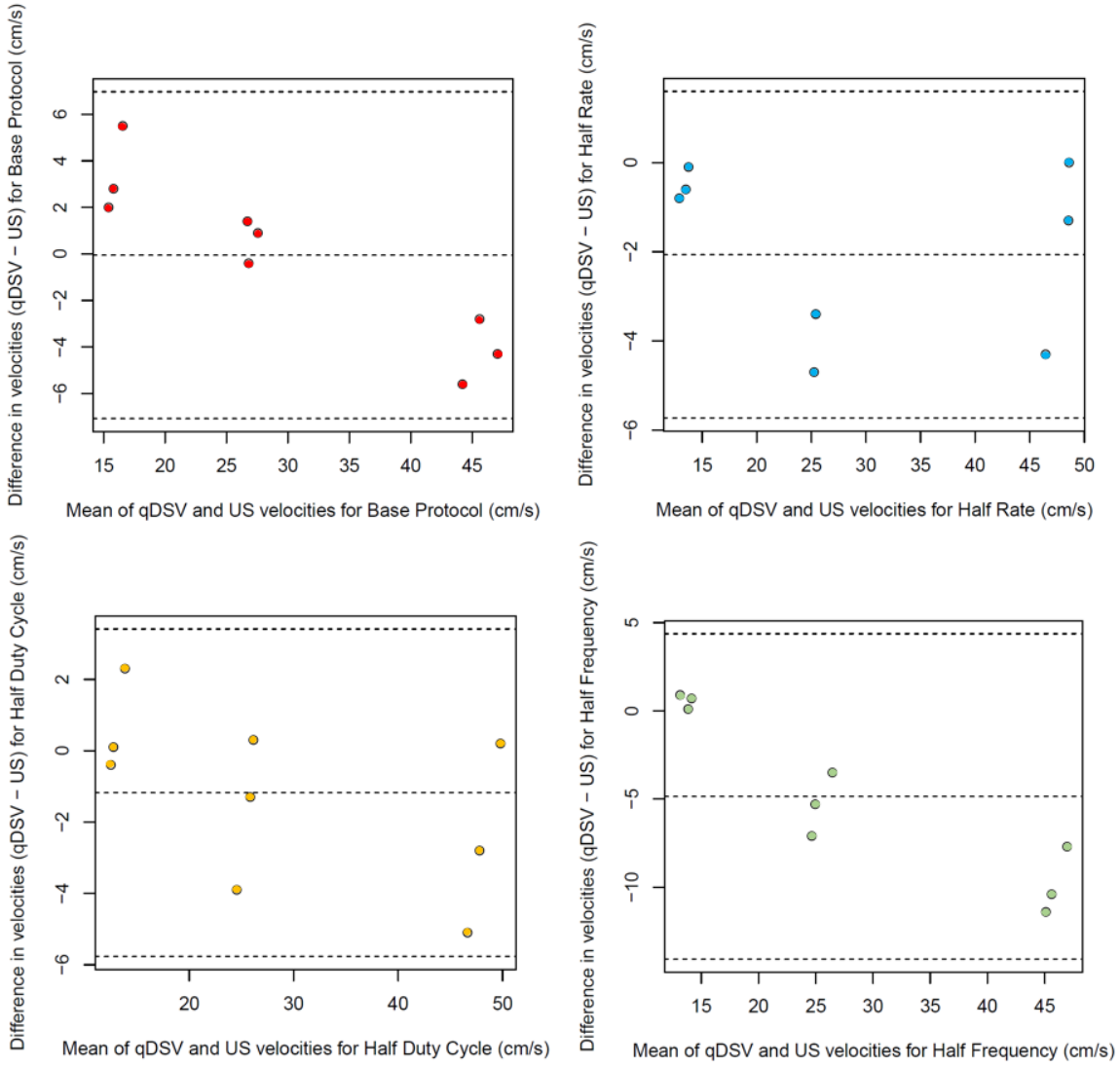

Figure 5: qDSV and US Bland-Altman analysis in phantom models

Bland-Altman plot of qDSV velocities and US velocities for the Base Protocol (red), Half Rate Protocol (blue), Half Duty Cycle Protocol (yellow), and Half Frequency Protocol (green). The middle dashed line represents the average of the differences between qDSV velocities and US velocities, and the top and

bottom dashed lines represent the mean difference + 1.96SD (standard deviation of the difference) and mean difference - 1.96SD, respectively. In the injection protocols with larger effective injection rates (base protocol, half-frequency), there appears to be a velocity dependent bias: higher velocities bias to US, lower velocities bias to qDSV.

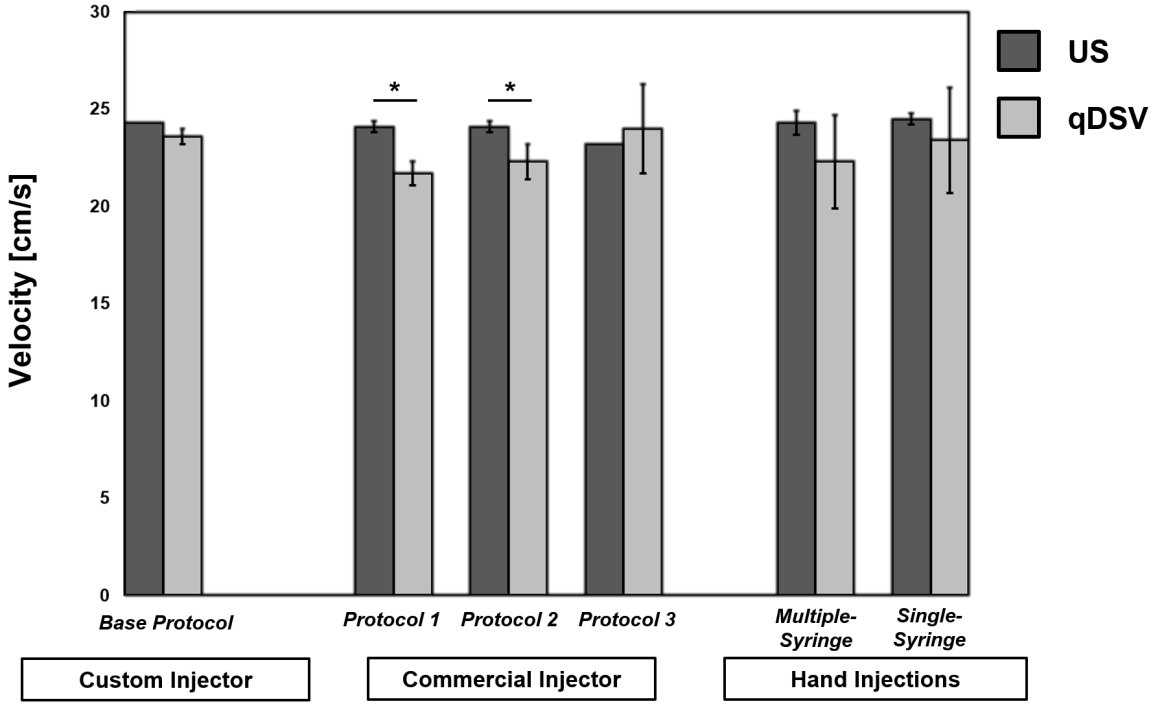

Figure 6: qDSV accuracy in phantom models across different contrast injection methods

A comparison of qDSV-calculated blood velocities using different injection methods. The calculated velocities using the custom injector, commercial injector (at different flow rates), and hand injections (using a single or multiple syringes) are similar to velocities measured by US.

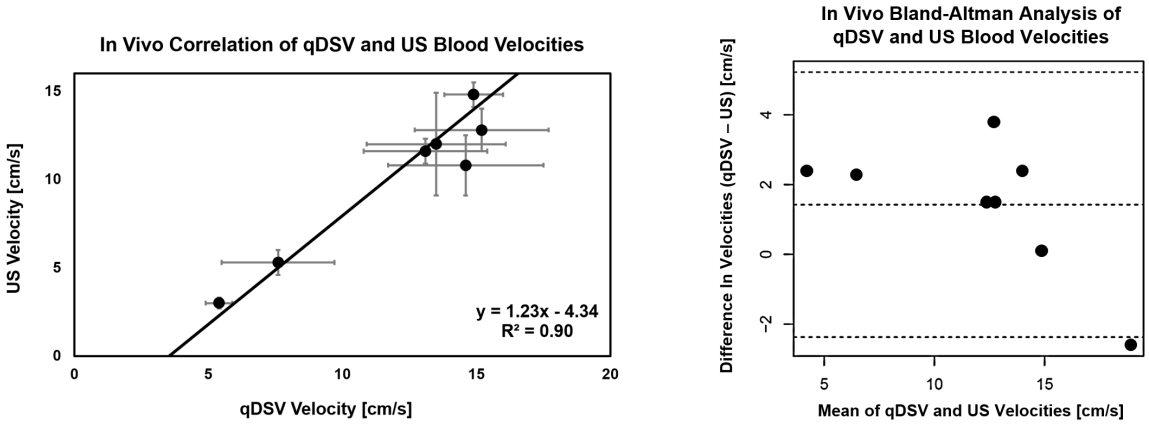

Figure 7: qDSV accuracy in in vivo porcine models of the iliac vein at different flow states

Correlation and Bland-Altman analysis of qDSV-calculated velocity with US-measured velocity in an in vivo model. There is a strong linear correlation between qDSV and US at different flow rates within the porcine iliac vein.

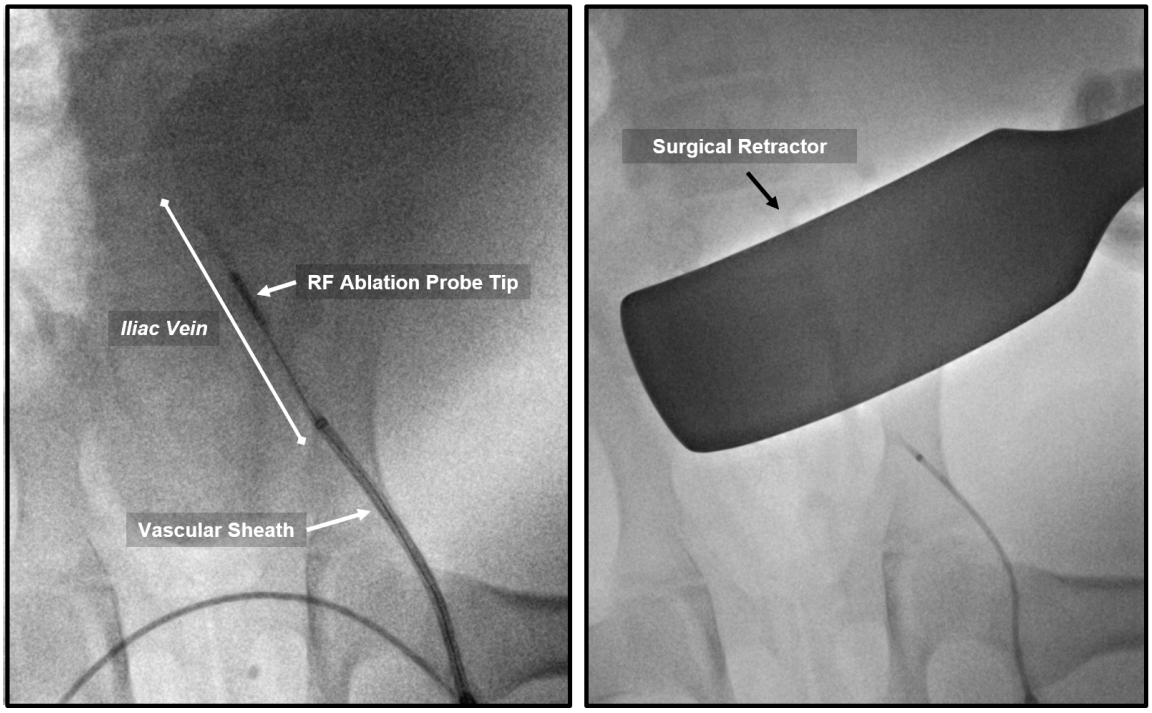

Figure 8: Endovenous RF ablation for in vivo venous stenosis creation

Intra-procedural setup for performing endovenous RF ablation in an in vivo porcine iliac vein model in order to create venous stenosis. Fluoroscopy is used to advance a custom-built endovenous RF probe through a large diameter vascular sheath (e.g. 8 Fr) until the metallic tip is centered on the target region of the vein. Prior to ablation, abdominal compression is applied to the target region (using either manual compression and/or tools such as a retractor) in order to provide sufficient contact of the venous endothelium with the probe tip. Once ablation has begun, compression is maintained until successful ablation is achieved.

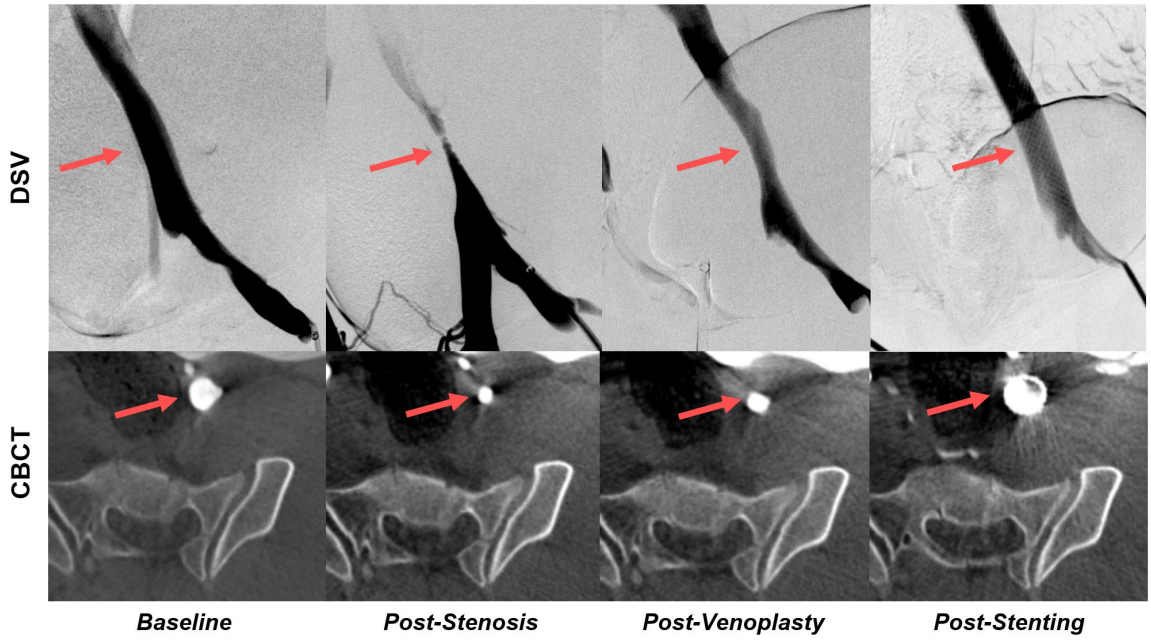

Figure 9: 2D and 3D venography of iliac venous stenosis and subsequent treatment

2D (digital subtraction venography, DSV) and 3D (cone-beam CT, CBCT) venograms from a porcine model of iliac venous stenosis. A decrease in vessel cross-sectional area is seen after endovenous radiofrequency ablation is performed. Subsequent increases in area are seen following venoplasty and deployment of a metallic stent.

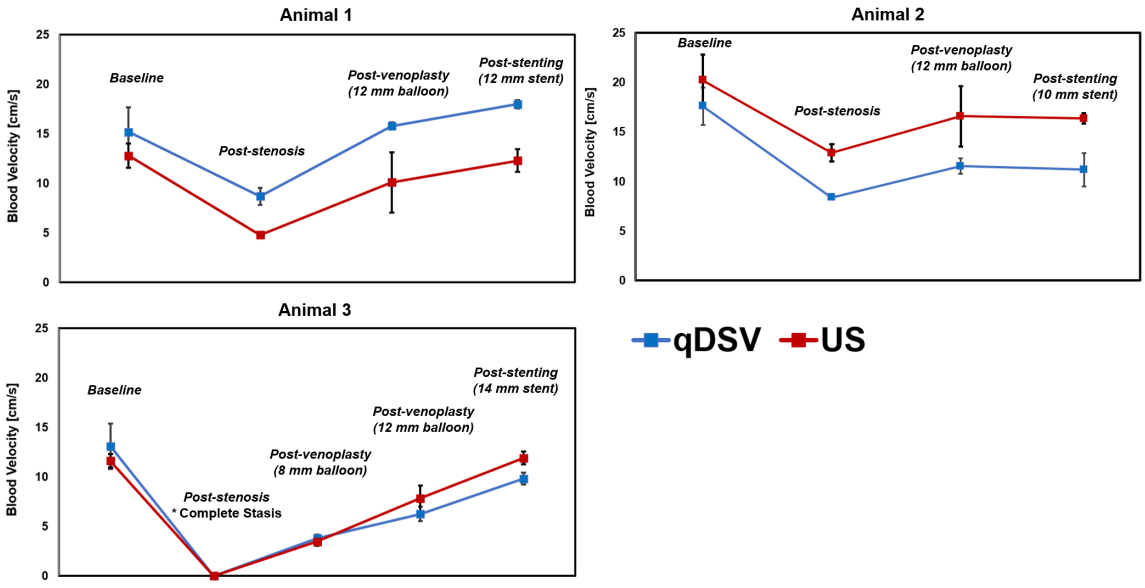

Figure 10: qDSV and US Blood Velocities During Stenosis Creation and Treatment

Blood velocity changes during a venous stenosis creation and treatment in a porcine model. Replicate velocity measurements were made at each intra-procedural time point using qDSV and US. Both techniques show similar decreases in mean blood velocity after stenosis formation and subsequent increases in velocity after venoplasty and stent placement.

5.4 Discussion

This study investigated the feasibility of a quantitative digital subtraction venography technique that employs a temporally modulated contrast injection to quantify venous blood velocity by assessing the correlation of qDSV-calculated blood velocities to Doppler US blood velocity measurements. In a phantom model, qDSV accurately quantified blood velocity across a range of baseline velocities and injection protocols using several different injection methods. In vivo, qDSV correlated strongly with US measurements in a normal iliac vein at different venous flow rates. In an in vivo endovenous RF ablation model of iliac venous stenosis, qDSV characterized changes in blood velocity after stenosis creation, venoplasty and stenting. At each step, changes on qDSV correlated with those on Doppler US.

The phantom studies indicate that different qDSV injection protocols may be used to quantify venous blood velocity. Injection protocols may be adapted based on patient- and venous pathology-specific factors. For example, in larger patients with more attenuating tissues, a higher rate protocol similar may be used to ensure stronger time-attenuation signals for qDSV calculation. In patients with lower native venous flow, a lower rate protocol may be used to minimize perturbation of blood flow. Of note, the

time-averaged velocity addition from injection was small (<10% of native blood velocity) in this study. A custom power injector with fine injection parameter control, similar to the one used in this investigation, may be desirable for such adjustments, but the results from this study indicate that similar venous velocity quantification may be achieved with conventional injection methods.

In vivo, qDSV enabled accurate iliac venous blood velocity quantification over a wide range of hemodynamic and pathologic states. Stenoses of different severity were created and treated with clinical angioplasty balloons and stents of different sizes. qDSV captured changes in venous velocity between baseline flow states and those with reduced arterial inflow, venous occlusion, venous recanalization, and restoration of baseline flow following venoplasty and stenting. A previously described method for creating venous stenoses in a large animal model was used, but modified to use an RF ablation generator and electrode made from off-the-shelf components (26). The anatomic (2D and 3D venography) and quantitative (qDSV, US) results from this study further validate this as an appropriate model for translational venous intervention research.

qDSV may address shortcomings of current techniques for determining treatment endpoints of venous intervention. Importantly, qDSV does not interfere with the procedural workflow and may complement other currently employed techniques. qDSV

may be used to characterize baseline blood velocity and determine whether a venous stenosis or compression is clinically significant, even if the vessel is not visible by ultrasound. It may help differentiate between patients with pathologic, clinically significant iliac venous compression and the large cohort of patients with normal physiologic iliac venous compression. Additionally, qDSV may be used in combination with IVUS to characterize changes in vessel patency with corresponding blood velocity changes. The two techniques may even be combined to calculate volumetric flow changes (velocity from qDSV and cross-sectional area from IVUS).

Our study had several limitations. The phantom study was performed in a flexible tube model which does not capture all of the features of venous vasculature including vessel compliance, convergent vessels, or turbulent flow. Despite this, qDSV correlated with Doppler US in an in vivo porcine model that more closely reflects human anatomy and physiology. In both models, qDSV-calculated velocities correlated strongly with US velocities across a range of velocities, but several factors may result in different absolute velocities between the two. The US velocities were temporally-averaged over the length of a scan, but were acquired at a single cross-sectional plane (in-line probe for phantom) or small region of interest (diagnostic probe for swine) near the iliofemoral venous junction due to an inability to visualize the iliac vein more centrally. This differs from the

spatially- and temporally-averaged velocity provided by qDSV, which calculates velocity along an entire segment of the common and external iliac vein, across a number of image frames. While in vivo ultrasound measurements were acquired immediately prior to or following qDSV scans, transient changes in native blood flow may have occurred between measurements. Blood velocity was also calculated by qDSV in the presence of a contrast injection. Although the injections used were intentionally brief and low volume, there may have been small transient increases in flow (and velocity) due to the injected contrast. While these factors affect the calculation of absolute blood velocity, relative changes in pre- and post-intervention velocities are still captured by qDSV. Lastly, this study used high-frame rate imaging to capture the temporal dynamics of the blood in the veins. For a typical venous segment and blood velocity, the frame rate can likely be reduced significantly (~7-10 frames per second) . Additionally, ongoing investigations indicate qDSV may be performed at significantly lower radiation doses, including levels comparable to conventional fluoroscopy.

In conclusion, using temporally-modulated contrast injections, qDSV was used to accurately quantify venous blood velocity in phantom and in vivo models. Furthermore, qDSV was able to characterize intra-procedural changes in blood velocity in a porcine model of venous stenosis with subsequent venoplasty and stenting. Further investigation

is warranted to assess the feasibility of using qDSV to determine objective treatment endpoints during clinical venous interventions.

5.5 References

1. Majeed GM, Lodhia K, Carter J, et al. A Systematic Review and Meta-Analysis of 12-Month Patency After Intervention for Iliofemoral Obstruction Using Dedicated or Non-Dedicated Venous Stents. J Endovasc Ther. 2021;152660282110570. doi: 10.1177/15266028211057085.

2. Bondarev S, Keller EJ, Han T, et al. Predictors of Disease Recurrence after Venoplasty and Stent Placement for May–Thurner Syndrome. J Vasc Interv Radiol. 2019;30(10):1549–1554. doi: 10.1016/j.jvir.2019.07.012.

3. Titus JM, Moise MA, Bena J, Lyden SP, Clair DG. Iliofemoral stenting for venous occlusive disease. J Vasc Surg. 2011;53(3):706–712. doi: 10.1016/j.jvs.2010.09.011.

4. Ahmed O, Ng J, Patel M, et al. Endovascular Stent Placement for May–Thurner Syndrome in the Absence of Acute Deep Vein Thrombosis. J Vasc Interv Radiol. 2016;27(2):167–173. doi: 10.1016/j.jvir.2015.10.028.

5. Hartung O, Loundou AD, Barthelemy P, Arnoux D, Boufi M, Alimi YS. Endovascular Management of Chronic Disabling Ilio-caval Obstructive Lesions: Long-Term Results. Eur J Vasc Endovasc. 2009;38(1):118–124. doi: 10.1016/j.ejvs.2009.03.004.

6. Lewandowski RJ, Wang D, Gehl J, et al. A Comparison of Chemoembolization Endpoints Using Angiographic versus Transcatheter Intraarterial Perfusion/MR Imaging Monitoring. J Vasc Interv Radiol. 2007;18(10):1249–1257. doi: 10.1016/j.jvir.2007.06.028.

7. Vries AR de, Engels PH, Overtoom TT, Saltzherr TP, Geyskes BG. Interobserver variability in assessing renal artery stenosis by digital subtraction angiography. Diagn Imag Clin Med. 1984;53(6):277–281.

8. Khaja MS, Obi AT, Sharma AM, et al. Optimal Medical Therapy Following Deep Venous Interventions: Proceedings from the Society of Interventional Radiology Foundation Research Consensus Panel. J Vasc Interv Radiol. 2021;33(1):78–85. doi: 10.1016/j.jvir.2021.09.009.

9. Funaki B, Kim R, Lorenz J, et al. Using pullback pressure measurements to identify venous stenoses persisting after successful angioplasty in failing hemodialysis grafts. Ajr Am J Roentgenol. 2002;178(5):1161–1165. doi: 10.2214/ajr.178.5.1781161.

10. Avery MB, Sambrano S, Eliyas JK, Eesa M, Mitha AP. Accuracy and precision of venous pressure measurements of endovascular microcatheters in the setting of dural venous sinus stenosis. J Neurointerv Surg. 2018;10(4):387. doi: 10.1136/neurintsurg-2017-013155.

11. Neglén P, Raju S. Intravascular ultrasound scan evaluation of the obstructed vein. J Vasc Surg. 2002;35(4):694–700. doi: 10.1067/mva.2002.121127.

12. McLafferty R. The Role of Intravascular Ultrasound in Venous Thromboembolism. Semin Intervent Rad. 2012;29(01):010–015. doi: 10.1055/s-0032-1302446.

13. Gagne PJ, Tahara RW, Fastabend CP, et al. Venography versus intravascular ultrasound for diagnosing and treating iliofemoral vein obstruction. J Vasc Surg Venous Lymphatic Disord. 2017;5(5):678–687. doi: 10.1016/j.jvsv.2017.04.007.

14. Gagne PJ, Gasparis A, Black S, et al. Analysis of threshold stenosis by multiplanar venogram and intravascular ultrasound examination for predicting clinical improvement after iliofemoral vein stenting in the VIDIO trial. J Vasc Surg Venous Lymphatic Disord. 2018;6(1):48-56.e1. doi: 10.1016/j.jvsv.2017.07.009.

15. Montminy ML, Thomasson JD, Tanaka GJ, Lamanilao LM, Crim W, Raju S. A comparison between intravascular ultrasound and venography in identifying key parameters essential for iliac vein stenting. J Vasc Surg Venous Lymphatic Disord. 2019;7(6):801–807. doi: 10.1016/j.jvsv.2019.03.015.

16. Zucker EJ, Ganguli S, Ghoshhajra BB, Gupta R, Prabhakar AM. Imaging of venous compression syndromes. Cardiovasc Diagnosis Ther. 2016;6(6):519–532. doi: 10.21037/cdt.2016.11.19.

17. Corriveau MM, Johnston KW. Interobserver variability of carotid Doppler peak velocity measurements among technologists in an ICAVL-accredited vascular laboratory. J Vasc Surg. 2004;39(4):735–741. doi: 10.1016/j.jvs.2003.12.017.

18. Periyasamy S, Hoffman CA, Longhurst C, et al. A Quantitative Digital Subtraction Angiography Technique for Characterizing Reduction in Hepatic Arterial Blood Flow

During Transarterial Embolization. Cardiovasc Inter Rad. 2021;44(2):310–317. doi: 10.1007/s00270-020-02640-0.

19. Hoffman C, Periyasamy S, Longhurst C, et al. A technique for intra-procedural blood velocity quantitation using time-resolved 2D digital subtraction angiography. Cvir Endovascular. 2021;4(1):11. doi: 10.1186/s42155-020-00199-y.

20. Shaughnessy G, Schafer S, Speidel MA, Strother CM, Mistretta CA. Measuring blood velocity using 4D-DSA: A feasibility study. Med Phys. 2018;45(10):4510–4518. doi: 10.1002/mp.13120.

21. Wu Y, Shaughnessy G, Hoffman CA, et al. Quantification of Blood Velocity with 4D Digital Subtraction Angiography Using the Shifted Least-Squares Method. Am J Neuroradiol. 2018;39(10):1871–1877. doi: 10.3174/ajnr.a5793.

22. Meram E, Harari C, Shaughnessy G, et al. Quantitative 4D-Digital Subtraction Angiography to Assess Changes in Hepatic Arterial Flow during Transarterial Embolization: A Feasibility Study in a Swine Model. J Vasc Interv Radiol. 2019; doi: 10.1016/j.jvir.2019.01.018.

23. Labropoulos N, Borge M, Pierce K, Pappas PJ. Criteria for defining significant central vein stenosis with duplex ultrasound. J Vasc Surg. 2007;46(1):101–107. doi: 10.1016/j.jvs.2007.02.062.

24. Sugaya K, Kadekawa K, Unten Y, Nishijima S, Ashitomi K, Yamamoto H. Relationship of blood flow in the common iliac vein to lower urinary tract disease. J Med Ultrason. 2019;46(2):223–229. doi: 10.1007/s10396-019-00927-5.

25. Oberstar EL, Periyasamy S, Laeseke PF, Speidel MA. Power injector for angiographic flow analysis using custom contrast density profiles. Medical Imaging 2020 Phys Medical Imaging. 2020;42. doi: 10.1117/12.2549656.

26. Li N, Ferracane J, Andeen N, et al. Endovascular Venous Stenosis and Thrombosis Large Animal Model: Angiographic, Histological, and Biomechanical Characterizations. J Vasc Interv Radiol. 2022;33(3):255-261.e2. doi: 10.1016/j.jvir.2021.10.036.

Chapter 6: Conclusion

6.1 Conclusions

Image-guided vascular interventions are minimally-invasive procedures that navigate and treat diseases through blood vessels. Digital subtraction angiography (DSA) is the primary intra-procedural imaging method for diagnosing pathology, determining procedural endpoints, and evaluating treatment efficacy. Currently, assessment of DSA images are largely subjective and qualitative, leading to high inter-observer variability and poor reproducibility. This has been shown to have negative outcomes for patients in a variety of treatments and conditions. A quantitative angiography technique would help develop objective treatment endpoints, standardizing procedures and improving their safety and efficacy.

In this dissertation, we investigated two novel quantitative angiography techniques, quantitative digital subtraction angiography (qDSA) and quantitative digital subtraction venography (qDSV). qDSA was validated in phantom and in vivo models as an accurate technique for performing intra-procedural blood velocity quantitation. In the oncologic application of liver embolizations, qDSA was able to quantitatively discriminate treatment endpoints, characterize intra-procedural blood velocity changes better than a commercially available technique, and correlated with histopathologic and

functional imaging measures of tissue perfusion. In developing advanced techniques, evaluations of super-selective qDSA, volumetric qDSA, and motion-compensation for 3D-DSAs demonstrated strong feasibility for integration into angiographic procedure workflow. In the non-oncologic application of spleen embolization, qDSA was able to characterize intra-procedural blood velocity changes, discriminate blood velocity changes due to different size particles, and correlate with multi-modal imaging measures of reduced portal venous blood flow. In the application of venous interventions, qDSV was accurate across a range of time-modulated injection protocols and methods, accurate in in vivo models, and was able to characterize intra-procedural blood velocity changes in an in vivo model of iliac vein stenosis.

Further development and validation of qDSA and qDSV are required, but this complete body of work successfully demonstrates the strong potential of these quantitative angiography techniques for improving patient outcomes related to image-guided vascular interventions.

6.2 Future Directions

6.2.1 Correlation of qDSA with immunohistochemistry in the liver

Ongoing studies are planned to correlate qDSA-based embolization endpoints with immunohistochemistry (IHC) markers of tissue hypoxia and inflammation. This will be done by performing a liver embolization to qDSA-calculated quantitative endpoints in a porcine model similar to the method outlined in Chapter 2 using several quantitativestasis endpoints(e.g. 25-100). There will be a survival period to allow acute ischemic changes take place, after which the animal will be euthanized. It will then be fixed and sectioned for histology and immunohistochemistry (IHC) analysis. On histology, our major findings of interest are degree of cellular necrosis and architectural changes. On IHC, our proteins of interest are hypoxia-inducible factor 1-alpha (HIF1a), tumor necrosis factor-alpha (TNFa),and vascular endothelial growth factor (VEGF). These markers will provide information about the degree of hypoxia, inflammation, and angiogenesis respectively. Subjective histopathologic assessment will be categorized into a 4-point rating scale and the IHC expression will be quantified using ImageJ. These pathology assessments will be compared with the relative reduction in blood velocity for the different partial-and complete-stasis endpoints.

6.2.2 Validation of qDSA-guided embolization in a large animal liver tumor model

Ongoing studies are planned to for validating qDSA-guided liver embolization in a large animal tumor model to demonstrate correlation with reduction in tumor volume and intra-tumoral changes. Liver tumors can have heterogeneity in size, architecture, and microvascularity. The development of a quantitative embolization endpoint would need to be relatively immune to these differences. Furthermore, there should be confidence that the method will allow for the selection of an endpoint that will effectively decrease tumoral enhancement without incurring significant off-target effects. We plan to use a newly developed liver tumor model, the *Oncopig*. In these genetically-modified swine, tumors are inducible through adenoviral vector (Cre-recombinase). Experiments will be conducted in a manner similar to 6.2.1, with the addition of a 4-week survival period with serial MRI tumor imaging, serial hematologic assays, and added tumor-specific markers of tumor necrosis and microvascularity (p53, Ki-67, CD-31, CD-34).

6.2.3 Determination of Optimal Partial Splenic Artery Embolization Endpoint

Ongoing investigations are planned to help determine the optimal qDSA-calculated quantitative blood velocity endpoint for partial splenic artery embolization procedures by correlating to measures of splenic perfusion. This will be done by performing a partial splenic embolization to qDSA-calculated quantitative endpoints in a porcine model similar to the method outlined in Chapter 4. Following embolization, the animals will undergo F18-MISO PET/MR to assess functional changes in splenic hypoxia, and changes in splenic arterial, venous, and portal venous blood flow using PC VIPR. During a survival period, serial hematologic assays will be acquired to assess any cytopenia or other abnormalities to blood counts. Gross and histopathology will be assessed for acute inflammatory any necrotic changes (similar to 6.2.1. Imaging and pathology changes will be correlated to the qDSA-determined degree of embolization. The quantitative endpoint which causes significant stasis whilst preserving splenic function and minimizing complications (e.g. abscess) will serve as a foundation for further clinical studies.

6.3 Collaborations

The following are several abstracts from ongoing collaborations related to qDSA and qDSV. These projects continue to improve and expand upon the described techniques.

6.3.1 qDSA Radiation Dose Reduction

Hoffman C, Whitehead J, **Periyasamy S**, Kutlu A, Speidel M, Laeseke PF. Low Dose Quantitative DSA for Intraprocedural Calculation of Blood Velocities. SIR 2022. June 2022. Oral Presentation

Purpose: Quantitative 2D digital subtraction angiography (qDSA) can be used to quantify blood velocity during interventions. Currently, qDSA is limited by radiation doses associated with the high frame rates required for blood velocity quantification. This study aimed to investigate the accuracy of qDSA utilizing lower dose DSA images in phantom and in vivo porcine models.

Materials and Methods: qDSA studies were performed in 4 vascular phantoms and 1 porcine model. 3D printed vascular models were created for the iliac, renal, hepatic, and splenic arteries. The same arteries were investigated for the porcine model. A total of 5 dose rates (0.08, 0.81, 1.82, 2.4, 3.6 μGy/frame) were acquired at 30 fps, with the highest dose rate being comparable to clinical DSA protocols. qDSA blood velocities were calculated using a shifted least squares approach that tracks contrast along a vessel centerline. A range of qDSA velocities were computed for the 4 vessel regions. Linear regression and Pearson's correlation coefficient were used to assess the agreement between the highest dose rate and the 4 remaining lower dose rates. In vitro and in vivo data sets were acquired in triplicate and duplicate respectively.

Results: The qDSA velocity measurements for the lower dose DSA techniques correlated with the highest dose DSA measurements (Pearson's $r = 0.96 - 0.99$) for the in vitro models. Similar correlation values were found for the in vivo model (Pearson's $r = 0.74 - 0.93$) with a slight reduction compared to in vitro. The linear regression of each dose rate resulted in slopes ranging from 0.80 to 1.14 and 0.77 to 1.06 for the in vitro and in vivo models respectively. The 95% confidence intervals included a slope of 1 for all cases.

Conclusion: Arterial blood velocities were accurately quantified with lower dose DSA imaging in both in vitro and in vivo porcine models. A strong positive correlation ($r > 0.8$) was maintained for up to an 80% reduction in radiation dose rate. The agreement between the lower dose and high dose DSA velocities is promising for clinical translation of the qDSA technique.

6.3.2 qDSA for Peripheral Arterial Disease

Meram E, **Periyasamy S**, Hoffman C, Pieper A, Kutlu A, Laeseke PF. Characterizing Blood Velocities in a Porcine Stenotic Iliac Artery Model Using Quantitative DSA. SIR 2022. June 2022. Oral Presentation

Purpose: Quantitative 2D digital subtraction angiography (qDSA) is a postprocessing technique that leverages the inherent pulsatility in arterial blood to quantify blood velocity1. It has been correlated with intravascular Doppler and 4D Flow MRI in normal porcine iliac arteries and was used to quantify velocities in a stenotic iliac artery phantom model2-3. This study aimed to assess the feasibility of using qDSA to quantify blood velocity in an in vivo porcine stenotic iliac artery model.

Materials and Methods: 120 2D-DSAs (30 fps) were performed in 4 swine (mean 63 kg). 100% or 50% contrast was administered at a 2.5 mL/s injection rate for 8 seconds via a 5 Fr angled glide catheter positioned in the proximal common iliac artery (CIA). Severe stenoses were created near the iliac artery bifurcation by performing a cutdown and tying 3-0 silk sutures around the vessel with a 0.035" wire in it. Pre- and post-stenosis 2D-DSAs were performed. qDSA velocities in the CIA (proximal to the stenosis) and external iliac artery (EIA, distal to the stenosis) were calculated and compared to peak systolic (PS) pulsed-wave doppler ultrasound. The results were evaluated with descriptive statistics, t-testing, Pearson correlation, and linear regression.

Results: The average qDSA and US blood velocities are shown in Table 1. Stenoses with >90% luminal narrowing were achieved (>200cm/s peri-stenotic PS velocities and tardus parvus waveforms in EIA). Distal to the stenosis, statistically significant reductions in velocity were noted in the EIA on both US and qDSA ($p < 0.05$). qDSA velocities obtained with 50% and 100% contrast strongly correlated ($r=0.82, p < 0.001$) with a slope of 0.97 and R2 of 0.69 ($y=0.97x+5.75$). The US and qDSA velocities also strongly correlated for all flow states (US vs 100% $r=0.71$; US vs 50% $r=0.76$). There was a 2.3-2.8:1 ratio between the PS US and mean qDSA velocities. Given that qDSA velocities are spatially and temporally averaged, estimated mean PS US velocities (assuming parabolic flow where mean PS velocity = 0.5 x PS velocity) are also provided in Table 1 for comparison

Conclusion: Pre- and post-stenotic iliac arterial blood velocities can be characterized using qDSA. Further studies are indicated to investigate the accuracy of qDSA velocity quantification with different degrees of stenosis as well as in clinical studies with diseased peripheral arteries.

6.3.3 Motion-Compensation for qDSA

Whitehead J, Hoffman C, **Periyasamy S**, Laeseke PF, Speidel M, Wagner M. "A motion compensated approach to quantitative digital subtraction angiography", Proc. SPIE 12031, Medical Imaging 2022: Physics of Medical Imaging, 120311L (4 April 2022); https://doi.org/10.1117/12.2611816

Quantitative digital subtraction angiography (qDSA) aims to standardize clinical endpoints for embolization procedures by measuring arterial blood velocity from 2D image sequences intra-procedurally until a predetermined reduction in velocity is achieved. qDSA determines velocity by tracking oscillations in iodine contrast induced from the cardiac cycle as they propagate along a vessel centerline. The purpose of this work was to investigate the influence of vessel motion on the accuracy of qDSA and to develop a motion compensated qDSA approach (MC-qDSA). MC-qDSA uses a deep learning-based frame-by-frame vessel segmentation approach followed by vessel registration. This allows automatic recalculation of centerlines for each frame and thus provides a dynamic centerline that moves with the vasculature. The approach was tested in a phantom study simulating physiologic blood flow, respiratory and cardiac motion. Errors in qDSA velocity measurements relative to the ideal case of a stationary phantom were quantified using the mean absolute percent difference (MAD). In the respiratory motion cases, no motion correction resulted in 160.0 ± 283.0% MAD and the proposed MC-qDSA approach improved the MAD to 6.5 ± 5.9%. In the cardiac motion cases, MAD was 11.9 ± 12.8% without motion correction and 5.4 ± 4.1% using MC-qDSA. A retrospective swine study was performed in motion corrupted image sequences to test the ability of MC-qDSA to correctly determine vessel centerlines with more anatomically realistic backgrounds and vessels. The average Hausdorff distance between non-motion-compensated vessel centerlines and manually annotated centerlines was 1.8 ± 1.5mm and for the motion compensated centerlines it was 0.5 ± 0.2mm. The proposed method provides a potential means of utilizing qDSA in motion corrupted image sequences.

6.4 Doctoral Publications

1. Longo KC, Zlevor AM, Laeseke PF, Swietlik JF, Knott EA, Rodgers AC, Mao L, Zhang X, Xu Z, Wagner MG, **Periyasamy S**, Lee FT Jr, Ziemlewicz TJ. Histotripsy Ablations in a Porcine Liver Model: Feasibility of Respiratory Motion Compensation by Alteration of the Ablation Zone Prescription Shape. Cardiovasc Intervent Radiol. 2020 Nov;43(11):1695-1701. doi: 10.1007/s00270-020-02582-7. Epub 2020 Jul 16. PMID: 32676957; PMCID: PMC8543737.

2. **Periyasamy S**, Hoffman CA, Longhurst C, Schefelker GC, Ozkan OS, Speidel MA, Laeseke PF. A Quantitative Digital Subtraction Angiography Technique for Characterizing Reduction in Hepatic Arterial Blood Flow During Transarterial Embolization. Cardiovasc Intervent Radiol. 2021 Feb;44(2):310-317. doi: 10.1007/s00270-020-02640-0. Epub 2020 Oct 6. PMID: 33025244; PMCID: PMC7855448.

3. Hoffman C, **Periyasamy S**, Longhurst C, Medero R, Roldan-Alzate A, Speidel MA, Laeseke PF. A technique for intra-procedural blood velocity quantitation using time-resolved 2D digital subtraction angiography. CVIR Endovasc. 2021 Jan 7;4(1):11. doi: 10.1186/s42155-020-00199-y. PMID: 33411087; PMCID: PMC7790988.

4. Wagner MG, **Periyasamy S**, Longhurst C, McLachlan MJ, Whitehead JF, Speidel MA, Laeseke PF. Real-time respiratory motion compensated roadmaps for hepatic arterial interventions. Med Phys. 2021 Oct;48(10):5661-5673. doi: 10.1002/mp.15187. Epub 2021 Sep 4. PMID: 34431111; PMCID: PMC8568648.

5. Wagner MG, **Periyasamy S**, Schafer S, Laeseke PF, Speidel MA. Three-dimensional catheter navigation of airways using continuous-sweep limited angle fluoroscopy on a C-arm. J Med Imaging (Bellingham). 2021 Sep;8(5):055001. doi: 10.1117/1.JMI.8.5.055001. Epub 2021 Oct 15. PMID: 34671695; PMCID: PMC8517428.

6. Pirasteh A, **Periyasamy S**, Meudt JJ, Liu Y, Lee LM, Schachtschneider KM, Schook LB, Gaba RC, Mao L, Said A, McMillan AB, Laeseke PF, Shanmuganayagam D. Staging Liver Fibrosis by Fibroblast Activation Protein Inhibitor Positron Emission Tomography in a Human-sized Swine Model. J Nucl Med. 2022 Apr 21:jnumed.121.263736. doi: 10.2967/jnumed.121.263736. Epub ahead of print. PMID: 35450958.

7. Wagner MG, **Periyasamy S**, Kutlu A, Pieper AA, Swietlik J, Hall T, Xu Z, Speidel M, Lee FT, Laeseke PF. An X-ray C-arm Guided Automatic Targeting System for Histotripsy. ***Under Revision for IEEE Transactions on Biomedical Engineering***. May 2022

8. **Periyasamy S**, Oberstar E, Kutlu A, Pieper AA, Whitehead J, Hoffman CA, Li G, Speidel MA, Laeseke PF. Quantitative Digital Subtraction Venography for Venous Interventions: Validation in Phantom and In Vivo Porcine Models. ***Submitted to Radiology***. April 2022

9. Mauch SC, Zlevor AM, Knott EA, Couillard AB, **Periyasamy S**, Williams EC, Swietlik JF, Laeseke PF, Zhang X, Xu Z, Abel J, Lee FT, Ziemlewicz T. Hepatic and Renal Histotripsy in an Anticoagulated Porcine Model. ***Submitted to JVIR***. April 2022

10. Pieper AA, **Periyasamy S**, Oberstar E, Hetzel SJ, Swietlik JF, Kleedhen M, Koepsel EK, Pinchot JW, Ozkan O, Speidel MA, Laeseke PF. Evaluation of Reduced Contrast Dose Digital Subtraction Angiography Reference Images in an In Vivo Porcine Model. ***Submitted to Diagnostic and Interventional Radiology***. May 2022